AN ABSTRACT OF THE DISSERTATION OF

Minalben B. Shah for the degree of Doctor of Philosophy in Materials Science presented on November 6, 2008.

Title: Mechanistic Aspects of Fracture and Fatigue in Resin Based Dental Restorative Composites.

Abstract approved:

Jamie J. Kruzic

For resin based dental restorative composites, one of the major challenges is to optimize the balance between mechanical and optical properties. Although fracture is the second leading cause of dental restorative failures, very limited mechanistic understanding exists on a microscopic level. In the present study, the fracture properties and mechanisms of two commercial dental resin composites with different microstructures are examined using double notched four point beam bending and pre-cracked compact-tension, C(T), specimens. Four point bend flexural strength was also measured using un-notched beam samples. The first material is a microhybrid composite that combines a range of nano and micro scale filler particles to give an average particle size of 0.6 μm, while the second is a nanofill composite reinforced

entirely with nano particles and their agglomerates. The influences of 60 days water hydration and a post-cure heat treatment were also examined.

Fracture resistance curve (*R*-curve) experiments have demonstrated the microhybrid composite to be more fracture resistant than the nanofill composite in both as-processed and hydrated conditions. Rising fracture resistance with crack extension was observed in all specimens, independent of the environmental conditions. Compared to the as-processed condition, a significant reduction in the peak toughness was observed for the nanofill composite after 60 days of water aging. Hydration lowered flexural strength of both composites which was attributed to hydrolytic matrix degradation with additional interfacial debonding causing larger strength decrease in the nanofill. Optical and SEM observations revealed an interparticle matrix crack path promoting crack deflection as a toughening mechanism in all cases except the hydrated nanofill which showed particle-matrix debonding. Crack bridging was another observed extrinsic toughening mechanism that was believed to be responsible for the rising fracture resistance curve (*R*-curve) behavior. Post-curing heat treatment changed the *R*-curve shape which was attributed to matrix toughening.

Fatigue crack growth resistance was also measured after water aging for 60 days and testing in wet conditions. The da/dN-ΔK curve showed sigmoidal behavior with three different fatigue crack growth regions. The nanofill composite had a lower fatigue threshold, ΔK_{th}, by ~ 0.13 MPa$\sqrt{m}$ compared to the microhybrid composite, with an observed plateau in the fatigue crack growth curve suggestive of environmental attack.

Toughening mechanisms of crack deflection and crack bridging were identified with evidence of cluster-matrix debonding in the nanofill composite. In general, fatigue crack growth ranged from ~10^{-9} to 10^{-5} m/cycle over ΔK of 0.54 to 0.63 MPa$\sqrt{m}$ for the microhybrid composite and ΔK of 0.41 to 0.67 MPa$\sqrt{m}$ for the nanofill composite.

© Copyright by Minalben B. Shah
November 6, 2008
All Rights Reserved

Mechanistic Aspects of Fracture and Fatigue in Resin Based Dental Restorative Composites

by
Minalben B. Shah

A DISSERTATION

submitted to

Oregon State University

in partial fulfillment of
the requirements for the
degree of

Doctor of Philosophy

Presented November 6, 2008
Commencement June 2009

Doctor of Philosophy dissertation of Minalben B. Shah presented on November 6, 2008.

APPROVED:

_____

Major Professor, representing Materials Science

_____

Director of the Materials Science Program

_____

Dean of the Graduate School

I understand that my dissertation will become part of the permanent collection of Oregon State University libraries. My signature below authorizes release of my dissertation to any reader upon request.

_____

Minalben B. Shah, Author

ACKNOWLEDGEMENTS

I would like to express my sincere gratitude and a deep sense of appreciation for my doctoral research advisor Dr. Jamie Kruzic for his stimulating suggestions, continuous motivation, and scholarly feedback throughout the course of my research and thesis writing. His deep sense of knowledge, guidance and thoughtfulness always triggered me to a great extent. It goes without saying that this research work would not have been completed without his help and support. I am more grateful to him than he knows.

I would like to express my gratitude to Prof. Jack Ferracane at Oregon Health and Science University, Portland, OR, for his collaboration on the present research work, providing necessary research material (from 3M™ ESPE™), and judicious feedback throughout my research project. I would like to acknowledge Kurt Langworthy and John Donovan at University of Oregon, Eugene, OR, for their help and support with SEM/ESEM analysis. Special thanks also go to my committee members Dr. William Warnes, Dr. David Cann, Dr. Ralf Busch, and my GCR (Graduate Council Representative) Dr. Sundar Atre for their time, interest, and valuable feedback on my research. My vote of thanks goes to Manfred Dietrich and Josh Hogg for machining my samples and Rawley Green, Nikole Wilkins, and Michelle Yang deserve special mention for their timely assistance. I thank the Materials Science program and Department of Mechanical, Industrial and Manufacturing Engineering for supporting

my research. I am grateful to all my colleagues in Materials Science for their invaluable assistance.

I am most grateful to my parents, my in-laws, other family members, and friends, especially Prashant Wadhwa and Manish Bothara, for standing besides me and supporting me throughout the course of my work. Finally, I would like to thank my husband Bhavin and our beloved son Aarav for their patient love, understanding, and encouragement. Without their care, affection, and tolerance, this study would not have been completed.

I would like to dedicate this
thesis to my husband Bhavin and our son Aarav

TABLE OF CONTENTS

TABLE OF CONTENTS (CONTINUED)

Page

LIST OF FIGURES

LIST OF FIGURES (CONTINUED)

LIST OF FIGURES (CONTINUED)

LIST OF FIGURES (CONTINUED)

LIST OF TABLES

1 INTRODUCTION

"The structure and composition of teeth is perfectly adapted to the functional demands of the mouth and are superior in comparison to any artificial material. So, first of all, do no harm [1]."

Resin composites are increasingly used in dental restorations since their introduction in 1962 [2], primarily due to their natural tooth like appearance and the absence of toxic mercury as is found in amalgam [3-5]. Some of the other advantages of resin composite include easy bonding with enamel and dentin [6], less removal of tooth structure [7] and their application in anterior as well as posterior restorations [3, 4, 8, 9].

Despite the above advantages and the ever increasing demand for highly aesthetic restoratives [5, 10], resin composites often suffer from in-service failures. Three primary reasons for composite failures are [6, 7, 10, 11]:

- Secondary caries,
- Restorative fracture, and
- Marginal defects.

Additionally, other short-comings of the resin composites include polymerization shrinkage [12], cytotoxicity [3], discoloration, poor wear resistance [13-15], post-operative sensitivity [11] and relatively poor mechanical properties compared to

amalgam [12]. Although a recent clinical survey at 3.5 years suggested satisfactory short-term clinical performance of resin composites [16], their longer term durability is still questionable [10]. A recently performed seven year clinical study comparing amalgam and resin composites for posterior restorations, on patients 8-12 years of age, showed much higher failure rate of the composite restorations, 0.9 to 9.4 %, compared to 0.2 to 2.8 % for the amalgam (N = 1748 restorations) [17]. In agreement with those findings, other studies have also suggested the use of amalgam over resin composites for large occlusal posterior restorations [5, 16].

Marginal chipping and/or bulk fracture [18, 19] are commonly reported restorative failures. Despite the fact that fracture (either by overload or fatigue) is the second leading cause of failure for composite dental fillings, a limited understanding exists on how fracture occurs in these materials and what mechanisms are responsible for the toughening in dental resin composites. Therefore, the purpose of the current research is to study the fracture and fatigue behavior of resin based dental restorative composites and to determine the microstructural influence in governing the fracture and toughening mechanisms.

Herewith, three manuscripts are attached which are submitted for publication in archival scientific journals. Though all three manuscripts stand alone, they have a common theme of addressing fracture behavior of resin based dental restorative composites. The first manuscript is titled "*R*-curve behavior and micromechanisms of fracture in resin based dental restorative composites" which characterizes the fracture

behavior of two different as-processed commercial resin composites, one microhybrid and one nanofill, in terms of resistance curves (*R*-curves) and also examines the role of microstructure in governing the toughening mechanisms. Results of first manuscript also forms baseline for comparing the fracture behavior of the same composites in hydrated conditions to simulate actual clinical oral conditions, which is addressed in the second manuscript titled "*R*-curve behavior and toughening mechanisms of resin based dental composites: Effects of hydration and post-cure heat treatment". Finally, as all restorations are subjected to masticatory stresses, it is important to understand the effect of cyclic fatigue stresses in inducing subcritical crack propagation in the resin composites. Accordingly the third manuscript addresses this topic and is titled "Mechanistic aspects of fatigue crack growth behavior in resin based dental restorative composites". In that article the fatigue resistance and the associated fatigue mechanisms for the microhybrid and nanofill dental composites were examined along with the cyclic crack growth behavior.

2 BACKGROUND

2.1 Tooth structure

Tooth is a complex hard tissue structure consisting of four major components:

- Enamel,
- Dentin,
- Pulp, and
- Cementum.

Each of these tooth components has distinct structure and functionality [3, 20], and each is briefly described below.

2.1.1 Enamel

Enamel is the hardest and stiffest tissue of a tooth [21] whose main function is to cover and protect the underlying dentin. Highly mineralized, enamel is composed of 92-96% inorganic substances, ~ 1% organic substances, and ~ 3% water by weight [3, 20]. Enamel rods are the fundamental morphological units of the enamel tissue which are formed by the ameloblasts cells. The enamel rods run through the enamel oriented parallel to each other. They define the final thickness of the enamel as they run outward from the dentinoenamel junction to the tooth surface. Enamel is acellular in its final form, extremely brittle, and it relies on the underlying structure of the dentin

for support. Its fracture toughness ranges from ~ 0.7 MPa√m for the cracks propagating in the direction parallel to the enamel rods to ~ 1.3 MPa√m in the direction perpendicular to the enamel rod [22].

2.1.2 Dentin

Dentin is a mineralized tissue that makes up the bulk of the tooth and its main function is to support the outer enamel. It consists of 70% by weight hydroxyapatite mineral, 20% organic mineral, and 10% water [3]. Odontoblasts are the primary formative cells for the dentin. Nanometer scale apatite minerals are distributed in a scaffold of collagen fibrils. Also, one of the characteristic microstructural features are the dentinal tubules that run from the soft interior pulp to the dentino-enamel junction. The tubules are surrounded by a collar of highly mineralized peritubular dentin and are embedded into an intertubular dentin matrix. Unlike enamel, formation of dentin continues throughout the life of the tooth. Due to the lower mineral content, it is softer than enamel and decays faster due to poor care.

2.1.3 Pulp

Pulp is a very soft tissue that occupies the innermost portion of the tooth and is made up of connective tissues, blood vessels, nerves, and cells called odontoblasts. The primary function of the pulp is to form dentin [3], but it also provides nutrients and acts as a sensor for changes in temperature and pressure. Coronal pulp resides within

the crown of the tooth whereas radicular pulp extends from the cervical region of the crown to the root apex [23].

2.1.4 Cementum

Cementum is a calcified tissue that covers the root of the tooth. It is thickest at the root apex and its main function is to anchor the periodontal ligaments to the root of the tooth. Cementum consists of cementum cells and is bone-like and yellowish in color. By weight it is approximately 61% inorganic material, 27% organic material, and 12% water [23].

2.2 Historical background and purpose of dental restorations

Despite efforts to preserve oral hygiene, human teeth are often subjected to problems associated with tooth decay requiring dental restoration. These restorations use specially fabricated materials to help restore the tooth structure. Restoration or dental filling materials are commonly used for applications such as i) to fill and repair dental caries and cavities, ii) cementation of dental prosthesis, and iii) surgical restoration due to external trauma. Restorations are also increasingly used for cosmetic purposes such as reconstruction of anterior teeth, correction of stains and erosion, and alignment of teeth. Gold was the first dental restoration material reported in the late fourteen hundreds [3, 12]. Many of the materials used in modern dental practices were developed between 1840 and 1900. Some of the dental restorative materials developed

include noble and base metals and their alloys, amalgam, resin composites, glass ionomers, ceramics, cements, dental waxes, etc. Although chemistry, physics, and other engineering sciences were the fundamental building blocks for developing restorative science, systematic improvement in the mechanical properties were achieved only after principles of mechanics were applied to biological restorative dentistry in the late nineteenth and early twentieth centuries [3].

2.3 Classification of dental restorations

Dental restorations are broadly classified into two categories:

- **Indirect restorations, and**
- **Direct restorations.**

Indirect restorations are prepared outside the tooth mostly in a laboratory, examples of which include inlays and onlays, crowns, veneers, and bridges. Direct restorations are applied in-situ into the tooth cavity and dental composites, amalgam, and glass-ionomers are the most common examples. Fig. 1 shows an organizational chart of various dental restorations.

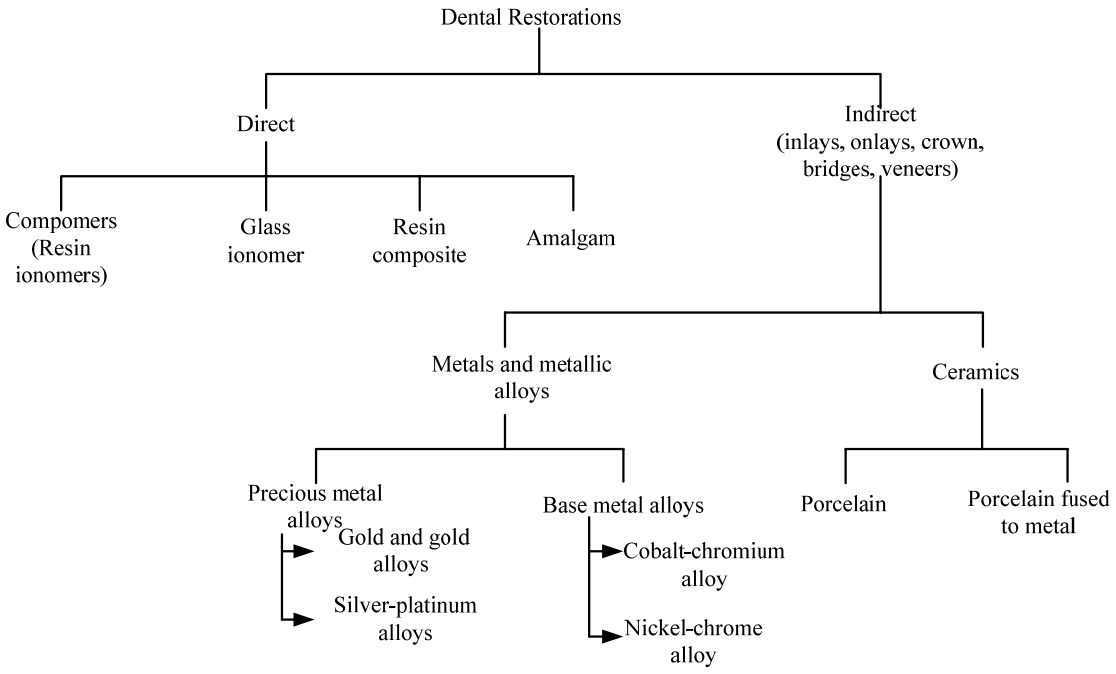

Fig. 1. Organizational chart of different types of dental restorations

2.3.1 Indirect restorations

2.3.1.1 Indirect restoration types

a) Inlays/Onlays

Inlays and onlays are very similar to fillings. An inlay lies inside the cusp tips of the tooth, whereas an onlay covers one or more of the cusps. Onlays in general require extensive reconstruction compared to inlays and they are custom made to fill the prepared cavity. Example materials commonly used for inlays and onlays include gold and porcelain.

b) Crowns

A crown is a fixed prosthetic restoration that is cemented over the entire tooth (enamel or dentin) to restore its function. It may be fabricated using metal, all-ceramic, or porcelain-fused to metal. One of the shortcomings of crown placement is it requires considerable tooth structure (~ 25%) removal.

c) Veneers

Dental veneer is typically a thin custom designed restorative layer that is placed on an anterior tooth to improve aesthetics. For example, by adjusting tooth alignment or covering chipped or worn teeth.

d) Bridges

A dental bridge is an artificial or false tooth that is used to fill the area left by the missing tooth. For example, two porcelain crowns are fused to the adjacent teeth on either side with a dummy tooth that fills the space of the missing tooth. Commonly used materials for bridges include gold, porcelain, or porcelain fused to metal.

2.3.1.2 Indirect restorative materials

a) Ceramics

Porcelain jacket crowns were the first ceramic restoratives developed. Due to the limited lifetimes of ceramic restoratives, ceramic fused metal restoratives were introduced at a later time. However, with increasing demand for improved aesthetics, all-ceramic restorations are increasing in popularity again [24]. In dentistry, ceramic restorations are used in all of the above mentioned applications such as crowns, inlays, onlays, veneers, and partial dentures. Modern all-ceramic restoratives have good aesthetics, high wear resistance, good biocompatibility, and good chemical inertness [25]. Traditionally used feldspathic porcelain and micaceous glass-ceramics have lower resistance to progressive slow-crack propagation than glass-infiltrated alumina and yttria-stabilized tetragonal zirconia polycrystals (Y-TZP) [25]. Current research is focused on evaluating more compliant bilayer (ceramic/polymer) and trilayer (ceramic/ceramic/polymer) configurations [26] for dental crown applications.

b) Metals and metallic alloys

Most metallic alloys are fabricated using a casting process where the metals are cast under pressure and post heat treated if required. An example of such a process is the lost-wax casting process. Although metal and metallic alloys are clinically proven to be the best materials for long-lasting dental restorations, the desire for cosmetically

appealing ‘metal-free’ alternatives is on the rise. Commonly used metallic materials in molar restorations include precious and noble metal alloys such as gold, silver, palladium and base metallic alloys such as nickel, cobalt, and titanium [20]. Other than aesthetics related limitations, thermally conductive metallic fillings also lead to higher sensitivity to heat and cold.

2.3.2 Direct restorations

2.3.2.1 Amalgam

Amalgam is the most widely used direct restorative material in today’s dental industry. It is a self-hardening mixture of liquid mercury and alloy powder of mostly silver and some amounts of tin, copper and zinc. Amalgam’s widespread usage is mainly attributed to its cost effectiveness, high strength, ability to apply in broad range of clinical applications, simple usage, easy handling, and durability [10]. Apart from gold, it has the longest service life compared to other restorative materials. Long term clinical evaluations suggests that amalgam has two to three times longer service life than dental composites [27]. Despite all the functional benefits, there are two major concerns:

- the aesthetics, and
- health concerns due to mercury related toxicity.

Despite the latter concern, there are no proven systematic or local effects from mercury contamination [3], which suggests that correct use of amalgam might not pose a health risk in terms of biocompatibility.

2.3.2.2 Glass Ionomer Cements (GIC)

Glass ionomer cements are mixture of ion-leachable fluoroaluminosilicate glass powder and liquid aqueous polymers and copolymers of acrylic acid, mostly in form of polyalkenoic acid. Glass ionomer cements use an acid/base setting reaction. As a part of this reaction, Al^{+++} and Ca^{++} ions forms due to acid attack on the glass powder which then cross-link the polyanion chains forming respective polyacrylate salts. The setting reaction usually continues for more than 24 hrs and may last up to 1 year [3, 28].

Glass ionomers and resin-modified glass ionomers are cements used in patients with high risk of dental caries, as it slowly releases fluoride into the mouth for a long time after restoration. Though initial applications of glass ionomers were limited due to its lower strength and slower setting time, modern glass ionomers have very good biocompatibility and their ease of bonding with bone and metals have created new applications as bone cements for implants [28]. Other advantages of the glass-ionomer cements include a similar thermal expansion coefficient to the tooth structure [28, 29], low shrinkage, and their high retention rate when used as a restorative material. Despite improvements in glass-ionomer formulations, e.g., resin-modified glass

ionomer adhesive, its flexural strength was reported to be significantly lower compared to the resin composite, regardless of the time of 10 minutes, 1 hour or, 7 days before fracture [30].

2.3.2.3 Compomers

Poly-acid modified compomers were introduced to combine the advantages of both glass ionomer cements and resin composites. Glass ionomers provide fluoride release and chemical bonding whereas resin composites impart good aesthetics and easy handling [29]. However, relatively poor mechanical properties like strength [30] and fracture toughness limits their clinical durability and usage as a restorative material.

2.3.2.4 Resin Composites

Resin composite restoratives are the subject of present research and are discussed separately in the following section.

3 RESIN COMPOSITES

Resin based composites were primarily introduced in an attempt to find an alternative to dental amalgam. Introduced in 1960 [2], the use of dental resin composites has increased immensely owing to increased aesthetics, increased ability to bond easily with enamel and dentin surfaces, increased desire to replace amalgam, and decreased tooth structure removal [31, 32]. These composites generally consist of an organic polymer matrix, typically dimethacrylate based resin, reinforced with hard inorganic ceramic particles such as glass, quartz, colloidal silica, or zirconia. In the last few years, nano-size fillers have been introduced to achieve substantial improvement in aesthetic properties while attempting to maintain the strength of the resin composites [33].

Some resin composites are optimized for low stress bearing anterior restorations while others are designed for high stress bearing posterior restorations [8]. Other than direct dental restorative purposes, dimethacrylate based resin composites have applications in diverse areas such as dentinal bonding agents, resin cements, pit and fissure sealants, and crown and bridge prostheses [34].

3.1 Classification of resin composites

Resin composites are most commonly classified according to the filler size and filler volume percentages and are commonly categorized as traditional, microfilled or

flowable, hybrid, microhybrid, and nanofill composites. Table I briefly summarizes the characteristics of these commonly used resin composites.

Table I Classification of resin based dental restorative composites based on filler volume % and filler size.

Properties	***Traditional***	***Microfilled***	***Hybrid***	***Microhybrid***	***Nanofill***
Filler vol.%	60 to 70	32 to 50	70-80	60-70	59-70
Filler Size	20-50 μm	0.02-0.15 μm	1 to 5 μm	0.2-0.8 μm	5-75 nm
Type of restoration	Anterior and posterior	Anterior	Mostly posterior	Anterior and posterior	Anterior and posterior
Pros	More durable	Smooth surface polish	Strong, high fracture strength and less discoloration	Fine polishing stronger than microfills	Better optical, mechanical and chemical Properties
Cons	Roughness, staining, discoloration	Poor mechanical properties	High wear and surface roughness	Poor fracture and fatigue resistance	Interface stability and fatigue resistance

3.2 Primary constituents of resin composites

Primary constituents of the resin composite are:

- Fillers,
- Resins, and
- Coupling agent.

The fillers are used as reinforcements, resin serves as matrix and the coupling agent acts as a bonding agent between the two. The function and desired properties of each constituent are discussed briefly in the following sections.

3.2.1 Fillers

Inorganic fillers provide strength, wear resistance, and translucency in addition to reducing the overall shrinkage of the composites. Commonly used reinforcements are glass, quartz, colloidal silica, silica nanoparticles, and zirconia-silica nanoclusters. Barium or strontium containing glasses, or zirconia particles, are often added to provide radiopacity and contrast needed for the clinical diagnosis of marginal leakage and secondary caries in resin based restorations [35]. As mentioned in sections 2.1.1 and 2.1.2, hydroxyapatite is a natural component of enamel and dentin and hence it has been considered as a filler material for resin composites. Hydroxyapatite is naturally radiopaque and moisture resistant. However, it was shown that porosity and filler particle aggregation lead to increased water uptake and solubility of the base resin [36], limiting their applicability as a filler.

Filler content, filler size, and distribution of filler play important roles in governing the physical and mechanical properties of resin composites [6]. Higher filler content and coarser size are usually associated with improved mechanical properties such as strength and modulus, but smaller particle size, which leads to enhanced volume fractions, provide higher wear resistance and aesthetic properties [6, 18, 37]. Hence,

recently developed composites have combination of micron and nano-size filler particles with filler loadings of ~ 70-80 wt. % [33].

Some studies have evaluated silica-glass fibers as reinforcing filler materials [38]. Although fiber reinforced composites have higher strength, toughness, and fatigue resistance, difficulties accommodating higher fiber content, insufficient fiber wetting, difficulty in manipulating free fibers, and rough surface characteristics [39] have restricted their widespread usage in dentistry [40]. Recently, silicon carbide and silicon nitride whiskers have also been tried as fillers with the purpose of enhancing the strength and toughness [41] of the composites.

3.2.2 Resins

Most present-day resin composites are based on dimethacrylate based resin systems. The two most common oligomers used in dental composites are Bis-GMA (bisphenol A-glycidyl dimethacrylate) and UDMA (urethane dimethacrylate). UDMA content is reported to be responsible for increasing the flexural and tensile strengths of the resin systems [42]. In order to reduce the viscosity of the oligomers, low-molecular weight TEGDMA (triethyleneglycoldimethacrylate) is added to many commercial resin composites [24]. Reduction in viscosity usually results in higher degree of polymerization [43] and hence composites containing equal amount of Bis-GMA/TEGDMA/UDMA are recommended for achieving optimal mechanical properties. Among the above mentioned resins, TEGDMA is most hydrophilic due to

hydrophilic ether linkages [44] and Bis-GMA has higher hydrophilicity than UDMA [45]. Hydrolytic degradation of the cross-linked polymer network often makes the resin less hard and more susceptible to fracture.

Heat-cured epoxy resins were used during the early years of resin composite development, but characteristically slow hardening rates prevented their widespread usage as a direct restorative material [46]. New monomers like siloranes have also been introduced by 3M™ ESPE™[47] in an effort to reduce the polymerization shrinkage and internal stress build-up in the composites.

The most commonly used light sources for the curing of dental composites are quartz-tungsten-halogen (QTH) visible light sources and blue light emitting diodes (LEDs) with peak wavelength of ~ 450-500 nm [3]. One of the limitations of the photocuring methods is that light attenuation increases with the composite sample depth due to absorption, reflection, and scattering. Therefore, 40-60 seconds of exposure time per 2 mm of composite thickness are recommended [48]. It has been shown that the use of high intensity light sources results in minimal increases in the depth of cure. Ferracane *et al*. [49] showed that laboratory light curing units produce similar depth of cure as the step-wise hand curing with a visible light source. Although recently developed blue LED sources appear to produce higher curing depths, similar flexural properties are usually achieved with the QTH light [3].

3.2.3 Coupling agent

A coupling agent is used to achieve good bonding between the inorganic reinforcing fillers and the organic resin matrix. The most commonly used coupling agent is organosilane (3-methacryloxypropyltrimethoxysilane), frequently reported in literature as a silane. Bifunctional silane is attached to the filler with a silanol group by a hydrolysis/condensation reaction that forms covalent bonding. Additionally, a methacrylic vinyl group is attached to the resin matrix through chemical reaction or chain entanglement [46]. Hydrolytic degradation of the coupling agent may occur in the oral environment and cause inferior properties of the resin composite.

3.2.4 Other additives

For composites that are light cured, a photo-activator is added to accelerate the polymerization reaction. The most commonly used photo-activator is camphorquinone. Chemical activation may be achieved by using an organic amine that produces free radicals that expedite the polymerization reaction. Additionally, pigments are added to match diverse tooth shades, polymerization inhibitors (e.g., 4-methoxy phenol) are added for storage stability, and color stabilizers are added to prevent discoloration with time.

3.3 Mechanical properties of resin composites

Various physical and clinically relevant properties of dental resin composites are important to understand, such as polymerization or volumetric shrinkage, thermal properties, solubility, water absorption, color stability, radiopacity, polish retention, optical translucency, surface morphology, toothbrush abrasion, and degree of cure. However, the scope of the current research is limited to studying the mechanical properties of resin composites with emphasis on strength, fracture toughness, and fatigue properties. There are a large number of different commercial and experimental composites, and their mechanical properties have been tested using a variety of methods and conditions, making it challenging to generalize their mechanical behavior. Hence only relevant findings are discussed in the following sections.

3.3.1 Flexural strength

Measurement of flexural strength is essential in selecting polymer based restorative composite according to ISO 4049 [50]. The standard requires a minimum flexural strength of 50 MPa. It is considered a clinically relevant test as it measures the collective response of tensile stresses at the lower surface of the specimen and compressive stresses at the upper surface of the specimen [34].

Flexural strength is commonly measured for the restorative material by either three or four point beam bending, but other methods such as bi-axial flexural testing have also

been reported [51, 52] in the literature. In general, three point bending tests result in higher strength compared to four point bending tests. This is because in the latter case a larger flaw population is exposed to the applied stresses, resulting into lower apparent strength. Surface flaws such as inclusions, voids, cracks, and inhomogeneous distribution of organic and inorganic phases have been shown to be the fracture initiation sites governing the strength of resin based composites [53].

In general, microfill/microfine composites have lower strength compared to hybrid and nanofill composites due to their lower filler content [54]. Although strength degradation is different for different material types when aged in water, no significant difference in strength was reported by Rodrigues *et al.* [53] for both a microhybrid and nanofill composite after 24 hrs of water hydration. Supporting those observations, Curtis and coworkers [51] reported no change in mechanical strength after 24 hrs of water hydration, but they also found a progressive reduction in strength over 12 months of aging for the same composites. In the case of the nanofill composite, the higher surface area to volume ratio and relatively porous nature of the agglomerated nanoparticle filler was suggested to be the reason for hydrolytic strength degradation [53]. Such results indicate that strength is dependent upon the size and morphology of the reinforcing filler. Besides filler content, filler-matrix interaction and matrix degradation also considerably influence the strength of resin composites [6, 34, 51]. Hydrolytic degradation of interfaces or the resin matrix restricts the effective transfer of the load from the matrix to the filler, thus reducing the strength of the composite. It has been observed that silane treated inorganic fillers demonstrate superior mechanical

properties compared to untreated or rubber treated fillers [55] due to enhanced interfacial bonding. Also, strength degradation was usually higher when aged in food simulating solvents such as ethanol/water mixtures (50/50 or 75/25 vol. %) or artificial saliva, in comparison to water aging. Reduction in strength after soaking in artificial saliva was suggested to be related to corrosive degradation of the filler [43, 56].

Varying results have been reported for the effect of resin viscosity on strength. Asmussen *et al.* showed that substitution of high viscosity Bis-GMA or relatively more flexible TEGDMA with UDMA increased the tensile strength. In other words, varying the relative amount of the resin components showed significant alteration of the mechanical properties of the resin composites [42]. However, Musanje *et al.* [57] reported no significant difference in the flexural strength for high, medium, and low viscosity hybrid composites.

Using continuous fiber preforms as reinforcements was first introduced in a direct resin composite by Xu *et al.* with the purpose of reducing polymerization shrinkage and fiber pull-out during polishing and wear. In that study, a fiber preform with a diameter of 1.3 mm was made by impregnating the resin in to the fiber bundle which was then cured using visible light and later cut into rods of desired length. Each sample consisted of single fiber preform which was placed longitudinally in the center. Composite samples with a fiber preform rod showed almost 2.5 times higher flexural strength compared to a typical hybrid resin composite.

3.3.2 Fracture toughness

Higher composite fracture toughness, K_{Ic}, is commonly associated with both improved fracture and wear characteristics of the restorations [8]. Also, by knowing the maximum inherent flaw size, a_0, and minimum K_{Ic} value the clinical performance of a restoration may be predicted under various levels of oral stresses [58].

3.3.2.1 Measurement methods

Commonly reported sample geometries and associated methods for measuring the fracture toughness of resin composites are noted in Table II [8, 11, 59-61]. Fujishima and Ferracane [61] showed that among the first four methods, double torsion method was the most conservative while Chevron short rod method gave much higher fracture toughness.

Table II Various sample geometries and associated fracture toughness test methods

Sample geometries	Methods
Single edge notch (SEN)	3-point beam bending
Compact tension specimen	Uniaxial tension
Chevron notch	Short rod design
Notched and grooved plate	Double torsion method
Disk shaped specimen	Brazilian disk test (diametral tensile test)

3.3.2.2 Pre-cracking concerns

From a fracture mechanics standpoint, a fundamental drawback of most fracture toughness studies on resin composites is the use of razor or micro-notched specimens rather than the pre-cracked specimens. Micro-notched specimens are often used due to the limited ductility of resin composites which makes pre-cracking difficult [35, 62]. For measuring fracture mechanics based plain strain fracture toughness of the resin composite under linear elastic loading conditions, all specimen needs to have an atomically sharp pre-crack. Pre-cracking complies with the definition of the fracture toughness which states "ability of a material to resist fracture from a *pre-existing* crack". Also, by simulating a sharp natural flaw in the material, conservative design estimates can be achieved. Although one study reported no significant difference in the fracture toughness, $K_{Ic,}$ measured using either notched or pre-cracked specimens [60], other studies have clearly demonstrated lower fracture toughness for the pre-cracked samples compared to the razor-notched samples [62, 63]. Although, notched samples as opposed to pre-cracked samples was the major difference between those studies, other factors such as notch radius, notch preparation method, and the material tested might have contributed in influencing the fracture toughness of the composite.

3.3.2.3 Effects of hydration on fracture toughness

A review of the available literature indicates that there is a varying degree of impact of hydration on the fracture toughness of resin composites. This difference in fracture behavior may be attributed to differences in experimental techniques, filler particle

sizes, filler-matrix interfacial adhesion, degree of cure of the resin matrix [61], aging time, and/or hydration media. Most studies report fracture toughness values for resin composites in the range of ~ 1 to 2 MPa√m [60, 61, 64, 65]. Such values are comparable to the fracture toughness of the enamel, ~ 0.6 to 1.8 MPa√m [3, 66, 67] and dentin, ~ 1 to 2 MPa√m [22, 68].

Some studies have shown an increase in K_{Ic} following water hydration. Lloyd and Iannetta [60] observed an increase in toughness following 7 days of water hydration which they explained by a plasticizing effect due to absorption of water molecules by the matrix. Consistent with that study, Indrani and coworkers [69] observed an increase in toughness over the initial 2 weeks of hydration followed by a plateau in toughness over the next four weeks. They attributed the high resistance to hydrolytic degradation to improved silanization of the filler particles over the years; compared to previous studies which reported degradation due to interfacial debonding [70, 71].

Ferracane and Marker [72] showed a significant degradation of fracture toughness of quartz and barium-glass filled composites after two months and fourteen months of aging in a food simulating liquid of 75/25 (vol.%) of ethanol/water mixture. The reduction in toughness was attributed mainly to softening of the resin matrix but also hydrolytic degradation of the filler/matrix interface was suggested as a possibility. Interfacial degradation of the silane coupling agent is largely related to hydrolysis of the Si-O-Si bonds by water which is expected to weaken the polymer-filler interface during aging [35]. However, the same composites when aged in *water* for the same

time period showed no reduction in fracture toughness. In a later study, Ferracane and Berge [65] measured fracture toughness of composites with varying degrees of light curing and a range of filler volumes after one and six months of hydration in the same food simulating liquid. Samples with insufficient cure and minimal filler volume showed decrease in K_{Ic} after one month of hydration. Almost a ~ 25% reduction in fracture toughness of all composites was found after six months of hydration which was again associated with weakening of the resin matrix. In another study, Ferracane *et al.* [73] showed 20-30% reduction in toughness after 6 months of water hydration with no changes thereafter up to 2 years. Similar degradation was observed by Ferracane and Condon for a composite aged for 30 days in deionized water [74]. Those authors hypothesized that the initial toughness reduction is associated with softening of the resin matrix and elution of unbound molecules, while saturation and stabilization of the polymer network at a later time prevents any further reduction in fracture toughness. In agreement with Ferracane's studies, Pilliar *et al.* [70] reported a decrease in the toughness following one and six months of water storage and suggested filler/matrix interface cracking as a possible cause. Recently, Drummond [35] examined several different composites and observed that fracture occurred through the resin matrix after 6 months of aging in air, distilled water, and a 50/50 (vol.%) ethanol/water mixture with the exception of a fiber-matrix composite, in which crack propagated along the fiber/matrix interface.

3.3.2.4 Effects of microstructure and filler content

In general, an increase in filler content increases the fracture toughness of the composite [62]. Resin composites with higher filler content, e.g hybrid composites, have higher fracture toughness compared to microfilled composites [54, 70, 75]. When compared with unfilled resin, the fracture toughness values for hybrid composites are typically almost 30-50% higher [62, 63]. Increases in fracture toughness have been attributed to an increase in fracture energy due to crack pinning at, and crack bowing between, particles. Rodrigues *et al.* [64] suggested that the increase in the toughness was due to the presence of round-shape filler particles which promoted toughening by the formation of microcracks that reduced stress concentration at the crack tip. Conversely, Bonilla *et al.* [8] found a very weak correlation between filler volume and fracture toughness when tested dry. They associated that finding with a difference in resin composition, filler size, and distribution of the filler particles compared to other studies.

Toughening offered by particulate reinforced composites is suggested to be less than for fiber-reinforced composites where fiber pull-out and other toughening mechanisms are important. Also, interfacial bond strength plays a more significant role in relatively higher aspect ratio, e.g. fiber, filler reinforced composites [55]. A different design was proposed by Xu *et al.* [76] who showed that continuous glass fiber preforms are more effective in improving toughness of composites without undergoing considerable hydrolytic degradation.

A fracture toughness study on nanofill composites [77] showed that nanoparticle reinforced composites have 2-3 times higher toughness than that of the matrix alone. Those authors identified crack deflection and interfacial crack growth mechanisms in the nanofill resin composites and stated that the increase in the nanofill composite fracture toughness originated from the improved interfacial toughness, which in turn resulted from the silanization treatment of the nanofiller particles. Computational modeling also has revealed the importance of the interface in accurately predicting the mechanical properties of the polymer composite, particularly when the reinforcement is in the form of well dispersed nanoparticles with high surface area to volume ratios [78].

3.3.2.5 Elastic modulus

Various conflicting results, as observed for strength and toughness, are also found in the literature for the elastic modulus. In general, heavily filled direct restoration composites show higher elastic modulus than indirect composites [79]. Also, as water induced degradation is a time dependent process, considerable degree of variation in modulus has been observed depending upon the hydration time. Momoi and McCabe [80] reported an increase in the elastic modulus following water storage but Indrani *et al.* [69] reported a continuous decrease in the modulus for 2 weeks followed by plateau until 6 weeks due to plasticization of the matrix. Another study [81] also showed a decrease in the elastic modulus after 90 days of water storage.

3.3.3 Fatigue of resin composites

Posterior restorations in actual oral environments frequently experience fatigue fracture due to relatively weak but repetitive masticatory forces [82]. Higher fatigue resistance is commonly associated with higher fracture toughness, small inherent flaw size, and higher wear resistance [83]. Fatigue failures of dental restorations are usually apparent as wear, marginal fracture, delaminated coatings, and/or bulk fracture [84] and often the service-life of dental prostheses or restorations are best determined by evaluating the fatigue resistance. Usually, fatigue fracture originates from internal or external microflaws, produced during fabrication or processing of the composite, which grow subcritically, eventually leading to final fracture. Although other mechanical properties such as hardness, modulus, and wear resistance often increases with increases in the filler content [37], an optimum level of filler content, ~ 60-80 wt.%, is required for the best fatigue resistance of the resin composite [85].

The common phenomenological approach of measuring the fatigue behavior of dental restorative materials is the stress-life, or S/N, approach [86]. Based on this approach, Baran and coworkers showed no fatigue/endurance limits under cyclic loading conditions [84] for dental resin composites. Other than cyclic fatigue, contact fatigue is also measured to understand the wear processes in resin composites [87, 88]. Another widely employed method for the fatigue testing of dental composites is the staircase method [87, 89, 90]. In this method, the cyclic lifetime and initial stress level is pre-selected. If a specimen fails at a pre-selected stress level, then a lower stress is chosen and experiment is repeated. However, if the specimen survives pre-selected

cycles, then it is cycled at a higher stress level. One of the limitations of this method is that it is less conservative in assuming that the material has a fatigue limit. Also, the number of cycles is pre-determined and hence if it is set to low levels then the information related to changes in the fatigue mechanisms could be lost [84].

As with other properties, the particle/matrix interface plays a major role in governing the fatigue resistance. In well bonded particle matrix composites, matrix failure is generally observed as the maximum stresses exists in the matrix above and below the poles of the particles [91]. Aging in water or other solvents generally showed a reduction in the fatigue properties [92] by plasticization of the matrix or interfacial debonding. Weak fillers also can leach out and contribute to failures. Resin composites, when tested under dry conditions, have shown evidence of stick-slip crack propagation behavior, but when tested under wet conditions interfacial degradation generated stable-slow crack growth behavior has been observed [84, 93].

Baran *et al.* [84] suggested that fracture characteristics of the resin composites are better understood by studying slow-crack growth mechanisms, i.e. using the damage tolerant approach. Relatively few studies [82, 94-97] have measured the fatigue crack growth resistance of dental composites using the fracture mechanics based approach and limited data are available to date. Generally, three different regions are identified in the fatigue crack growth curve, as shown in Fig. 2. Region I is characterized by a rapid acceleration in fatigue crack growth following the onset of crack extension. Region II is where the crack grows more slowly, while region III is characterized by a

rapid acceleration in crack propagation, usually leading to unstable fracture. The mid growth region II is best described using the Paris power law [98] expression:

$$\frac{da}{dN} = C(\Delta K)^m \quad \textbf{(1),}$$

where, $\Delta K = K_{max}$-K_{min}, maximum and minimum stress intensities respectively. The m and C are scaling constants. Scaling constant, m, varies between 2-4 for ductile materials like metals but it goes as high as > 100 for some highly brittle ceramic materials.

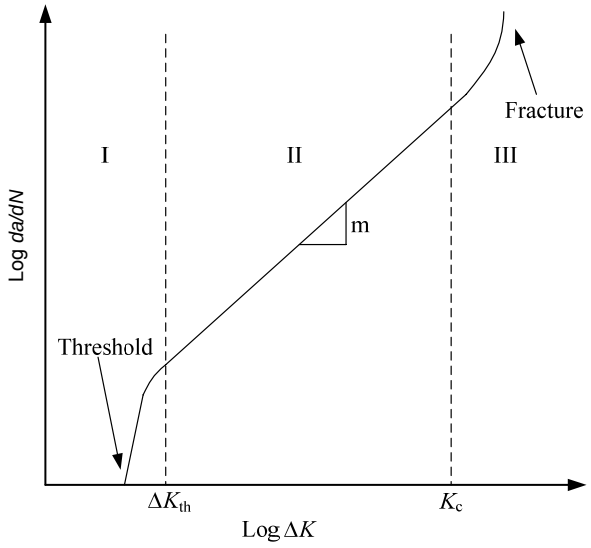

Fig. 2. Sigmoidal curve showing three different regions of fatigue crack growth illustrating the fatigue threshold, ΔK_{th}, and scaling constant, m [98].

Different fatigue crack growth behavior has been observed when a resin composite was either water hydrated for long-term or tested in wet conditions without prior

aging. Long-term hydration deteriorated the fatigue resistance whereas improved fatigue resistance was observed when unaged composites were tested under wet conditions [95]. Kawakami *et al.* reported lower fatigue threshold values, ΔK_{th}, for composites with organic fillers compared to inorganic suggesting limited effectiveness of the former in retarding crack propagation behavior [82] irrespective of the environmental conditions. In general, the collective results indicate that the filler-matrix interface plays a critical role in governing the fatigue resistance of resin composites.

Finally, when a dentin/resin bi-layer composite bonded using an adhesive resin bonding agent was fatigue tested, the dentin/resin adhesive interface showed the lowest fatigue crack growth resistance when compared to the composite or dentin, while dentin showed the highest fatigue crack growth resistance [97].

3.3.4 Effect of post-curing heat treatment

One limitation of direct resin composites when placed in the posterior restorations is polymerization shrinkage stress induced failures [12]. To overcome such limitations, resin composite inlays were introduced which utilize heat curing following the initial light-curing to achieve improved physical and mechanical properties. Post curing has been reported to increase wear resistance, marginal integrity, post-operative sensitivity, tensile strength, hardness, abrasion resistance, flexural strength, elastic modulus, and fracture toughness [13, 45]. Post cure heat treatment also offers the

advantage of improving the biocompatibility of the resin composite through the reduction of leachable, unreacted monomer in the polymer resin matrix [99].

Post curing is carried out in an oven usually above the glass transition temperature of the matrix, e.g., 100 to 120 °C for typical dimethacrylate based resins. For the post-curing time, it has been shown that as low as 10 min of heating is as effective as 3 hr in improving the properties of the composite [74]. Delay time, which is a time between initial light curing and post heat treatment, showed no influence in governing the properties of the composite.

Fractography has showed greater filler/matrix adhesion and filler fracture following post-curing treatment which was attributed to matrix toughening. An increase in the degree of cure due to enhanced cross-linking was found to be the primary reason for the property improvements [74, 100]. Other possibilities include increased mobility of the free radicals that formed during irradiation [100]. However, when the resin composites were aged in water for 30 days after post-curing [45], degradation of fracture toughness, flexural modulus, and flexural strength were observed, suggesting that the improvement in properties after post-cure heat treatment may only be short-term.

De Gee *et al.* [101] studied the influence of the post-cure heat treatment on the wear resistance of a composite and reported that homogenous distribution of shrinkage stresses around the filler particle was primarily responsible for the post anneal

improvement. Their study did not support improved degree of polymerization as a cause for increasing the wear resistance of the composite.

3.4 Fracture resistance curve *(R*-curve) behavior

In brittle materials like ceramics and some composites where the innate low toughness is a major drawback [102], microstructural alteration is found to be the most efficient way in improving such properties. The contribution of such microstructural modifications in improving the inherent fracture resistance, or toughness, of the material can be measured using the fracture resistance-curve (*R*-curve) method. *R*-curves measure the increase in the toughness of a material with crack extension and the presence of a rising *R*-curve affects unstable as well as sub-critical crack propagation. Although fracture behavior in terms of *R*-curves has been studied considerably for brittle materials like ceramics for the past 30 years [103], dental composite materials still remain unexplored in terms of their *R*-curve behavior.

3.4.1 Stable and unstable crack growth

In materials exhibiting *R*-curve behavior, crack extension occurs when the applied driving stress intensity, K_{app}, is equal to the crack growth resistance, K_R. Applied stress intensity, K_{app}, is similar to the strain energy release rate, G, in that they both govern crack extension and their relationship is given by [98]:

$$G = \frac{K_{app}^{\ 2}}{E} \quad \textbf{(2),}$$

where E is the modulus of elasticity. While K_{app} is a function of the applied load, crack size, shape, and specimen geometry, K_R, depends on the material toughening mechanisms and the formation of a process/bridging zone during crack propagation [104]. The crack growth can be stable or unstable. Conditions for the stable crack growth are given by:

$$K_{app} = K_R \text{ and } \frac{dK_{app}}{da} < \frac{dK_R}{da} \quad \textbf{(3),}$$

and unstable crack growth occurs when

$$K_{app} = K_R \text{ and } \frac{dK_{app}}{da} \geq \frac{dK_R}{da} \quad \textbf{(4)}$$

In general, material behavior can be categorized in terms of two types of *R*-curves:

1) Flat *R*-curve

When fracture resistance doesn't increase with crack extension, unstable fracture occurs always at a single value of K, resulting in a flat R-curve. As shown in Fig. 3a, when the applied stress is σ_1 the crack is stable but when the stress increases to σ_2,

crack propagation becomes unstable because material resistance doesn't increase with the increase in the applied stress intensity. Hence, the fracture resistance for a material with a flat *R*-curve is usually characterized in terms of a single toughness value, K_{Ic}.

2) Rising *R*-curve

A rising *R*-curve is achieved when the fracture resistance of the material increases with crack extension. Crack is stable until the applied stress intensity curve is tangential to the *R*-curve and $\sigma_1 < \sigma_{fracture}$, as shown in Fig.3b. The condition of tangency indicates the equilibrium state and defines the strength of the material. Unstable fracture, where $\sigma_2 = \sigma_{fracture}$, occurs thereafter as the rate of change of the applied stress intensity equals or exceeds the slope of the *R*-curve [105]. Hence, crack growth toughness is best expressed by taking the slope of the rising *R*-curve.

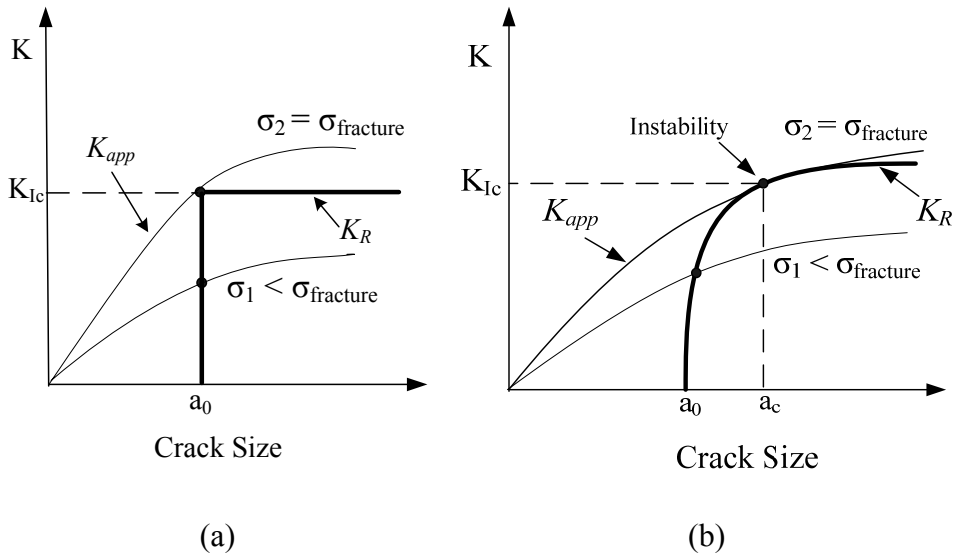

Fig. 3. Applied stress intensity, K_{app} and fracture resistance, K_R, as a function of crack extension for (a) flat *R*-curve and (b) rising *R*-curve.

When the material behavior is characterized by a rising *R*-curve, the condition of tangency depends on the shape of the *R*-curve, which in turn is governed by both the intrinsic material properties and the geometrical configuration of the material. Thus, the fracture behavior cannot be determined by a single toughness value [101]. Though shape of the *R*-curve influences the crack growth toughness and strength, the crack initiation toughness is usually considered an intrinsic property of the material. The crack initiation toughness at the onset of crack growth, i.e. $\Delta a = 0$, is difficult to determine experimentally from fracture experiments and generally measured using a separate experimental technique.

Rising *R*-curve behavior is also common for ductile metals where the plastic zone size increases with the crack extension. However, when unstable crack propagation by cleavage fracture occurs and the plastic deformation is almost completely suppressed due to high strain rates, the material might show falling *R*-curve behavior [98].

The *R*-curve is usually affected by the size and shape of the cracked body. For example, shape of the *R*-curve sometimes depends on the stress triaxiality at the crack tip. In case of a thin sample, it tends to give steeper *R*-curve due to lower degree of triaxiality at the crack tip.

R-curve behavior for brittle materials is most commonly measured by quantifying the *G* or *K* value to cause crack extension while also measuring the crack length. The crack length may be measured either optically, by compliance methods, or by the

electric potential drop method. The origins of the *R*-curve behavior are best understood by examining the toughening mechanisms.

3.5 Toughening mechanisms

In general, toughening mechanisms are characterized into two classes:

- Intrinsic toughening mechanisms, and
- Extrinsic toughening mechanisms.

3.5.1 Intrinsic toughening mechanisms

Critical and subcritical crack extension is generally governed by the mutual competition between intrinsic (damage) and extrinsic (shielding) mechanisms, as is illustrated in Fig. 4. Intrinsic mechanisms are related to the inherent resistance of the material to microstructural damage and cracking. Intrinsic mechanisms generally occur *ahead* of the crack-tip [102, 103] by controlling the driving forces, e.g. stress intensity, to cause crack extension under monotonic loading.

Ductile materials like metals are usually intrinsically toughened by formation of a plastic deformation zone. Such materials usually fail by cleavage, intergranular cracking, or microvoid coalescence. In the case of cyclic loading conditions, intrinsic mechanisms are characterized by blunting and resharpening of the crack tip. In the

case of brittle materials like glass and ceramic, any efforts to improve the intrinsic toughness by promoting crack-tip plasticity have had little or no success [103].

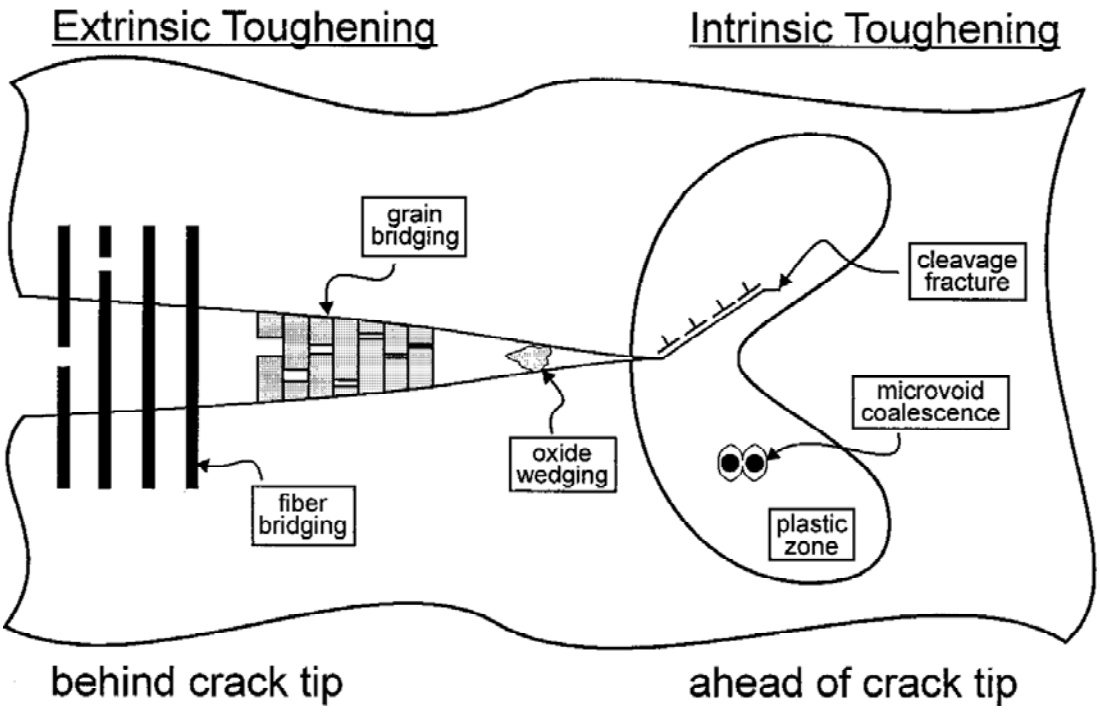

Fig. 4. Examples of intrinsic (damage) and extrinsic (crack-tip shielding) toughening mechanisms [103].

3.5.2 Extrinsic toughening mechanisms

In brittle materials that have limited or almost no ductility, extrinsic toughening mechanisms are far more important in improving the crack growth resistance. These mechanisms generally act in the crack wake and promote crack-tip shielding by reducing the applied stress intensity experienced at the crack tip by mechanical, microstructural, or environmental factors [106]. Some extrinsic toughening

mechanisms produce inelastic deformation in the material and a non-linear stress-strain relationship. Crack-wake mechanisms are dependent upon the size of the crack when crack extension causes a more substantial shielding zone in the crack wake. Initially a crack growth commences at the crack initiation toughness, K_0, but higher stress intensities are required to further the crack extension until sometimes a "plateau", or steady state, toughness is reached. Rising *R*-curve behavior is a direct consequence of the extrinsic toughening mechanisms [107, 108] that cause a crack size dependence of the toughness.

Extrinsic toughening mechanisms involve the formation of either a process zone or bridging zone. Process zones involve transformation toughening, microcracking, or twin toughening whereas bridging zones are usually governed by the presence of ductile particles, fibers, whiskers, or grain/particle reinforcements.

Rising *R*-curve behavior has been observed in ceramics, metals, intermetallics [109], composites [110, 111], and biomaterials like bone [107, 108, 112] and dentin [113, 114] where extrinsic mechanisms have been reported to be responsible for the rising toughness with crack extension. Extrinsic mechanisms are commonly determined by the microscopic examination of the microstructure-crack path interactions. The following section discusses some of the important extrinsic toughening mechanisms.

3.5.2.1 Crack deflection

In composites and reinforced ceramics, crack deflection around second phases or reinforcing fillers can provide significant toughening. Optimum separation between reinforcements is one key to gaining crack deflection benefits. In addition, the geometrical shape of the second phases or fillers can make considerable differences in imparting toughening. For example, rod like particles rather than spherical particles can induce higher angle crack deflections and also promote crack bridging as an additional toughening mechanism. This is because twist deflections around rod shape particles are more effective at lowering the stress intensity at the crack tip than tilt deflections caused by spherical or discs shape particles due to the higher aspect ratio achieved by the rod shape [105].

3.5.2.2 Microcrack toughening

Microcrack toughening is categorized as process zone shielding [105]. For this mechanism, a diffused zone of microcracks forms ahead of the crack tip and extends as the crack propagates, leaving a microcracked zone in the crack wake. If the microcracking zone size is constant from the onset of crack extension, no rising *R*-curve behavior is observed. Rising *R*-curve only obtained when the zone expands with the crack extension [115]. Crack-tip shielding achieved from the microcracking mechanism depends largely on the size and shape of the process zone.

Microcracks are formed in materials with high residual stresses and low fracture energy interfaces [106]. If the volume expansion resulting from the formation of microcrack damage zone is constrained by the surrounding material [116], the crack tip experiences compressive forces from the surrounding material which contributes to increasing the toughness of the material. Reduction in the modulus within the microcrack process zone can also contribute in improving the toughness of the composite. On the contrary, when large number of microcracks connect to the main crack, contributing to crack advancement, it adversely affects the toughness of the material. Toughening contributions from microcracks are usually small since the formation of large volumes of microcracks reduces the intrinsic toughness of the material. So, significant toughness improvement from microcracking is only achieved when extrinsic toughening contribution is much higher than the reduction in the intrinsic toughness, such is the case of multiphase ceramic materials with high internal residual stresses [117]. So, toughening from microcrack formation is realized mainly when it leads to bridges behind the crack tip, as will be described in section 3.5.2.4.

3.5.2.3 Transformation toughening

Transformation toughening is another example of process zone shielding which is dominated by a volume increase around the crack tip. In transformation toughened zirconia, an in-situ phase transformation from tetragonal to monoclinic martensite occurs ahead of the crack tip. This dilatant transformation results in the formation of a inelastic deformation zone in the crack wake imparting closing tractions on the crack

surfaces, leading to reduced stress field ahead of the crack tip [103]. Other than martensitic transformations, ferroelastic transformations and twinning are also examples of transformation toughening. Martensitic transformations have both dilatational and shear stress components whereas twinning has only a shear stress component that induces transformation [106].

Y-TZP (yttria-tetragonal-zirconia polycrystals) is used in biomedical applications such as dental ceramics and hip implants due to its stress induced transformation toughening mechanism. Y-TZP has applications in all-ceramic inlays, crowns, bridges, and partial dentures primarily because of its high strength, toughness, [66] and damage tolerance [118] compared to other dental ceramics.

3.5.2.4 Crack bridging

In many ceramic and composite materials, crack bridging leads to rising *R*-curve behavior as shown in Fig. 5. In absence of crack bridging or similar extrinsic toughening mechanisms, a material will fail at the crack initiation toughness, K_0, giving single value fracture toughness, K_{Ic}, and a flat *R*-curve.

Crack bridging reduces the driving forces, e.g. the stress intensity, at the crack tip by formation of intact elastic regions or frictionally loaded bridges in the crack wake, as depicted in Fig. 6. Such crack bridges promote crack tip shielding by sustaining some of the applied load [114]. This phenomenon results in increasing crack growth

resistance with crack extension under monotonic increasing loading conditions. In many grain bridging ceramics, the size of the bridging region in the crack wake was found to be similar to the crack extension required to reach the steady state *R*-curve toughness. This is usually on the scale of a few tens of micrometers up to many millimeters [119].

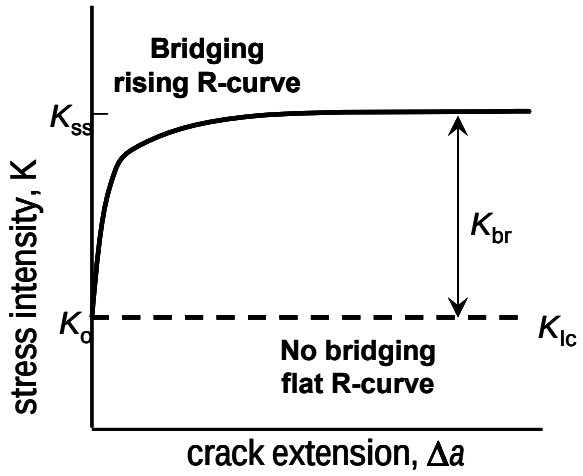

Fig. 5. Contribution of crack bridging and rising *R*-curve behavior.

In bridging materials, the applied stress intensity, K_{app}, is equal to sum of the bridging stress intensity, K_{br}, and near-tip stress intensity, K_{tip}, and accordingly, K_{tip} may be expressed as,

$$\boldsymbol{K_{tip} = K_{app} - K_{br}} \quad \textbf{(5)}$$

In brittle materials, formation of bridging requires either microstructural residual stresses, weak interfaces, or both. Residual stresses are often produced from thermal

expansion mismatch between grains or phases. This suppresses local crack propagation, leading to the formation of intact regions behind the crack tip. In the case of weak interfaces, crack deflection occurs along low fracture energy interfaces that may lead to formation of intact regions in the crack wake. A micromechanical model was recently used to gain insight into the formation of crack bridges [120] which reinforces the initial concepts given by Evans [106]. According to this 2-D model, depending on the orientation and aspect ratio of the grain/particle with respect to the crack, either complete debonding occurs leading to frictional pull-out or a new crack nucleates ahead of the primary crack due to crack arrest induced stress concentration, creating an uncracked bridge. Alternatively, in 3-D the crack may bifurcate around the particle at the arrest point, and then join ahead to form a crack bridge. According to the 2-D model of the Foulk *et al.*, a considerable increase in the fracture resistance is achieved even before the bridge has formed due to the crack deflection and arrest process [120].

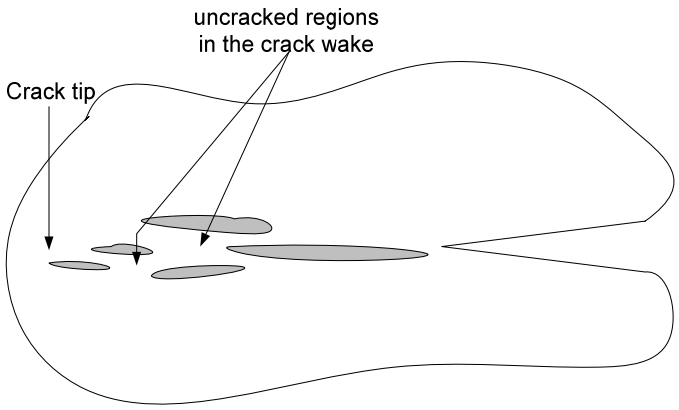

Fig. 6. Schematic showing crack bridging by uncracked regions in the crack wake sustaining some of the applied load thus promoting crack-tip shielding.

In general, a rapidly rising *R*-curve and high toughness can be obtained by enhancing the number of bridging reinforcements, and the length of the debonded interfaces [121]. In grain bridging ceramics, uniform dispersion of large elongated grains in a fine sub-micrometer grain sized matrix have been shown to be very important in improving the fracture resistance. This promotes steeply rising *R*-curves and higher fracture strengths [121]. For interfacial debonding, it has been shown that there is a small window for optimal boundary adhesion [122, 123]. If the boundaries are too strong, transgranular fracture occurs with no bridging and no toughening. However, if the boundaries are too weak the toughness rises very slowly giving lower strength and fatigue resistance.

Crack bridging has been observed in metals, ceramics [124], intermetallics, fiber/whisker reinforced and layer composite materials [125, 126], and biomaterials such as dentin and bone [107, 114, 127].

4 MANUSCRIPT I: *R*-CURVE BEHAVIOR AND MICROMECHANISMS OF FRACTURE IN RESIN BASED DENTAL RESTORATIVE COMPOSITES

M. B. Shah[a], J. L. Ferracane[b] and J. J. Kruzic[a 1]

[a] Materials Science, School of Mechanical, Industrial, and Manufacturing Engineering, Oregon State University, Corvallis, OR 97331, USA

[b] Division of Biomaterials & Biomechanics, School of Dentistry, Oregon Health & Science University, Portland, OR 97239, USA

Submitted to

Journal of Mechanical Behavior of Biomedical Materials

September 2008

---

[1] Corresponding author. Tel: +1-541-737-7027; fax: +1-541-737-2600.

E-mail address: jamie.kruzic@oregonstate.edu (J. J. Kruzic)

ABSTRACT

The fracture properties and micromechanisms of fracture for two commercial dental composites, one microhybrid (Filtek™ Z250) and one nanofill (Filtek™ Supreme Plus), were studied by measuring fracture resistance curves (*R*-curves) using pre-cracked compact-tension specimens and by conducting both unnotched and double notched four point beam bending experiments. Four point bending experiments showed about 20% higher mean flexural strength of the microhybrid composite compared to the nanofill. Rising fracture resistance was observed over ~ 1mm of crack extension for both composites and higher overall fracture resistance was observed for the microhybrid composite. Such fracture behavior was attributed to crack deflection and crack bridging toughening mechanisms that developed with crack extension, causing the toughness to increase. Despite the lower strength and toughness of the nanofill composite, based on micromechanics observations, the large nanoparticle clusters appear to be as effective at deflecting cracks and imparting toughening as the solid particles of the microhybrid. Thus, with further microstructural refinement, it should be possible to achieve a superior combination of aesthetic and mechanical performance using the nanocluster approach for dental composites.

KEYWORDS: Dental Composite; Fracture; *R*-curve; Crack Bridging; Flexural Strength

4.1 Introduction

In the past few decades, one notable transition in the dental restorative field is the widespread usage of resin based composites as an alternative to traditional amalgam for direct restoration of tooth structure. Key driving forces behind the increased use of composite materials are 1) their tooth-like appearance [128] and 2) their lack of the potentially toxic element mercury that is present in amalgam [129, 130]. Additional clinical advantages include minimal removal of native tooth structure [131], the ability to be bonded to enamel and dentin surfaces [6], convenient handling, and the ready availability of a wide range of tooth shades.

Despite the above mentioned advantages, there are some disadvantages associated with restorative composites that are recognized as a concern among dental researchers and practitioners. Polymerization shrinkage is one issue which can lead to marginal leakage of the oral fluid between the cavity walls and restoration and allow secondary caries to form, requiring subsequent retreatment of the tooth [132]. Low fracture resistance is another concern which can lead to chipping and/or bulk fracture of the restorations [5, 58, 133]. Fractures of restorations are most common in high stress bearing posterior locations [8]. As fracture is the second leading cause of restorative failures to secondary caries [4], understanding the fracture mechanisms and how they relate to the structural performance are important for the continued use and improvement of resin based composites as dental restorative materials.

Until recently, change in filler technology has been the main approach for improving the properties and performance of resin based dental composite materials [9, 63]. The overall mechanical properties have remained relatively unchanged over the years, possibly because a complete understanding of the fracture and toughening mechanisms in these materials is still lacking. Accordingly, the purpose of this study is to investigate both qualitatively and quantitatively the salient fracture and toughening mechanisms in two commercially available resin based dental composite materials. Specific attention is paid to the influence of microstructure in governing the fracture behavior.

4.2 Background

The mode I fracture toughness, K_{Ic}, is a material property that measures the resistance to catastrophic or critical failure in terms of the stress intensity, K.[2] While the use of K_{Ic} as a single-value measure of the toughness is appropriate for many materials, such as engineering metal alloys and ideally brittle ceramics, in some materials the fracture resistance actually increases with crack extension, promoting stable crack growth and requiring a fracture resistance-curve (*R*-curve) approach [98, 105] Specifically, *R*-curves are necessary to describe the fracture resistance of materials toughened by

---

[2] The stress-intensity factor, K, is a global parameter which fully characterizes the local stress and deformation fields in the immediate vicinity of a crack tip in a linear-elastic solid, and thus can be used to correlate with the extent of crack advance. It is defined for a crack of length a as $K = Y\sigma_{app}(\pi a)^{1/2}$, where σ_{app} is the applied stress and Y is a geometry factor of the order of unity [98].

crack-tip shielding [106, 115, 122], i.e., by extrinsic toughening mechanisms such as crack bridging or in-situ phase transformations. Such mechanisms act to lower the stress intensity experienced locally at the crack tip, K_{tip}, thereby "shielding" the crack from some of the applied load. Furthermore, these mechanisms develop as the crack extends, giving the observed increase in fracture resistance. In such instances, crack extension commences at a *crack-initiation toughness*, K_0, while sustaining further crack extension requires higher driving forces until sometimes a "plateau" or steady-state toughness, K_{ss}, is reached.

Such rising *R*-curve behavior is not uncommon among dental materials; indeed, certain dental ceramics [134] and natural tooth dentin [114] both show increasing fracture resistance with crack extension, or rising *R*-curve behavior. Furthermore, extrinsic toughening mechanisms and rising *R*-curve behavior are very common in composite materials [110, 111], so it can be expected that such behavior may be found in resin based dental restorative composites as well. Accordingly, this study utilizes an *R*-curve approach to characterize the fracture behavior of two dental composites. Additionally, attention is paid to also assess the specific toughening mechanisms responsible for the rising *R*-curve behavior, as well as the role of microstructure in promoting those mechanisms.

4.3 Materials and methods

4.3.1 Materials

Two commercially available particle reinforced resin based dental restorative composites, Filtek™ Z250 and Filtek™ Supreme Plus (3M™ ESPE™, St Paul, MN, USA), were investigated in this study. The compositions and the curing times used are listed in Table III. It should be noted that both microstructures have a mixture of large and small filler particles, but in the case of the nanofill the large particles are actually clusters of smaller nanoparticles rather than solid particles.

Table III Composition and light-curing times for the commercial resin based dental composites

Brand name	Composite	Matrix	Filler	Shade	Curing time (sec)
Filtek Z250™ Universal Restorative	Microhybrid	Bis-GMA[a], Bis-EMA[b] UDMA[c], and TEGDMA[d]	0.01 to 3.5 μm, average 0.6 μm, zirconia/silica (60 % by volume)	A2	80
Filtek Supreme Plus™ Universal Restorative	Nanofill	Bis-GMA, Bis-EMA, UDMA and TEGDMA	20 nm silica and zirconia/silica clusters of 0.6 to 1.4 μm with individual particle size of 5-20 nm (59.5 % by volume)	A2B	80

[a] Bis-GMA, bisphenol A-glycidyl dimethacrylate, [b] Bis-EMA, bisphenol A ethoxylate dimethacrylate

[c] UDMA, urethane dimethacrylate, [d] TEGDMA, triethyleneglycoldimethacrylate

4.3.2 Specimen preparation

Compact-Tension, C(T), specimens of microhybrid and nanofill composites were prepared for fracture resistance curve (*R*-curve) testing using an aluminum split mold. The mold was filled with uncured composite and both the top and bottom surfaces were covered with polyester strips that were pressed flat against each side of the mold to remove excess material and provide uniform sample thickness. The composite was then illuminated for total of 80 sec (40 sec each on top and bottom surfaces) using a visible light curing unit (Triad II, Dentsply International, York Division, PA). After removing the sample from the mold, pin holes were machined (Bridgport Mill, Elmira, NY) using a conventional end mill and notching was performed using a high precision slot cutter. The final sample had a nominal width W of ~ 14 mm, thickness B of 2 ± 0.5 mm and initial notch length a_0 of 3.5 ± 0.2 mm. The sample surfaces were then ground and mirror polished up to a 0.05 μm finish using alumina suspensions followed by Buehler™ MasterPolish for a finishing step. A micro notch was then introduced by repeatedly sliding a razor blade over the machined notch in the presence of 1 μm diamond slurry using a custom built razor micronotching machine. This process was continued until a sharp pre-crack initiated and grew from the micronotch, as shown in Fig. 7a and b.

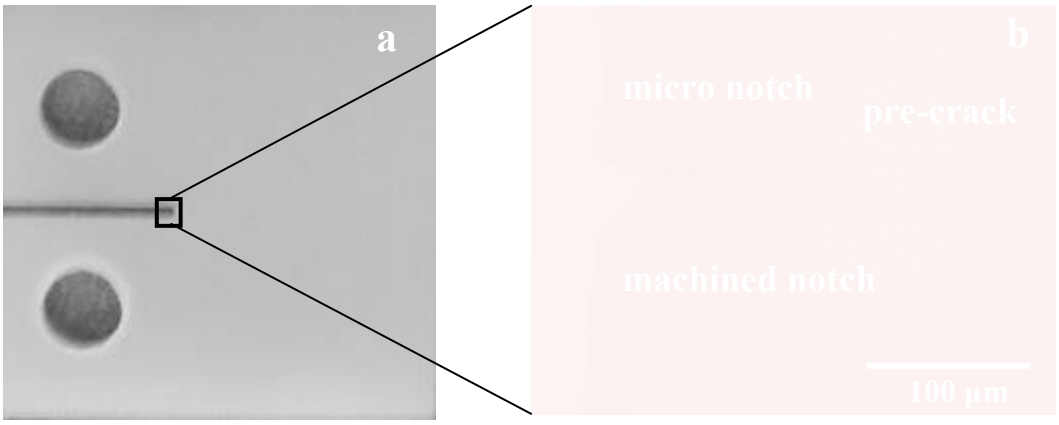

Fig. 7. Compact-tension, C(T), specimen showing (a) machined holes and notch and (b) localized view of micronotch and pre-crack emanating from the machined notch.

Both unnotched (25 x 2 x 2 mm^3) and double notched (33 x 3 x 2 mm^3) rectangular bar shaped specimens were also produced for beam bending experiments using the same procedures. The double notched specimens were molded with two identical notches, each separated by 5 mm with a width and depth of 400 μm and 600 μm, respectively (Fig. 8).

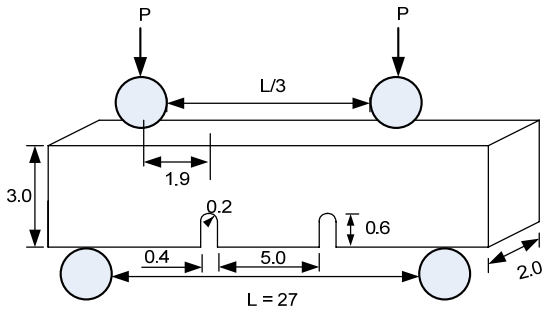

Fig. 8. Schematic diagram of a double notched four point bend specimen showing dimensions and loading configuration.

4.3.3 *R*-curve testing

R-curves measure the change in the fracture resistance, usually in terms of the stress intensity, K_R, or strain energy release rate, G_R, as a function of crack extension, Δa. *R*-curve experiments ($N = 3$ for each microstructure) were carried out using an Instron© 8501 servo-hydraulic testing machine. Additional samples beyond $N = 3$ were actually produced, but unstable fracture occurred prior to the successful measurement of the *R*-curve for some samples. The pre-cracked compact tension, C(T), specimens were monotonically loaded using manual displacement control until the onset of crack extension, which was determined by a sudden drop in the load. At this time, the sample was promptly unloaded by about 10-20% of the peak load to register the sample compliance at the new crack length. The sample was reloaded again and the loading-unloading sequence was repeated until the end of the test when the plateau of the *R*-curve was definitively reached. Load-point displacements were measured using a capacitance displacement gauge which was connected to the clevis grip fixture. After completion of the test, the crack length, a, at each unload was calculated using a load-point compliance calibration for the C(T) specimen geometry [135]. The standard fracture mechanics based solution for a compact tension specimen was used to determine the fracture resistance, K_R, at each crack length [136]. In addition, crack lengths were periodically measured by interrupting the test, removing the sample, and using optical microscopy. When necessary, compliance crack length data was then corrected for each test to reflect the actual measured crack lengths. Student's t-tests were used to compare differences in the steady state toughness values measured for the two composites ($p=0.05$).

4.3.4 Flexural strength testing

Flexural strength was measured at ambient temperature using a Bose/EnduraTEC ELF® 3200 mechanical testing machine using the unnotched bend beams (N = 12 for each microstructure) in four point bending. Samples were loaded in displacement control at a crosshead speed of 0.01 mm/sec with an inner span of 10 mm and an outer span of 20 mm. The flexural strength was calculated using simple beam theory and the student's t-test was used to compare any differences between the composites ($p=0.05$).

4.3.5 Double notched experiments

Double notched four point beam bending experiments (N = 12 for each microstructure) were performed to help qualitatively evaluate the fracture mechanisms. Testing was carried out at ambient temperature using a Bose/EnduraTEC ELF® 3200 mechanical testing machine. The samples were centered in the loading fixture (Fig. 8) and the notched bars were then monotonically loaded in bending using displacement control at a rate of 0.01 mm/sec until the sample fractured from one of the notches. The other notch was frozen at the onset of instability whereby the microstructural damage could subsequently be observed in the vicinity of the notch tip. Observation of the damage zone surrounding the unbroken notch tip showed the interaction of cracks with the underlying microstructural features.

4.3.6 Fracture and toughening mechanism characterization

After coating the samples with a Au-Pd alloy, fracture surfaces, unfractured C(T) samples, and the unfractured notches of the double notched samples were examined using a Zeiss Ultra scanning electron microscope (SEM) to identify the microstructural fracture and toughening mechanisms.

4.4 Results

Fig. 9 shows that the flexural strength results of the microhybrid composite (134.3 ± 10.9 MPa) was significantly higher than that of the nanofill composite (107.9 ± 17.2 MPa).

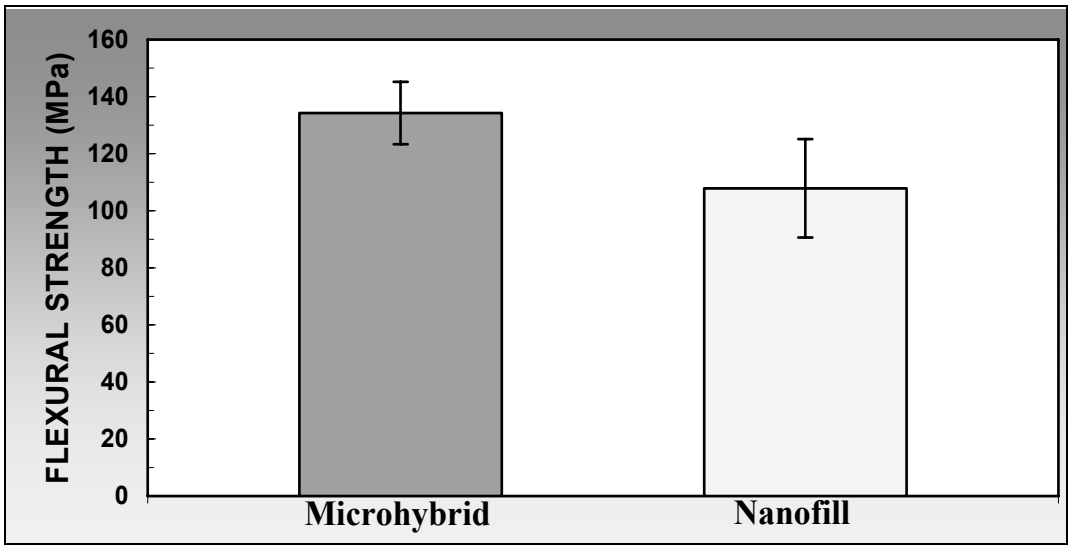

Fig. 9. Comparison of mean flexural strength of microhybrid and nanofill dental resin composite.

4.4.1 Resistance-curve (*R*-curve) behavior

A representative load-load point displacement curve for stable crack extension in the nanofill composite is shown in Fig. 10a. The microhybrid composite also showed similar load-displacement behavior. The resulting *R*-curves for the microhybrid and nanofill dental composites are shown in Fig. 10b. Solid filled symbols designate *R*-curve data for the microhybrid composite whereas crossed symbols designate the nanofill composite.

As the energy approach is often commonly used to describe fracture of materials, the *R*-curves were also converted to be in terms of the strain energy release rate, *G*. In Fig. 10b, the strain energy release rate, G_R, is shown on the right axis. This was calculated using the relation for plane strain conditions [98],

$$G_R = \frac{K_R^{\,2}}{E/(1-\upsilon^2)}, \qquad \textbf{(6),}$$

where E is the elastic modulus and ν is Poisson's ratio. Average E and ν values of 11 GPa and 0.33 were used to scale G_R estimates on the right axis of Fig. 10b based on the manufacturer and published reported values [137, 138].

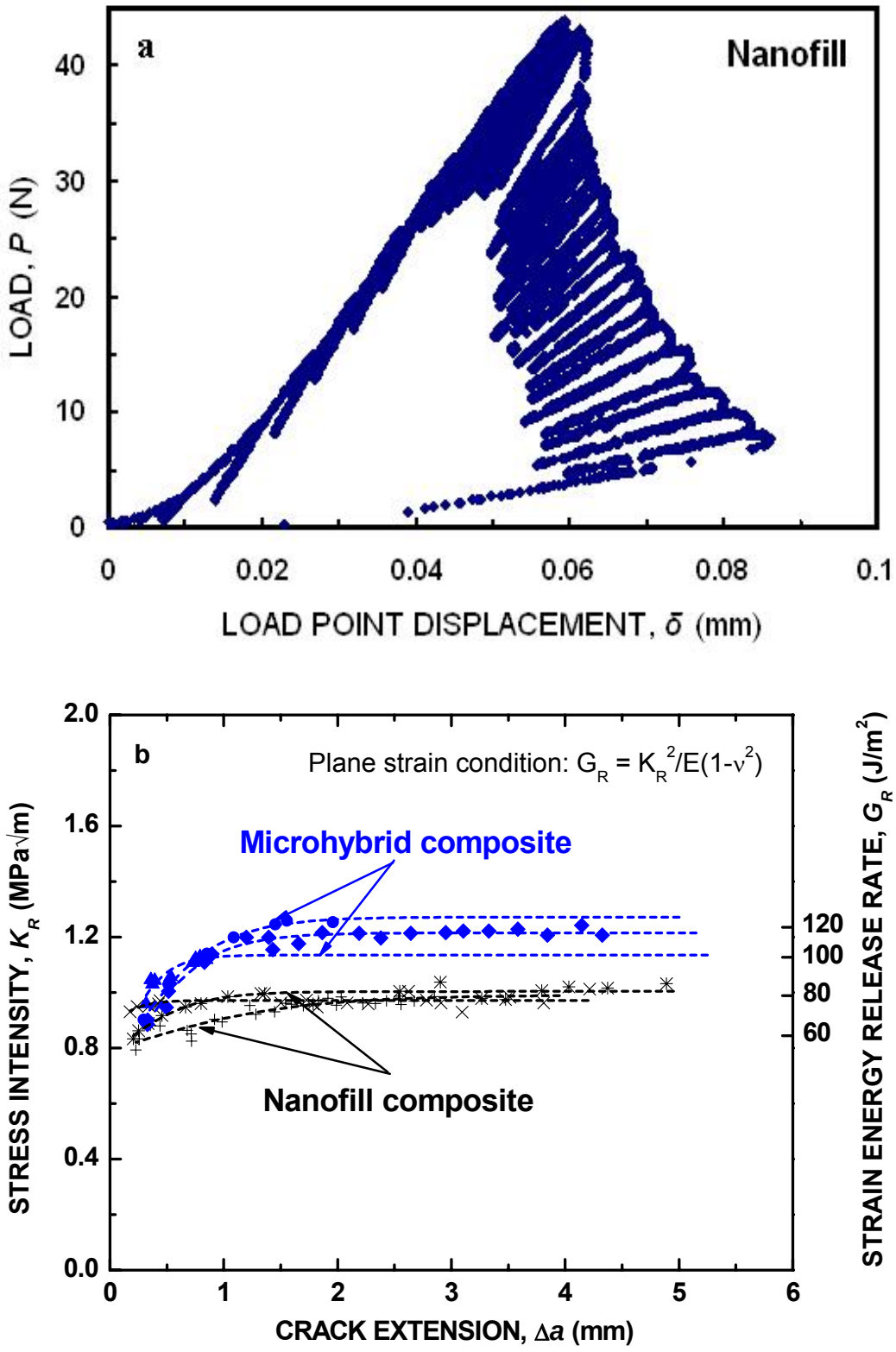

Fig. 10. (a) Representative load-load point displacement curve for stable crack extension in a nanofill dental composite sample. Both composites showed similar

load-displacement behavior. (b) Resistance-curve, $K_R(\Delta a)$, for microhybrid and nanofill dental composites. Note the *R*-curve for the microhybrid composite rises faster and higher in comparison to that of the nanofill composite. Also, estimates of G_R (Δa) are plotted on the secondary axis.

Comparing the data in Fig. 10b, it is generally necessary to make independent measures of the initiation toughness as extrapolating the data back to $\Delta a = 0$ is often unreliable [119, 122, 139]. Accordingly, at this time it is difficult to make any firm conclusions about differences in K_0 between the microstructures. However, after about a millimeter of crack extension, both composites showed a "plateau" region where toughness remained essentially constant with the crack extension. The steady state toughness, K_{ss}, was 1.21 ± 0.07 MPa√m and 0.99 ± 0.02 MPa√m for the microhybrid and nanofill composite, respectively. These differences in steady state or peak toughness were statistically significant ($p = 0.0059$).

4.4.2 Microstructural characterization and crack path interactions

R-curve and double notched bend experiments allowed for stable crack extension and hence made it possible to study the toughening mechanisms and the influence of microstructure on the fracture behavior. Fig. 11(a) and (b) shows SEM micrographs of crack propagation and interaction of crack with the microstructural features in the microhybrid and nanofill dental composites, respectively. It is evident that cracks propagate within the matrix along an interparticle (or intercluster) crack path in both microhybrid and nanofill composites. This interparticle crack growth influences the

fracture process by promoting crack deflection as a toughening mechanism in both resin based dental composites.

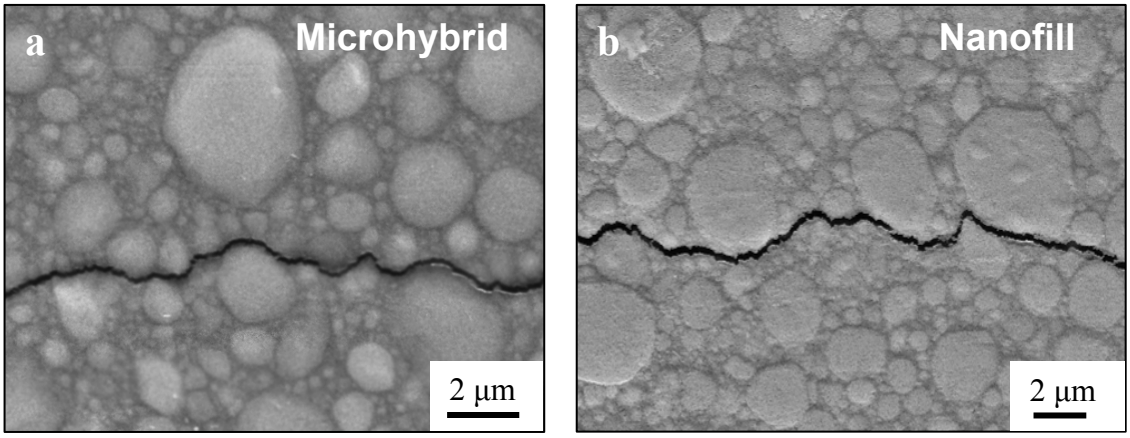

Fig. 11. SEM micrographs of the (a) microhybrid and (b) nanofill dental composite, showing the interactions of the crack path with salient microstructural features. It is apparent that both composites show interparticle crack growth which promotes crack deflection. The general direction of crack growth was from left to right.

Observations of localized crack tip zones revealed intact bridges spanning the wake of the crack in both composites (Fig. 12). These uncracked bridges sustain a portion of the load that would otherwise contribute to advancing the crack, thereby raising the fracture resistance of the material. Essentially, the crack bridging mechanism reduces the stress concentration experienced at the crack tip and hence acts as a source of extrinsic toughening. It is important to note that these bridges develop with the crack extension and thus give rising *R*-curve behavior.

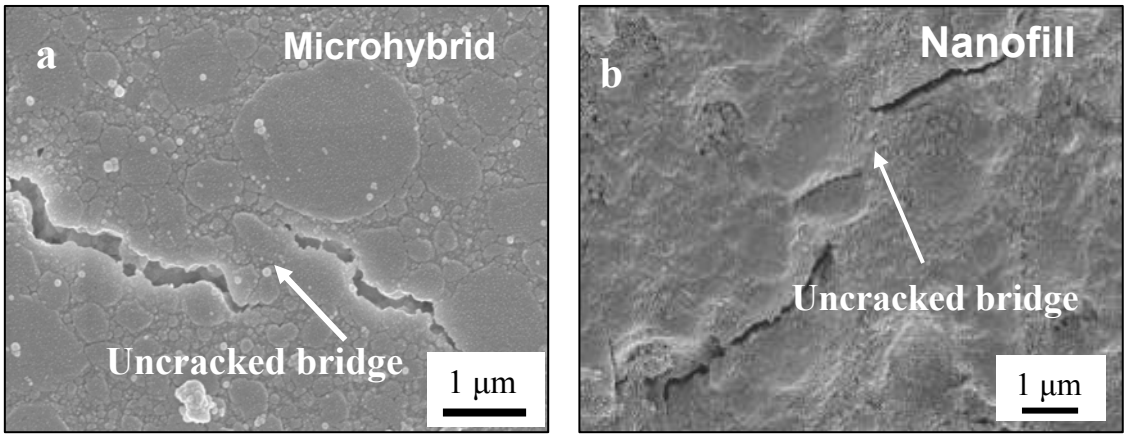

Fig. 12. SEM images showing the localized formation of intact regions behind the crack tip for (a) microhybrid and (b) nanofill dental resin composites. These uncracked bridges provide extrinsic toughening by shielding the crack tip from some of the applied load. The general direction of crack growth was left to right.

Examination of the fracture surfaces confirmed the predominantly interparticle crack path. Fig. 13a & b compares identically magnified SEM images of the two opposite surfaces of a fractured nanofill composite at the exact same fracture location. The fracture surfaces for the microhybrid composite were similar. In Fig. 13, examination of the morphology on both the fracture surfaces at the exact same position reveal the absence of cracking of the large clusters of nanoparticles, confirming what was seen on the sample surfaces in Figs. 11 & 12. Careful observation of the images shows that the clusters on one surface correspond to holes on the other surface and vice versa. Several such spots (1-5) are identified in Fig. 13, and close observation of many additional locations reveal the same behavior, confirming a predominantly interparticle crack growth mechanism. Higher magnification observations of both composites generally revealed the presence of matrix around and in-between the filler

particles indicating that crack propagation was predominantly through the matrix, as shown in Fig. 13c.

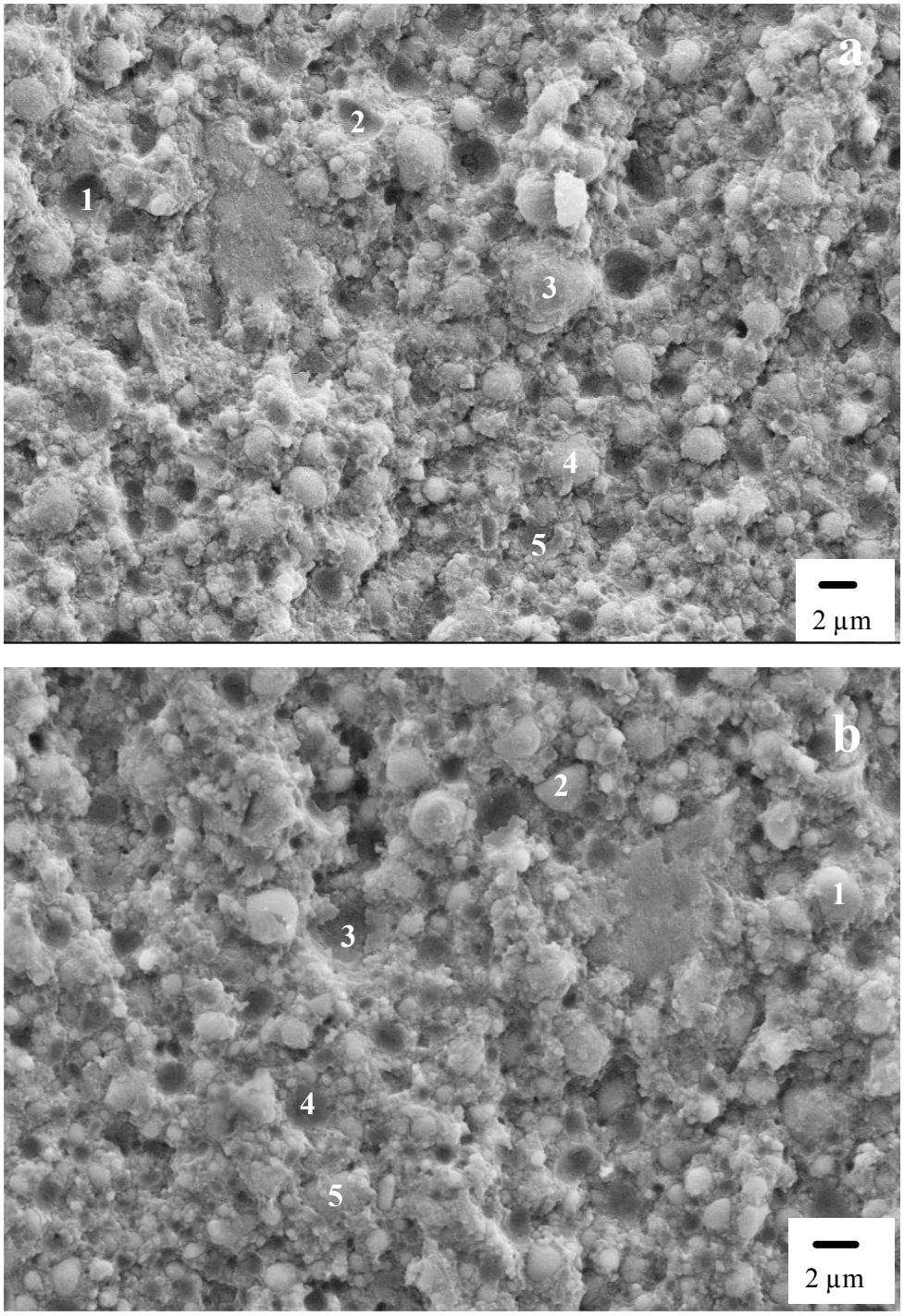

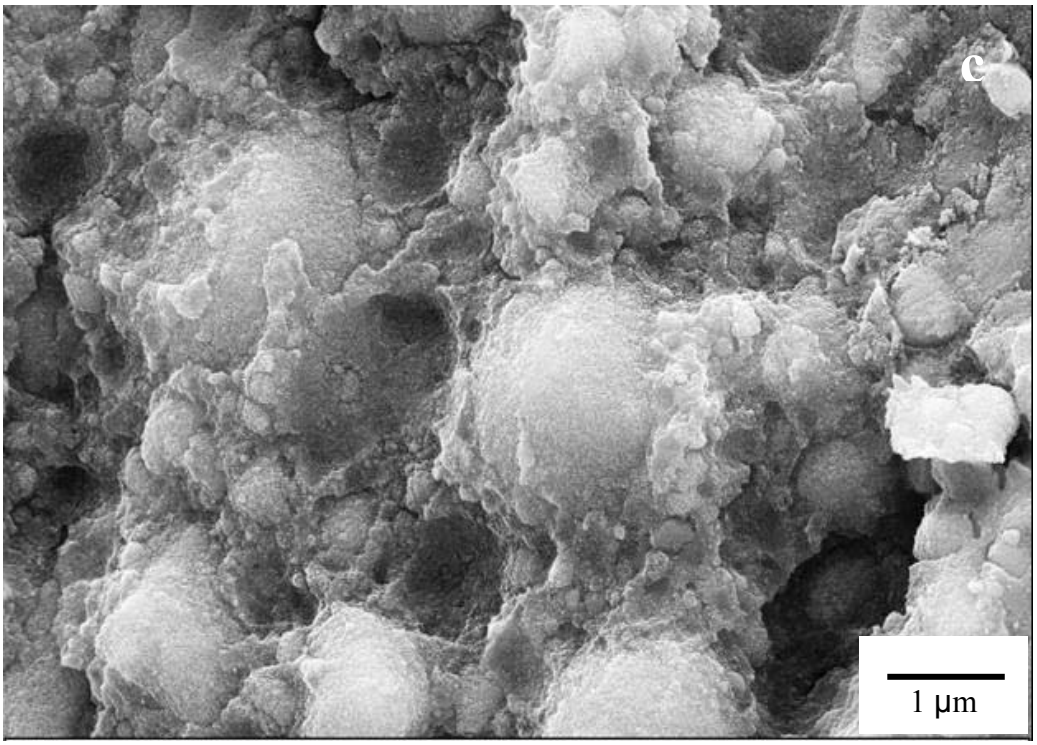

Fig. 13. SEM mirror images of nanofill composite showing identical locations (e.g. 1 to 5) on the two opposing fracture surfaces on a single specimen (a) and (b). Detailed observations of these surfaces revealed that a filler nanoparticle cluster on one surface corresponds to a hole on the other and vice versa, confirming an absence of cluster fracture. Higher magnification of a nanofill composite fracture surface in (c) reveals that interparticle crack growth was predominantly through the resin matrix. The microhybrid composite also showed similar fracture paths.

Finally, observations of fracture surfaces showed the presence of internal pores and inclusions (Fig. 14a and b respectively) on the fracture surfaces of both composites. Energy Dispersive X-ray Spectroscopy (EDS) analysis of 4-5 inclusion sites showed that silica was the major constituent. Such defects likely acted as fracture initiating sites during the flexure strength experiments.

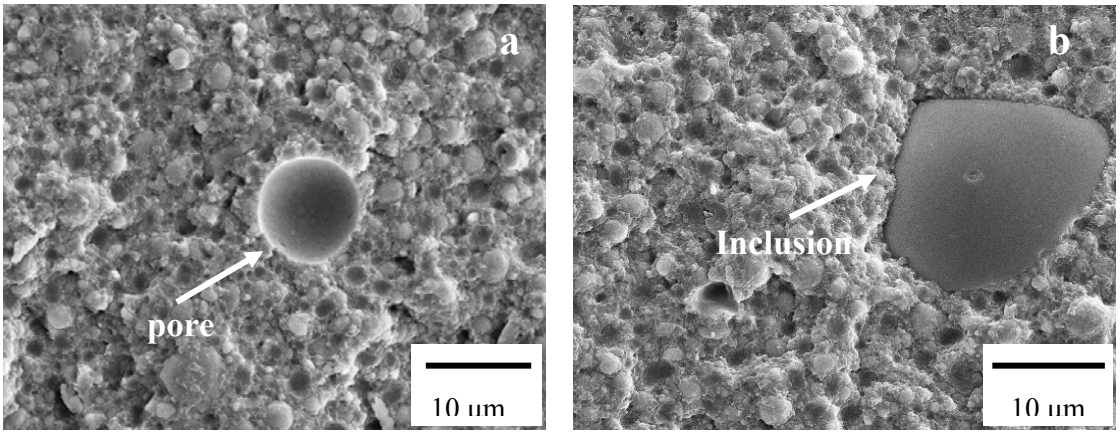

Fig. 14. Fracture surface defects of (a) internal pore and (b) inclusion in nanofill composite. Similar flaws have also been identified in microhybrid composite.

4.5 Discussion

4.5.1 Rising *R*-curve and role of extrinsic toughening mechanisms

A number of studies have measured the fracture toughness of the resin based composites in terms of a single toughness value, K_{Ic}, [6, 11, 55, 63, 69, 73], and also have identified the predominantly interparticle crack path [62, 77, 140]. Interparticle crack propagation through the matrix is indicative of good filler/matrix adhesion in both the composites [62, 141], who also observed interparticle matrix failure in dry dental composites, reasoned that compressive hoop stresses in the resin developed during polymerization shrinkage may be partially responsible for mechanically holding the filler particles in the matrix.

However, to the authors' knowledge, the present work is the first time that fracture resistance has been evaluated in terms of an *R*-curve for particle reinforced resin dental composites. Both the microhybrid and the nanofill dental composites exhibited rising *R*-curve behavior over roughly the first millimeter of crack growth. Rising *R*-curve behavior is a desirable mechanical effect, especially in brittle materials, as a portion of the crack growth toughness can contribute to greater flaw tolerance and higher strength.

This study also has identified two extrinsic toughening micromechanisms thought to be responsible for this effect, namely crack deflection and crack bridging, which are promoted by the interparticle crack path. Crack pinning and crack branching are two other toughening mechanisms that have been reported for polymer based composites [62, 140, 142]. Kim *et al*. reported these mechanisms for dental resin based composites that were reinforced with < 25% spherical filler particles, but with increased filler volume percentages (> 40%), they observed that crack deflection by filler particles became the more prominent toughening mechanism. This was also observed in the present study for composites with ~ 60% by volume of filler. Microcrack induced toughening has also been mentioned as a potential toughening mechanism at higher filler volumes. However, that mechanism requires large volumes of microcracks that are constrained by residual stresses so as to not propagate and counteract any gains in toughness [117]; such behavior was not observed in the present composites.

Crack deflection and bridging are two toughening mechanisms that often act in concert; indeed, crack deflection commonly leads to crack bridging. A recent two-dimensional cohesive-zone fracture modeling study has provided some insight into this process by demonstrating that for a crack intersecting a single reinforcing grain or particle, significant toughening above that for simple crack kinking is generated during the bridge formation process, even before the crack has propagated far enough for a bridge to form [120]. In that study, depending on the orientation and aspect ratio of the reinforcing grain or particle with respect to the crack, either complete debonding occurs, creating a frictional pullout, or a new crack nucleates ahead, creating an uncracked bridge. In that 2-D model, the main crack could arrest while kinking around a particle and create a stress concentration ahead of the main crack tip large enough to nucleate a new crack [120], leaving a bridge behind, although any local flaws in the microstructure would certainly ease the nucleation process. However, when considering the full 3-D case, local arrest could allow the main crack to propagate around the arrest point on each side and rejoin ahead, also forming a bridge.

In the present composites, once intact particles, or groups of particles, span across the crack flanks, those bridges sustain part of the applied load that would otherwise be experienced at the crack tip, effectively toughening the material by lowering the near-tip stress intensity, K_{tip}, relative to the applied stress intensity, K_{app}:

$$K_{tip} = K_{app} - K_{br}\text{,} \qquad \textbf{(7),}$$

where K_{br} is the bridging stress intensity, which is a function of crack extension, Δa. Similar crack bridging mechanisms have been reported to provide significant toughening and be responsible for *R*-curve behavior in elephant [143] and bovine dentin [144], human cortical bone [107], ceramics [122], as well as fiber and layer reinforced composite materials [125, 126]. Observation of a "plateau" toughness in both composites (Fig. 10b), following the initial crack growth, implies that specimen dimensions were large enough to accommodate the entire bridging zone. This steady state or "plateau" toughness indicates that bridges are forming and breaking in the crack wake at a similar rate.

4.5.2 Role of Microstructure

4.5.2.1 Fracture resistance

Comparisons of the measured *R*-curve behavior between the two microstructures (Fig. 10b), suggest that the fracture resistance rises more quickly, and to a higher level, for the microhybrid composite relative to the nanofill composite. Steeper and higher rising *R*-curves are indicative of superior fracture properties; indeed, in bridging ceramic materials such behavior imparts greater defect tolerance and higher strength [119, 122, 123]. This behavior can be related to the extrinsic toughening mechanisms involved, namely crack deflection and crack bridging.

With regard to crack deflection, it is apparent from Figs. 11-13 that the particles in both composites appear equally effective at deflecting the crack. Although one might expect the nanoparticle clusters of the nanofill composite to be more prone to cracking than the solid particles in the microhybrid composite, no instances of cluster fractures were observed by examining crack profiles on the sample surfaces of C(T) and double notched samples and by examining the fracture surfaces. Accordingly, it is believed that if cluster fractures occur, they are rare occurrences, and thus other microstructural differences account for the difference in fracture and strength behavior.

In this regard, it is useful to draw experience from the published literature on bridging ceramics, which are essentially composites of a weak glass matrix (for example ~ 10% volume in Si_3N_4) surrounding crystalline ceramic grains that fracture mostly intergranularly. Several microstructural factors govern the fracture resistance of bridging ceramics, including grain size, shape, size distribution, and the adhesion between the grains. With regards to grain size, larger grain size generally gives higher peak toughness via larger deflections and larger bridge sizes [121, 145]. This concept agrees with trends seen in the mechanical behavior of dental composites, whereby composites with coarser reinforcements generally have better mechanical properties [62]. In the present case, the reported particle size for the microhybrid is somewhat higher than for the nanofill composite (Table III), indicating that this may impart some of the improved fracture resistance.

Considering particle shape, it is well known that elongated fibers, rods, or plates give superior *R*-curve behavior over equiaxed grains [121, 146]; however, in the present case the reinforcing particles appear to be roughly equiaxed for both composites, thus this is an unlikely contributor. Much less is known about the effects of size distribution on the fracture properties. However, it is clear that the maximum bridging zone size may be governed by the largest reinforcements in the distribution rather than the mean value. On the other hand, it is known that grain adhesion can have a significant effect on toughness and strength [122, 123]. Crack deflection and bridging mechanisms rely on interparticle crack growth, and thus a sufficiently weak interface between the particle and matrix, or a sufficiently weak matrix, is needed. However, if the interparticle crack growth occurs too easily, a slower rising *R*-curve and inferior strength properties generally result [122, 123]. Thus, a weaker and/or more poorly bonded matrix can actually be detrimental to the fracture resistance. For the present composites the resin formulation is very similar for both, although slight differences may be affecting the matrix toughness. Additionally, although the manufacturer reports nearly identical filler volume fraction, recent ashing results for the two composites have shown a higher filler content in the microhybrid relative to the nanofill composite [64]. Thus, even if the matrix composition were identical, the matrix is likely more highly constrained by the non-deforming filler particles in the microhybrid composite, giving higher local strength.

4.5.2.2 Flexural strength

The dental composites used in this study had high filler content (~ 60%) and accordingly failed in a brittle manner, based on both the low overall toughness and the highly linear elastic load displacement curves for the flexural strength tests. For brittle materials, the fracture resistance (K_{Ic} or R-curve), along with the defect population, plays an important role in determining the fracture strength. For the R-curve case, assuming an initial penny shaped flaw radius of a_i, the applied stress, σ_{app}, equals the fracture strength when the following two conditions are satisfied:

$$K_{app} = 2\sigma_{app}\sqrt{\frac{\Delta a + a_i}{\pi}} = K_R \text{ and } \frac{dK_{app}}{da} = \frac{dK_R}{da}, \quad \textbf{(8),}$$

where K_R is the fracture resistance from the R-curve. Flexural strength predictions based on Eq. 8 have proven to be quite accurate for two Si_3N_4 ceramics provided the early part of the R-curve is accurately measured back to $\Delta a = 0$ [122]. Although this was not possible in the present study, as will be explained later, qualitative insight can be gained into the toughness-strength relations for these composites.

Eq. 8 predicts, and for Si_3N_4 and Al_2O_3 ceramics it has been experimentally confirmed, that steeper and higher rising R-curves give higher strength [122, 123]. The results of this study are consistent with this concept; indeed; the microhybrid composite exhibits a steeper and higher rising R-curve (Fig. 10b) and ~ 20% higher

mean flexural strength (Fig. 9). Thus, a connection can be made between the observed extrinsic toughening mechanisms and trends in flexural strength. Developing microstructures that more effectively exploit these mechanisms has the potential to improve both the toughness and strength of resin based dental composite.

Eq. 8 also illustrates the importance of initial crack size in determining the strength, i.e., larger defects give lower strength. Defects are usually produced during manufacturing or processing of dental composites and can reduce the strength depending on their location relative to regions of high stress [53]. Observations of fracture surfaces (Fig. 14) revealed the presence of both pores and silica inclusions that, along with surface scratches and voids, may act as initiation points for fracture during the flexural strength tests. Another advantage of steeper *R*-curves is that not only does the overall strength increase, but the scatter in strength decreases since the influence of the initial flaw size is lessened [122]. Again, this is consistent with the present results where a lower standard deviation was measured for the flexural strength of the microhybrid composite.

4.5.3 Limitations of this study

This study provides new insight into the micromechanisms of fracture and toughening in resin based dental composites, and how those relate to fracture resistance and strength. While testing in the as-processed state allowed quick data collection, it is recognized that dental composites actually are used in the oral environment. Current

efforts by the authors are extending this study to investigate the fracture behavior of these same two resin based restorative composites in the hydrated state to more closely stimulate actual clinical conditions. The results of the present paper will provide baseline properties to help understand the mechanistic role hydration plays in affecting the fracture and strength properties.

Additionally, while the present techniques have proven very useful for qualitatively rationalizing the relations between micromechanisms, strength, and toughness, in order to make quantitative predictions of behavior (e.g., using Eq. 8) the early part of the *R*-curve must be accurately measured [122]. This can be achieved by direct measurements using specialized experimental techniques [147], or can be deduced by independently measuring K_0 and interpolating the data rather than extrapolating [119, 122, 123]. Unfortunately, for the former case custom testing apparatus is required, and for the latter case there are experimental challenges associated with stress relaxation of the resin matrix during K_0 measurements. Thus, such experiments were not completed at this time.

4.5.4 Further composite development

Dental composites must achieve a balance of esthetic and mechanical performance to find clinical success, and the major advantage of using a nanofill composite is improved polishability and polish retention over microhybrids. This is due to the capability of the nanoclusters to wear by fracturing off the nanoscale subparticles

rather than entire clusters pulling out of the composite [33]. Unfortunately, in the present case this coincides with a sacrifice in strength and toughness. However, in terms of providing fracture resistance, no fundamental differences were seen between the nanoclusters and solid particles; indeed, no observations of nanocluster fracture were made on crack profiles and fracture surfaces (Figs. 11-13). Accordingly, the nanoclusters should, in principle, be capable of providing equally effective toughening as the solid particles in the microhybrid assuming their behavior does not degrade in a wet oral environment. It may be concluded that with further microstructural refinement, a nanofill composite could be developed with a superior combination of aesthetic and mechanical performance.

4.6 Conclusions

Based on a study of strength and *R*-curve behavior, and the fracture micromechanisms, of two commercially available resin based dental restorative composites, one microhybrid and one nanofill, the following conclusions can be made:

1. Four point bending experiments showed about a 20% higher mean flexural strength of the microhybrid composite compared to the nanofill composite. Scatter in the strength values is attributed to pore and inclusion defects in both composites.

2. The fracture resistance of both composites increases with crack extension over ~ 1 mm of crack length, and this can be analyzed in terms of a fracture resistance curve (*R*-curve).

3. The steeper and higher rising *R*-curve of the microhybrid dental composite is indicative of higher fracture toughness and may be correlated with its higher flexural strength and less scatter in flexural strength.

4. Two different extrinsic toughening mechanisms were identified from the post-test observation of crack profiles, crack deflection and crack bridging. Crack deflection resulting from interparticle crack growth showed failure predominantly in the matrix. Crack bridging was induced by the formation of uncracked regions in the crack wake that sustain some of the applied load. Bridges form with crack extension, causing the observed rising *R*-curve behavior.

5. Despite the lower strength and toughness of the nanofill composite, based on micromechanics observations, the nanoparticle clusters appear to be as effective at deflecting cracks and imparting toughening as the solid particles of the microhybrid. Thus, with further microstructural refinement, is should be possible to achieve a superior combination of esthetic and mechanical performance using the nanocluster approach.

ACKNOWLEDGEMENTS

The authors wish to thank 3M™ ESPE™ for providing the restorative materials tested in this study.

5 MANUSCRIPT II: R-CURVE BEHAVIOR AND TOUGHENING MECHANISMS OF RESIN BASED DENTAL COMPOSITES: EFFECTS OF HYDRATION AND POST-CURE HEAT TREATMENT

M. B. Shah[a], J. L. Ferracane[b] and J. J. Kruzic[a3]

[a] School of Mechanical, Industrial, and Manufacturing Engineering, Oregon State University,
Corvallis, OR 97331, USA

[b] Division of Biomaterials & Biomechanics, School of Dentistry, Oregon Health & Science University, Portland, OR 97239, USA

Accepted for publication in

Dental Materials

November 2008

[3] Corresponding author. Tel: +1-541-737-7027; fax: +1-541-737-2600.

E-mail address: jamie.kruzic@oregonstate.edu (J. J. Kruzic)

ABSTRACT

Objectives: To test the hypothesis that the fracture resistance of two different particulate resin composites degrade after water hydration and improve after post-cure heat treatment, and to correlate those changes with salient failure micromechanisms.

Methods: Two composites with different filler morphology were selected, denoted microhybrid (Filtek™ Z250) and nanofill (Filtek™ Supreme plus). Following initial light curing, hydrated samples were aged in water for 60 days at room temperature while post-cured samples were heat treated at 120 ºC for 90 min. Fracture resistance was assessed using fracture resistance curves (*R*-curves) utilizing pre-cracked compact tension, C(T), specimens. The flexural strength of the hydrated composites also was evaluated in four point bending using unnotched beams. Scanning electron microscopy of crack paths and fracture surfaces was performed to determine the micromechanisms of fracture and toughening. The results were compared by two-way ANOVA and Tukey's multiple comparison test ($p \leq 0.05$).

Results: SEM observations revealed a predominantly interparticle matrix crack path for all cases except the hydrated nanofill composite, which showed evidence of particle matrix debonding. Hydration lowered the strength for both composites and the peak toughness for the nanofill composite. The strength decrease was attributed to resin matrix plasticization and hydrolytic degradation in both cases, with additional interfacial degradation causing a larger strength decline and concomitant peak

toughness decrease in the nanofill composite. The post-cure heat treatment noticeably changed the *R*-curve shape causing the peak toughness to be reached after shorter amounts of crack extension. Such changes help explain the increases in strength reported in other studies and is attributed to improved resin matrix properties.

Significance: Results from this study provide new insight into the micromechanisms of fracture in resin based dental composites which should aid the future development and improvement of these materials.

KEYWORDS

Resin composite; *R*-curve; Crack bridging; Fracture; Hydration; Post-cure; Toughening

5.1 Introduction

A number of studies have investigated the fracture toughness of resin based dental composites using either notched or pre-cracked samples to estimate or measure, respectively, a single value of fracture toughness, K_{Ic} [6, 62, 63, 148].[4] However, it has recently been reported that dental composites actually exhibit *rising* fracture resistance with crack extension [149]. Such behavior is similar to many other materials such as cortical bone [107] , dentin [114], layered composite ceramics [126], and dental ceramics [134], and is generally associated with extrinsic toughening mechanisms that develop during crack extension. Examples of important extrinsic toughening mechanisms include crack bridging and in-situ phase transformation toughening [116, 150] . These mechanisms improve the toughness of the material by shielding the crack from some of the applied load, thus reducing the stress intensity experienced at the crack tip. The development of such crack tip shielding mechanisms increases the fracture resistance of the material as the crack propagates. Accordingly, fracture resistance curves (*R*-curves) are generally used to measure the fracture resistance of such materials, usually in terms of the stress intensity, K_R, or strain energy release rate, G_R, as a function of crack extension, Δa [98, 151].

---

[4] The stress-intensity factor, *K*, is a global parameter which fully characterizes the local stress and deformation fields in the immediate vicinity of a crack tip in a linear-elastic solid, and thus can be used to predict crack advance. It is defined for a crack of length *a* as $K = Y\sigma_{app}(\pi a)^{1/2}$, where σ_{app} is the applied stress and Y is a geometry factor of the order of unity [98].

While rising *R*-curve behavior attributed to crack bridging has been observed in as-processed dental composites [149], restorative materials are exposed to the oral environment throughout their lifetime, and it is vital to understand the properties of these composites in hydrated conditions. Findings of many studies have shown significant changes in the mechanical properties of resin composites due to aging in water [81, 152, 153]. Prolonged exposure to aqueous media is believed to produce adverse effects such as degradation of the silane coupling agent that bonds filler particles to the resin matrix [72], resin degradation [141], leakage or pullout of filler elements [41, 154], and softening of the resin matrix [155]. Though a number of studies have addressed the effect of long-term hydration on the fracture toughness of resin composites, there is no general consensus on the effects of water on fracture properties [57, 70, 73, 81]. Ferracane *et al*. reported a 20-30% reduction in fracture toughness after 6 months hydration [73], while another study by Indrani *et al*. reported an increase in K_c over the first 6 weeks of hydration after which it remained constant [69]. For the latter case, it was suggested that an increase in the plastic zone size ahead of the crack under the influence of water caused an increase in the fracture toughness. It is conceivable that various composites react differently to hydration, making this an important area for further research.

Additionally, numerous studies have shown heat curing induced improvements in the mechanical properties of dental resin composites. Most composite restoratives achieve only 45-70% monomer conversion after the initial light curing [156]. Post-curing above the glass transition temperature of the resin matrix can enhance the degree of cure and improve the mechanical properties of the composite [74]. Also, relief of

internal stresses which are generated during the initial light-curing may also improve the mechanical properties of resin composites [101]. Furthermore, studies show increased biocompatibility of the resin composite after heat treatment [99, 101]. Depending on the post-cure temperature, time, and resin composite formulation, researchers have reported increases in hardness, tensile and flexural strength, and fracture toughness [13, 74, 100]. Such results have clinical importance, for example in producing indirect composite restorations with improved properties, while also giving insight into how to improve light cured direct restorations, for example through chemical modifications that enhance light curing to achieve a similar final state to the heat treated composites.

Accordingly, the objective of this study was to measure *R*-curves to test the hypothesis that the fracture behavior of resin based dental composites degrades after water hydration and improves after post-cure heat treatment while also gaining insight into the microscopic fracture and toughening mechanisms of these composites in the hydrated and heat treated states. To achieve these goals, mechanical tests were combined with microscopy to examine the fracture behavior of one microhybrid (Filtek^{TM} Z250) and one nanofill (Filtek^{TM} Supreme Plus) commercial resin based dental composite, and results were compared to a previous study on the same composites in the as-processed state without subsequent treatments [149].

5.2 Materials and Methods

5.2.1 Materials

The two commercial resin composites used in this study were Filtek Z250™ and Filtek Supreme Plus™ Universal restoratives manufactured by 3M™ ESPE™ (St Paul, MN, USA). The composition details provided by the manufacturer for both composites are listed in Table 4. It should be noted that both microstructures have a mixture of large and small filler particles, but in the case of the nanofill the large particles are actually clusters of smaller nanoparticles rather than individual solid particles.

Table IV Summary of composition for commercial resin based composites

Commercial name	Shade	Type	Matrix	Filler
3M™ESPE™ Filtek Z250™ Universal Restorative	A2	Microhybrid	Bis-GMA[a], Bis-EMA[b], UDMA[c] and TEGDMA[d]	0.01 to 3.5 μm, average 0.6 μm, zirconia/silica (60 % by volume)
3M™ ESPE™ Filtek Supreme Plus™ Universal Restorative	A2B	Nanofill	Bis-GMA[a], Bis-EMA[b], UDMA[c] and TEGDMA[d]	20 nm silica and zirconia/silica clusters of 0.6 to 1.4 μm with individual particle size of 5-20 nm (59.5 % by volume)

[a] Bis-GMA, bisphenol A-glycidyl dimethacrylate, [b] Bis-EMA, bisphenol A ethoxylate dimethacrylate

[c] UDMA, urethane dimethacrylate, [d] TEGDMA, triethyleneglycoldimethacrylate

5.2.2 Sample preparation and *R*-curve testing

Sample preparation was the same as described in a previous paper [149], differing only in terms of the post cure treatments, and thus the details are only briefly described here. The uncured composite samples were molded using aluminum split molds and photopolymerised for 40 sec each on the top and bottom surfaces in a laboratory curing unit (TRIAD II; Dentsply International, PA). Following the initial curing, samples were either 1) hydrated by soaking in de-ionized water for 60 days or 2) immediately (5 min delay time) post-cured at 120 ºC for 90 min with no subsequent hydration treatment.

R-curves were evaluated for both the composites using standard compact tension, C(T), specimens (W= 14 mm, B = 2.2 ± 0.3 mm). The initial notch length, a_0, was 3.5 ± 0.1 mm. The samples were ground to 600 grit using silicon carbide papers and polished to 0.05 μm using alumina powder slurries followed by a final finishing polish using Buehler™ MasterPolish suspension. A custom built razor micronotching machine was used to produce a pre-crack in the sample. A micronotch was cut into the machined notch by repeatedly sliding a new razor blade in the presence of a 1 μm diamond slurry under applied loading of about 200-300 grams, until a sharp pre-crack initiated from the micronotch (Fig. 15a and b).

Following pre-cracking, hydrated (N = 3 for each composite) or post-cured C(T) samples (N = 3 for nanofill, N = 2 for microhybrid) were tested on an Instron© 8501 servo-hydraulic testing machine to measure the *R*-curves. A capacitance displacement

gauge was attached to the clevis grips to precisely measure the load-point displacement. Samples were manually loaded using displacement control until the onset of the sub-critical crack extension determined by a sudden drop in the load. The samples were immediately unloaded by about 15-20 % of the maximum load and then were reloaded until subsequent crack extension. This loading and unloading sequence was continued until the end of the test. The tests were generally concluded after several millimeters of crack growth when a steady-state toughness in the *R*-curve was clearly achieved, although some samples didn't survive and failed by unstable fracture. A compliance method was used to determine the crack length at each unloading step using the load point displacement data. Crack lengths, *a,* after each unload were calculated using a load-point compliance calibration for the C(T) specimen [135]:

$$a / W = 1.0025 - 3.8256U + 2.0734U^2 - 11.443U^3 \quad \textbf{(9),}$$

where W is the sample width and U is given by:

$$U = \frac{1}{\sqrt{EBC} + 1} \quad \textbf{(10)}$$

In Eq. 10, B is the sample thickness, C is the measured unloading sample compliance, and E is the elastic modulus. To maximize the accuracy of the technique, rather than using an average reported value, E was calculated for each sample as the value which

gave the best agreement between the initial compliance and the optically measured crack length before the start of the test for each specimen.

During each test, samples were unloaded several times and removed from the test machine for an optical measurement of the crack length. These intermittent optical measurements were performed to confirm accuracy and allow corrections of any errors in the compliance crack length measurements. Finally, the fracture resistance, K_R, at each new crack length was computed from the standard fracture mechanics based solution for the compact tension specimen [136].

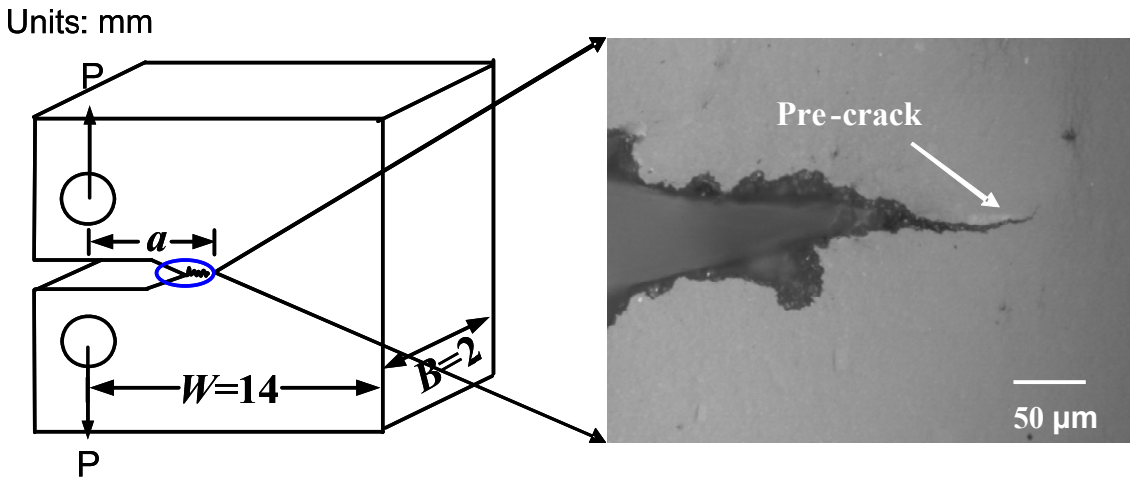

a) **b)**

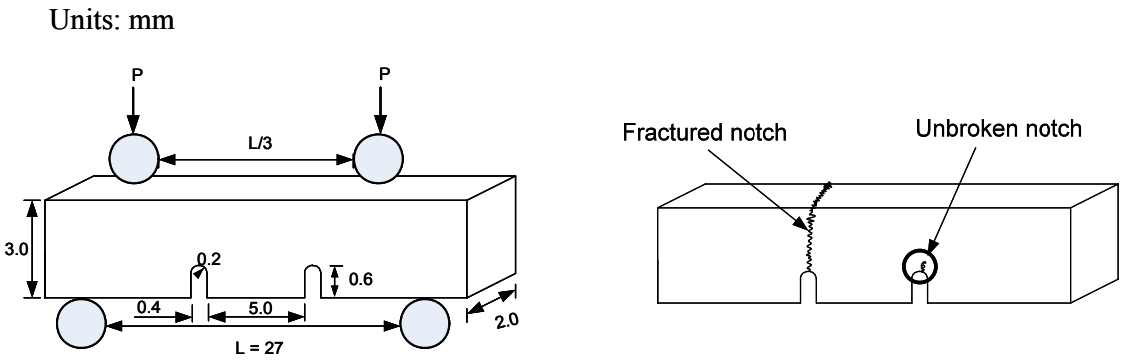

c) **d)**

Fig. 15. (a) Schematic of a standard fracture mechanics based compact tension, C(T), specimen with a micronotch and pre-crack. (b) Optical micrograph of a pre-crack which was created using a custom built razor micronotching machine. Due to the high magnification, only the micronotch and pre-crack can be seen. (c) Double notched sample geometry with four point loading configuration. (d) Post test sample schematic showing the fractured and unbroken notch. The circle surrounding the unbroken notch indicates the area to be analyzed for observing the fracture micromechanisms.

5.2.3 Double notched beam testing

To supplement the *R*-curve experiments for the hydrated specimens, double notched four point bend specimens were used to further examine the fracture and toughening mechanisms. Following a similar fabrication procedure as for the C(T) specimens, rectangular double notched specimens ($N = 12$ for each composite) were made in a double notched aluminum split mold (33mm x 3 mm x 2mm). Special attention was paid in producing identical notches to avoid preferential fracture from a particular notch. Four point bend testing (Fig. 15c) was performed on a Bose/EnduraTEC ElectroForce® 3200 testing instrument. Here, samples were loaded in displacement control at a cross head speed of 0.01 mm/sec until fracture took place from one of the

notches. Invariably, each sample fractured from one of the notches, while the other notch was at the point of instability and the microstructural phenomena preceding the fracture were frozen in at the notch tip. Accordingly, the areas surrounding the unbroken notches were analyzed in a scanning electron microscope (SEM) to study the fracture micromechanisms (Fig. 15d).

5.2.4 Unnotched flexural strength testing

Unnotched rectangular bars (25 x 2 x 2 mm) were fabricated from each composite (N=12), hydrated and tested in four-point bending using similar procedures as for the double notched specimens. Flexural strength was calculated using simple beam theory.

5.2.5 Hydration time estimation

With the goal to obtain nearly complete hydration in all the resin composite sample geometries, hydration times were estimated using Fick's second law for non-steady state diffusion. The solution was based on a boundary condition where surfaces were kept at a constant concentration, $C_s = 1$, while the rest of the sample was assumed at an uniform initial concentration, $C_0 = 0$. The diffusion constants were taken from the literature to be 4.1×10^{-9} $cm^2 s^{-1}$ [132] and 9.57×10^{-9} $cm^2 s^{-1}$ [157] for the microhybrid and nanofill composite, respectively. The diffusion concentration profile for the average thickness (0.22 cm) C(T) specimens of microhybrid composite (Fig. 16) showed that after 60 days, about 98% hydration was achieved at the center of the

specimen. Diffusion concentration values might be underestimated here as all the calculations assumed rectangular samples without the notch and holes of the actual C(T) samples. The nanofill composite showed close to 99.9% hydration at the center after 60 days. Double notched and flexural strength samples also showed about 99% hydration at the center thickness for both composites. Consequently, all the samples were hydrated for 60 days in de-ionized water at room temperature as longer hydration time resulted in a minimal increase in water uptake.

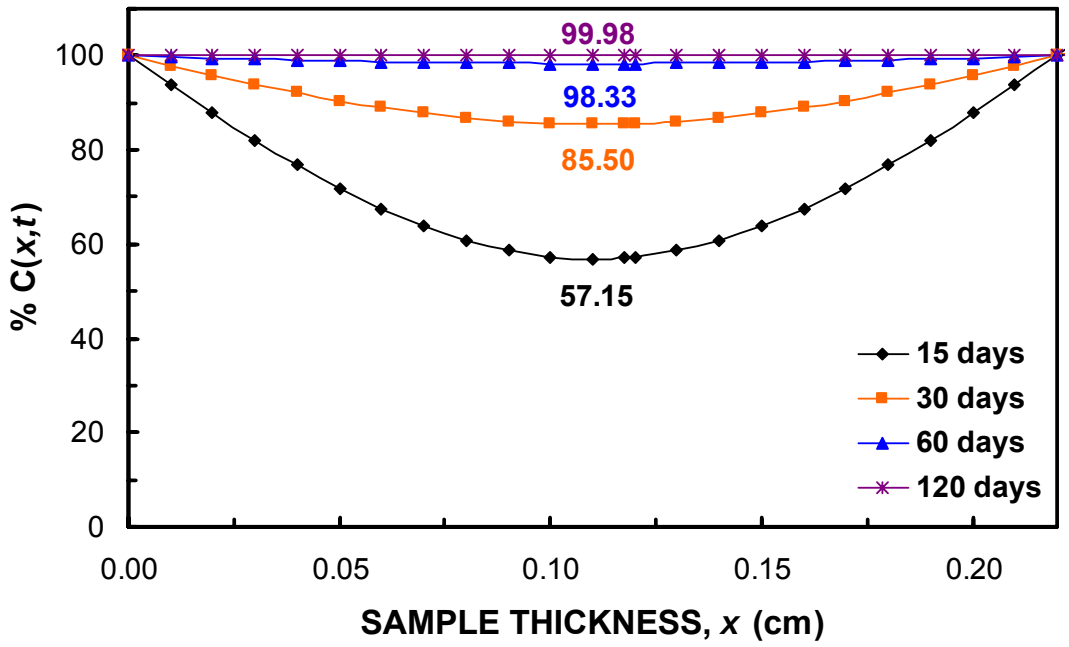

Fig. 16. Illustration of the diffusion concentration profile for the microhybrid compact tension, C(T), specimens. Diffusion calculations were based on Fick's second law for non-steady state diffusion. It is seen that > 98% hydration is achieved after 60 days with minimal increase in hydration at longer times and this was the lowest hydration level estimated for any sample.

5.2.6 Microstructural characterization

After sputter coating (Scancoat Six SEM Sputter Coater, Edward Limited, UK) the sample surfaces with ~ 20 nm of gold, microscopic crack path observations and fractography of the fractured samples were performed using a digital Zeiss Ultra SEM to identify the microstructural fracture and toughening mechanisms.

5.2.7 Statistical analysis

A two-way analysis of variance (ANOVA) was performed on strength and peak toughness for both resin composites, microhybrid and nanofill, with two different storage conditions, as-processed and hydrated. Strength and peak toughness data of both composites in the as-processed condition were obtained from a previous study [149]. Pairwise multiple comparison Tukey tests were performed at a significance level of $p = 0.05$. Additional student's t-test, also at a significance level of $p = 0.05$, were performed to compare the as-processed and post cured nanofill composite data.

5.3 Results

5.3.1 Flexural strength evaluation

Mean flexural strength was calculated from the unnotched four point beam bending test for the microhybrid and nanofill composite after 60 days hydration (Fig. 17). Mean flexural strength of the microhybrid, 91.44 ± 14.75 MPa, showed ~ 40%

superior strength compared to the nanofill composite, 52.7 ± 12.87 MPa. Also shown in Fig. 17 are the strength results for the as-processed composites from a previous study [149]. A two-way ANOVA comparison demonstrated that material and storage conditions both were significant, however, no significant interaction was identified between them. Pairwise comparison tests further demonstrated that the nanofill composite has significantly lower strength than the microhybrid composite in both conditions. Also, hydration caused significant reduction in strength for both composites, with a ~ 32% and ~ 50% reduction for the microhybrid and nanofill composites, respectively.

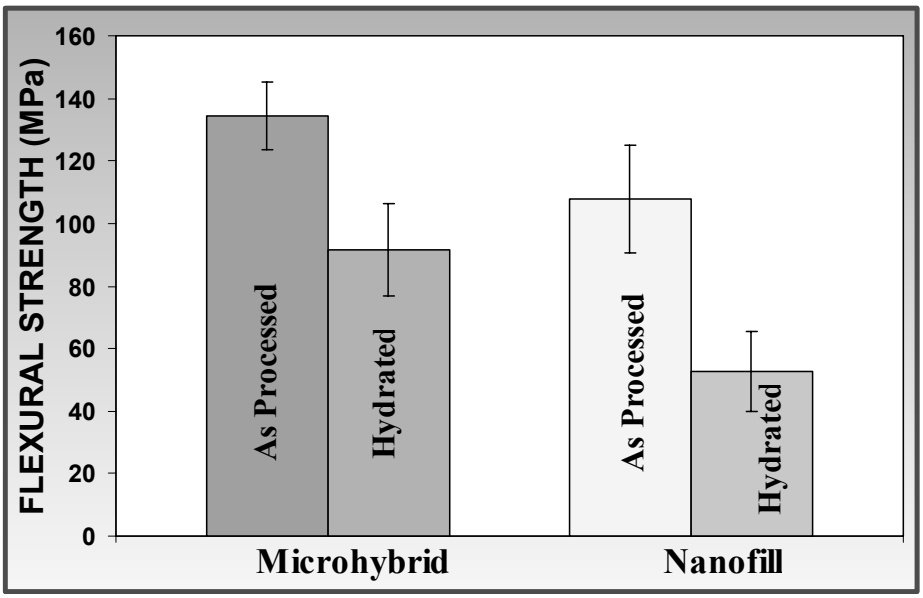

Fig. 17. Bar chart comparing the mean flexural strength for the microhybrid and nanofill composite with and without 60 days of water hydration. Note the significant decrease in strength for both composites with water hydration.

5.3.2 Fracture resistance (*R*-curve) and peak toughness measurements

Load-load point displacement plots (e.g., Fig. 18a) for C(T) specimens were analyzed to deduce *R*-curves as described in Section 5.2.2. Both microhybrid and nanofill composites showed similar stable crack growth behavior. *R*-curves are plotted in terms of the stress intensity, K_R, as a function of crack extension, Δa, with the strain energy release rate, G_R, on the right axis (Fig. 18b). The latter was calculated using the relation for plane strain conditions [98]:

$$G_R = \frac{K_R^2}{E / (1 - \nu^2)} \quad \textbf{(11),}$$

where E is the elastic modulus and ν is Poisson's ratio. Average E and ν values of 11 GPa and 0.33 were used to scale G_R estimates on the right axis of Fig. 18b based on the manufacturer and published reported values, respectively [137, 138].

It is clear from Fig. 18b that both composites exhibited rising *R*-curve behavior over roughly the first 1 mm of crack growth in the hydrated state. Two-way ANOVA and Tukey's test highlighted that the microhybrid composite showed significantly higher *R*-curve peak toughness of 1.26 ± 0.05 MPa√m compared to the nanofill composite, 0.80 ± 0.06 MPa√m. Furthermore, peak toughness comparison of as-processed (1.21 ± 0.07 MPa√m) and hydrated (1.26 ± 0.05 MPa√m) microhybrid composite, Fig. 18c and f, showed no significant difference. On the contrary, as observed from Fig. 18d

and f, toughness of the hydrated nanofill composite (0.81 ± 0.06 MPa√m) was significantly reduced when compared to the as-processed condition (0.99 ± 0.02 MPa√m).

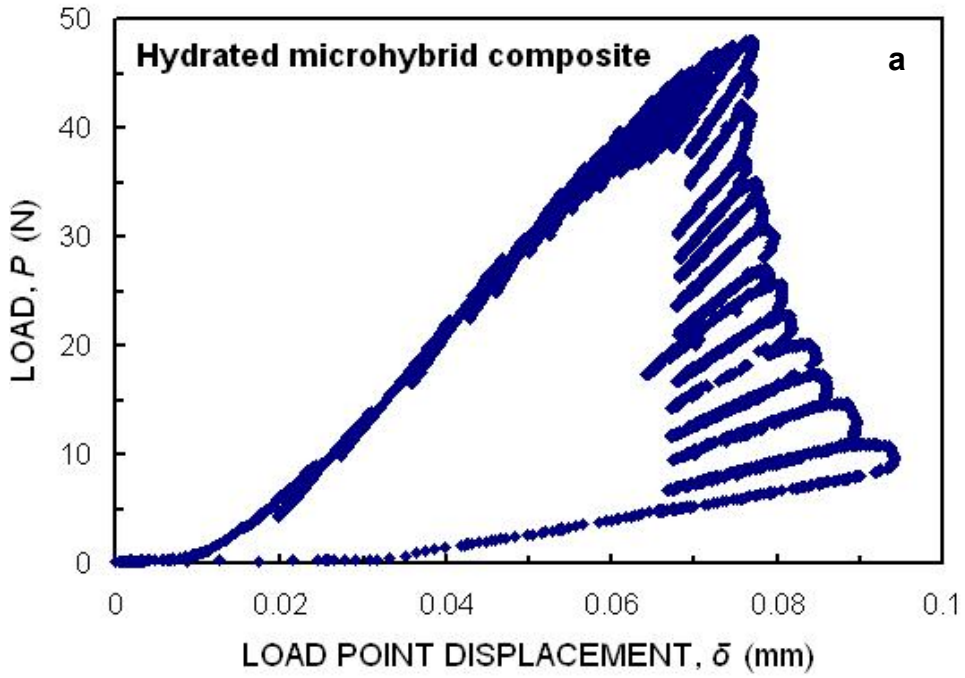

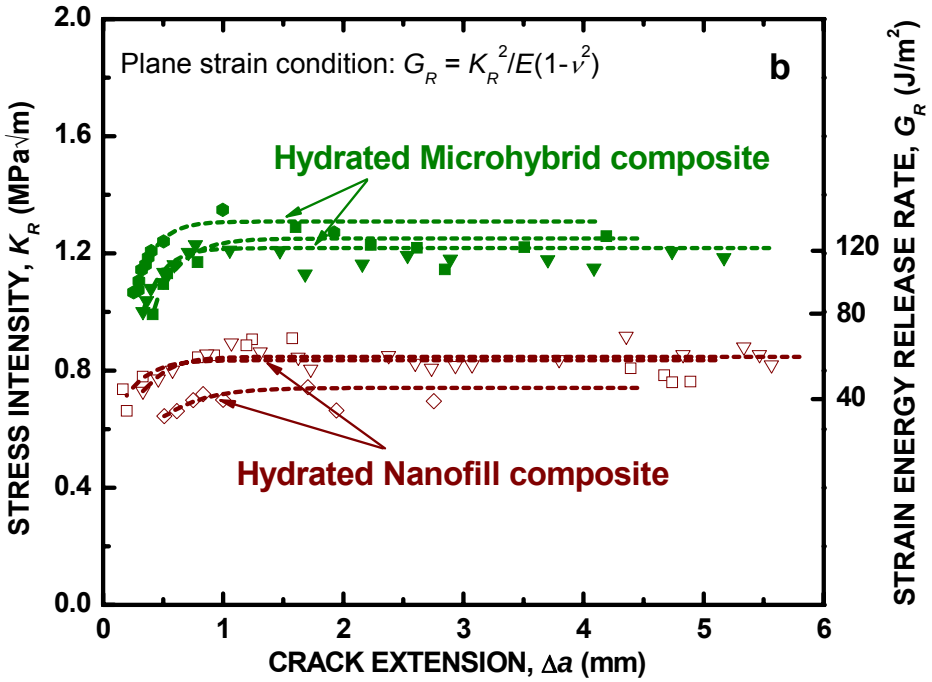
Plane strain condition: $G_R = K_R^2/E(1-\nu^2)$
b
Hydrated Microhybrid composite
Hydrated Nanofill composite
STRESS INTENSITY, K_R (MPa√m)
STRAIN ENERGY RELEASE RATE, G_R (J/m^2)
CRACK EXTENSION, Δa (mm)
2.0
1.6
1.2
0.8
0.4
0.0
120
80
40
0
1
2
3
4
5
6

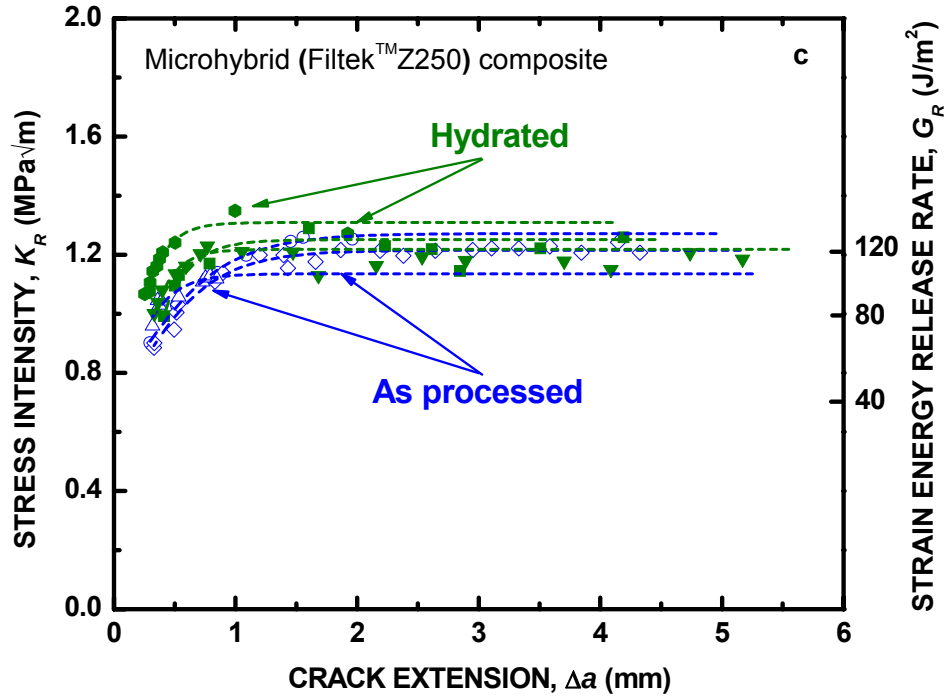
Microhybrid (Filtek™Z250) composite
c
Hydrated
As processed
STRESS INTENSITY, K_R (MPa√m)
STRAIN ENERGY RELEASE RATE, G_R (J/m^2)
CRACK EXTENSION, Δa (mm)
2.0
1.6
1.2
0.8
0.4
0.0
120
80
40
0
1
2
3
4
5
6

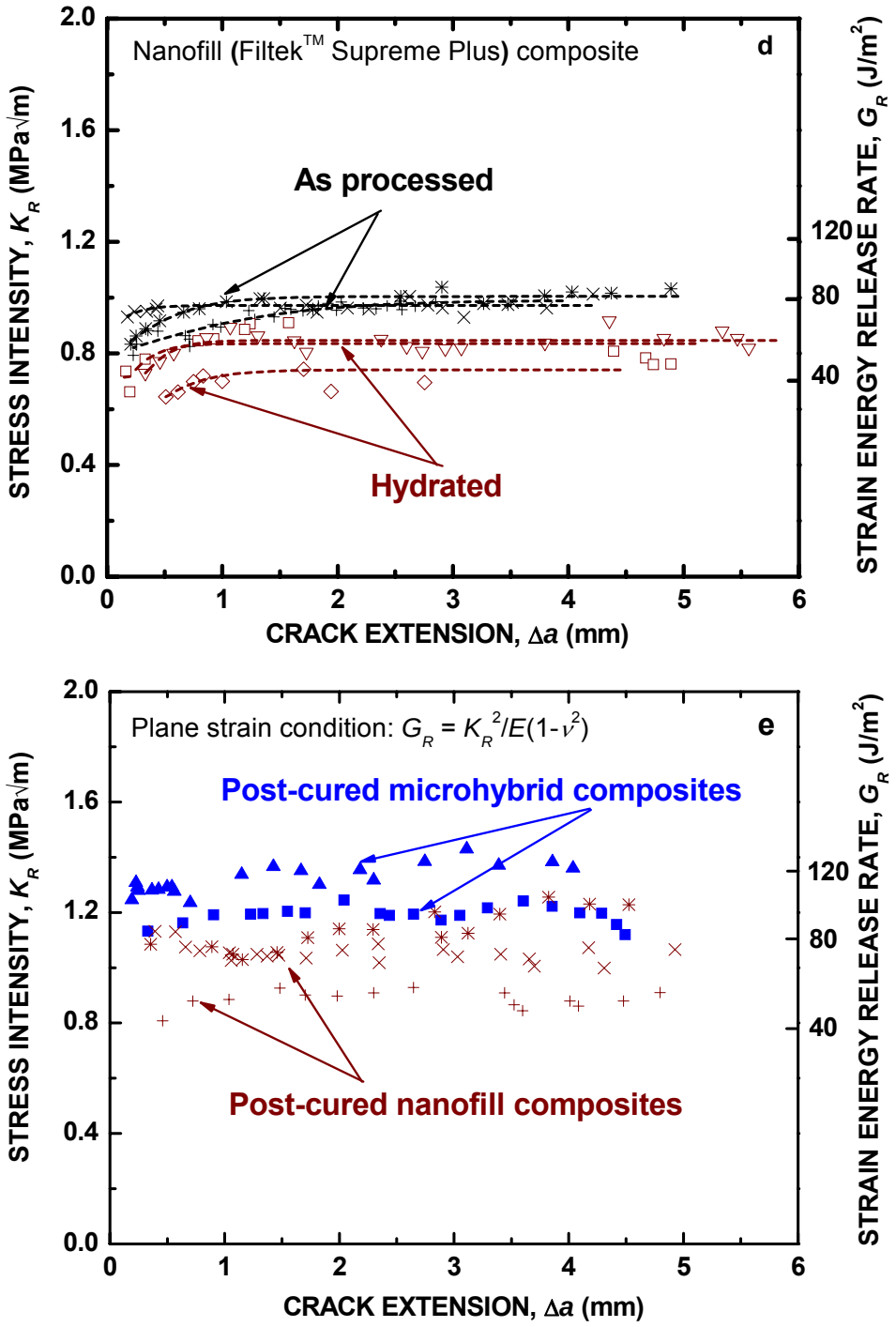
Nanofill (Filtek™ Supreme Plus) composite
d
As processed
Hydrated
STRESS INTENSITY, K_R (MPa√m)
STRAIN ENERGY RELEASE RATE, G_R (J/m²)
CRACK EXTENSION, Δa (mm)
Plane strain condition: $G_R = K_R^2/E(1-\nu^2)$
e
Post-cured microhybrid composites
Post-cured nanofill composites

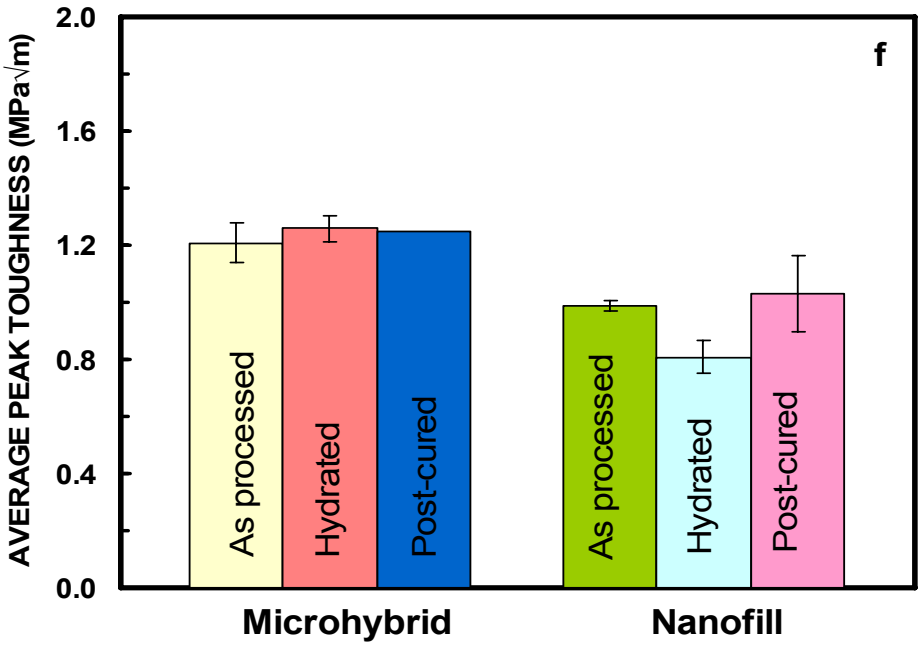

Fig. 18. (a) Example load-load point displacement curve showing stable crack growth for a hydrated microhybrid composite C(T) sample. The nanofill composite also showed similar behavior. (b) Fracture resistance curves (*R*-curves) for the hydrated microhybrid (open symbols) and nanofill (solid symbols) composites plotted in terms of the stress intensity, K_R, as a function of crack extension, Δa. Note the higher initial increase in toughness for the microhybrid composite. (c) *R*-curve comparison of the as-processed (open symbols) and hydrated (solid symbols) microhybrid composite samples. (d) *R*-curve comparison of as-processed (crossed symbols) and hydrated (open symbols) nanofill composite samples. (e) *R*-curves for the post-cured microhybrid (solid symbols) and nanofill (crossed symbols) composite. The right axis in all *R*-curve plots show the estimated strain energy release rate, $G_R(\Delta a)$. (f) Average peak toughness comparison of as-processed, hydrated, and post-cured microhybrid and nanofill composites, error bars indicate the standard deviation and are absent for the post cured microhybrid samples where only two complete *R*-curves were obtained.

Post-cured composites were also tested to determine their *R*-curve behavior (Fig. 18e). Approximations of average strain energy release rate, $G_R(\Delta a)$, for both post-cured composites is shown on the right axis. Modulus, E, was taken as 13.5 GPa based on post-cured flexural modulus of Z-100 composite [45], which has similar average

particle size of 0.6 μm as Z-250, although its resin composition is different in that it contains only Bis-GMA and TEGDMA. Poisson's ratio, ν, was again taken to be 0.33. All post-cured samples reached their peak toughness rapidly after a very short amount of crack extension, generally < 0.5 mm. The average peak toughness from the *R*-curve was calculated to be 1.25 MPa√m for the microhybrid composite and 1.03 ± 0.13 MPa√m for the nanofill composite. Statistical comparison of peak toughness between post-cured and as-processed microhybrid composite was not practical as only two samples provided *R*-curve results for the post-cured microhybrid composite; however, the values were essentially identical. Also, no significant difference ($p = 0.63$) was found between *R*-curve peak toughness of post-cured and as-processed nanofill composites. Fig. 18f compares the *R*-curve derived mean peak toughness of as-processed [149], hydrated, and post-cured composites. The microhybrid shows superior peak toughness compared to the nanofill composite in all conditions.

5.3.3 Crack profiles and fractography

Post-test SEM images of crack paths for hydrated microhybrid and nanofill composites are shown in Fig. 19. It is evident from the micrographs that cracks propagated predominantly between the filler particles in both composites, either near, or at, the filler/matrix interface (Fig. 19a and b). This interparticle (or inter-cluster) crack growth suggests crack deflection is an important toughening mechanism in both restorative composites.

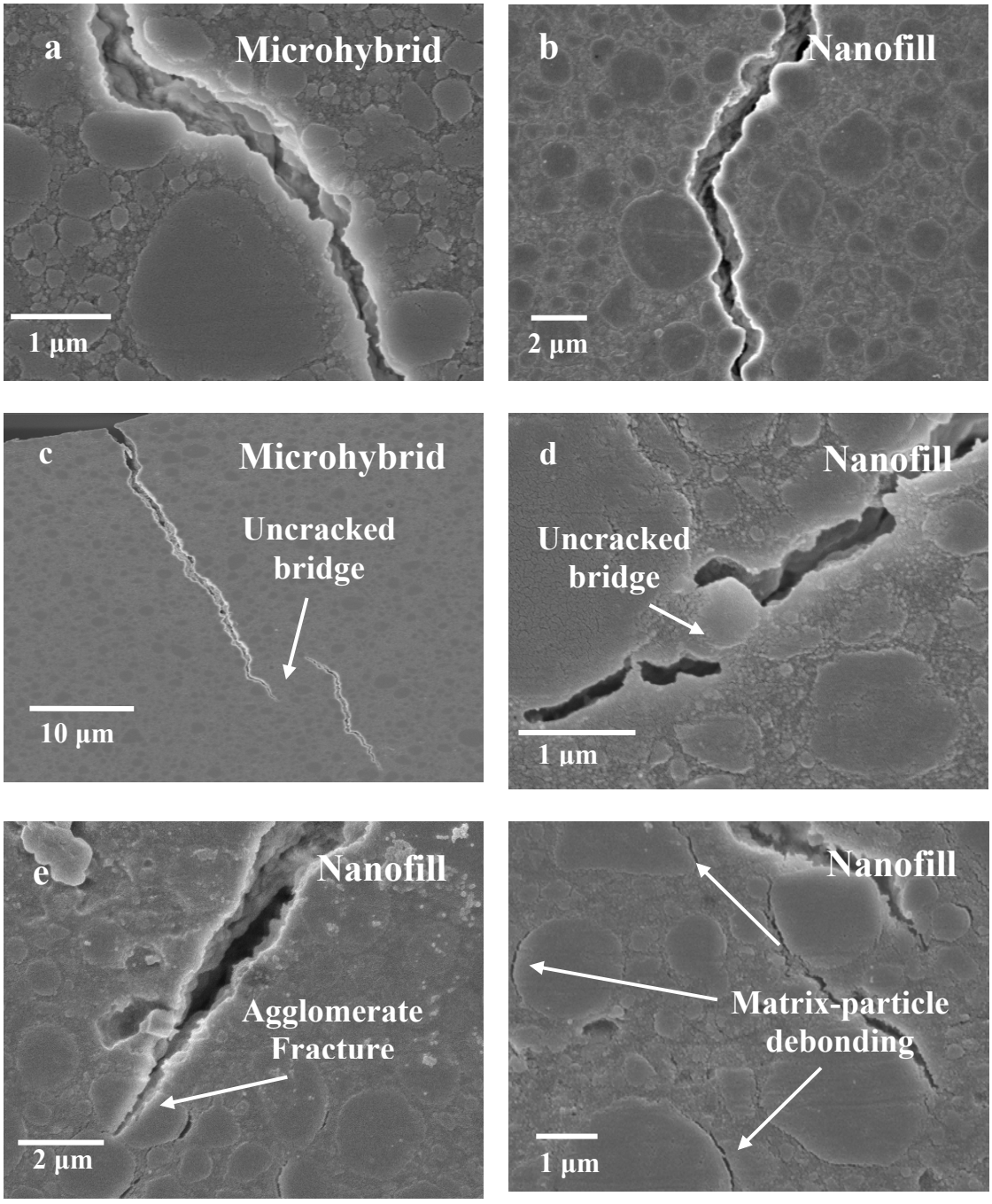

Fig. 19. SEM micrographs of hydrated (a) microhybrid and (b) nanofill composites showing the interparticle crack path. Crack bridging was observed in both hydrated (c) microhybrid and (d) nanofill composites. An isolated instance of agglomerate/cluster fracture in the hydrated nanofill composite is shown in (e) while matrix-particle debonding in the proximity of the crack tip in the hydrated nanofill composite is seen in (f). In all micrographs the crack is propagating generally from top to bottom.

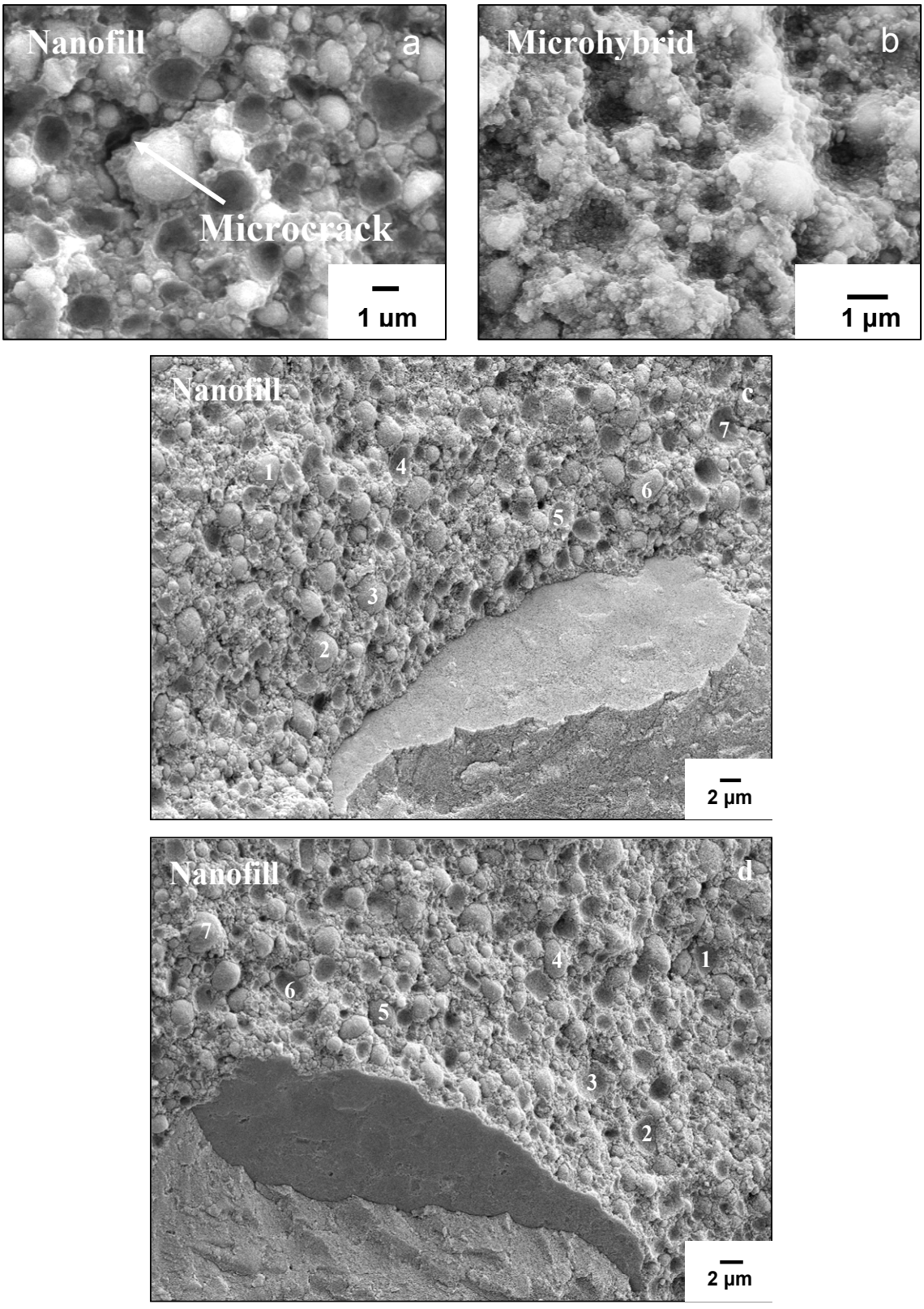

Fig. 20. SEM micrographs of fracture surfaces: (a) Hydrated nanofill fractograph showing clear interfacial debonding and the presence of

microcracking along the filler-matrix interface. (b) Micrograph showing coverage of the fracture surface with resin matrix and no evidence of interfacial microcracks in a hydrated microhybrid composite. (c) and (d) show SEM images of matching fracture surfaces of a nanofill composite sample confirming interparticle crack growth. Each filler particle on one surface corresponds to a hole on the other and vice versa as seen in example locations 1 – 7. The microhybrid composite also showed no evidence of particle fracture. The inclusion in (c) and (d) was used as a landmark for locating matching regions.

Observations of the areas surrounding the crack tips revealed the presence of intact bridges spanning the crack wake. These crack bridges were observed in both the hydrated microhybrid and nanofill composites (Fig. 19c and d respectively). Such bridges sustain a portion of the applied load that would otherwise go toward crack extension. Thus, in addition to crack deflection, crack bridging is another toughening mechanism present in both resin composites. The same crack deflection and bridging toughening mechanisms were also observed in the crack profiles of the post-cured specimens, as well as the as-processed specimens in a previous study [149].

No particle cracking was observed in any of the microhybrid samples whereas one instance of cluster/agglomerate fracture was observed in the hydrated nanofill composite (Fig. 19e). Matrix-particle debonding was evident in multiple hydrated nanofill composite samples, particularly in the area surrounding the crack tip (Fig. 19f). Further confirmation of interfacial debonding was obtained by observing the fracture surfaces of the nanofill composites (Fig. 20a). In Fig. 20a there is clear evidence of particles that have debonded from the matrix, with distinct lines outlining the particles and holes, and a microcrack showing additional particle-matrix debonding out of the plane of the photo. In contrast, Fig. 20b shows almost

exclusively interparticle failure in the matrix for hydrated microhybrid composite. Here the morphology is different with the matrix completely covering each particle and no microcracks. A similar interparticle matrix crack path as seen in Fig. 20b was observed for the post-cured nanofill and microhybrid composites with very little evidence of any matrix-particle separation, as well as in the as-processed composites in a previous study [149].

Further fracture surface imaging was performed for the hydrated nanofill composite, and no other instances were found of particle or cluster fracture (Fig. 19e). For example, Figs. 20c and d show identical locations on matching fracture surfaces of the nanofill sample. In every location, interparticle crack growth is confirmed. Matching locations are labeled 1 to 7 and show that each particle on one surface corresponds to a hole on the other surface and vice versa. No evidence of split clusters or particles were apparent in all of the fracture surfaces observed from both composites with either treatment. Also, as was observed in the as-processed composites [149], voids and inclusions were also identified on the fracture surfaces, with an inclusion of unknown origin seen in Figs. 20c and d.

5.4 Discussion

5.4.1 Flexural strength: Role of hydration

5.4.1.1 Strength degradation and aging time

Comparing the flexural strength of both composites (Fig. 17) reveals that the microhybrid has superior strength compared to the nanofill in the hydrated condition, which is the same trend previously observed for the as-processed composites [149]. However, 60 days hydration causes a degradation in flexural strength for both composites with a ~ 32 % and ~ 50 % reduction for the microhybrid and nanofill composites, respectively. This trend is in general agreement with a recent study by Curtis et al. [51] who observed a decrease in biaxial flexural strength in the same composites after three and six months of hydration. It is also important to note that those same authors did not observe any significant reduction in strength after 24 hrs of water aging, which is similar to the finding of Rodrigues et al. [53] that there is not a significant difference in four-point bending flexural strength of the same microhybrid and nanofill composites after 24 hrs of hydration.

As discussed in Sec. 5.2.5, water absorption of these dimethacrylate based composites is estimated to take roughly 60 days to achieve close to 99% hydration in both composites for the sample sizes used in this study. Our theoretical calculations are in compliance with other studies [153, 158], where most materials reached their water

uptake saturation within 7-60 days of hydration. Such results indicate that long term hydration may be more clinically relevant than the 24 hrs storage recommended by ISO 4049 [50], as has been suggested by other researchers [128].

5.4.1.2 Strength degradation mechanisms

Several studies have reported significant reductions in strength for dental polymer resins and composites due to water uptake [14, 51, 128, 141]. Possible reasons for a degradation of composite mechanical properties include the degradation of the resin, the filler, or the resin/filler interface. With regard to the filler, although one isolated instance of cluster fracture was observed in a hydrated nanofill sample (Fig. 19e), it is likely a rare occurrence as extensive fracture surface imaging (e.g., see Fig. 20c & d) confirmed interparticle crack growth and showed no further evidence of agglomerate/cluster splitting. Thus, it may be concluded that filler degradation is not a likely source for the observed loss in strength with hydration.

Resin degradation may be associated with either volumetric changes such as swelling, physical changes such as plasticization, or chemical changes such as oxidation and hydrolysis [44]. As for the interfaces, in dimethacrylate based resin composites, filler particles are chemically bonded to the resin with a bifunctional silane coupling agent where one functional silica group is connected to the inorganic filler through a condensation reaction while a methacrylate group provides compatibility and bonding to the resin matrix [33]. Particle-matrix debonding can diminish the transfer of stresses

to the filler particles thus reducing the overall strength of the composite. Moreover, interfacial degradation of the silane coupling agent has been reported in some dental composites [14, 35, 72].

Both composites in this study experience degradation in strength with hydration. But despite having very similar resin and filler chemistry and similar filler volumes [33], hydrolytic strength degradation of the nanofill composite was significantly greater than the microhybrid composite.

Additionally, interfacial separation was clearly observed in the fracture surface imaging of the hydrated nanofill composite (Fig. 20a), while no such debonding was observed in the as-processed state [149]. Comparing fracture surfaces at high magnification, the microhybrid composite has a "lumpy" looking appearance as the matrix covers the particles (Fig 20b), which also has been observed in a previous study [149]. The particles appear to be very well adhered to, and covered by, the matrix, suggesting fracture through the resin matrix. Crack growth through the resin matrix indicates good filler/matrix adhesion [73] which should give good strength and toughness. For the hydrated nanofill composite, crack path observations (Fig. 19a) show clear interfacial separation between some particles and the matrix while fracture surfaces (Fig. 20a) show particles protruding from the matrix or evidence for interfacial separation between the particles and the matrix. This indicates a lesser degree of adhesion between the resin and filler in the nanofill composite when hydrated, as no such behavior was seen in the as-processed condition [149]. Curtis *et*

al. [51] reported the presence of microcracks on the fracture surfaces of both of these composites after 6 months of hydration and suggested that it could have been a consequence of degradation of the resin matrix or the silane layer surrounding the filler particles. In the present study, after 60 days of hydration, the nanofill composite showed a greater presence of microcracks (Fig. 20a) along the filler/matrix interfaces on the fracture surfaces, while such behavior was either very limited or nonexistent in the microhybrid composite (Fig. 20b).

Thus, it may be concluded that strength loss by resin degradation occurs in both composites, while the additional strength loss in the nanofill composite may be attributed to interfacial degradation. Interfacial debonding suggests there is some hydrolytic degradation of the silane coupling agent for the nanofill composite. This latter effect is likely due to the fact the nanofill composite actually contains clusters of agglomerated nanoparticles in contrast to the solid particles present in the microhybrid composite. Although the fillers in both composites are silane treated, differences in hydrolytic degradation may be attributed to different interfacial properties due to the larger surface area to volume ratio and more irregular porous structure [51] of the nanoclusters compared to the solid particles in the microhybrid composite. The porous surfaces associated with the agglomerates may not as effectively accept the silane treatment or may simply be more prone to hydrolytic degradation.

5.4.2 *R*-curve behavior: Role of hydration

Both composites show rising *R*-curve behavior in the hydrated state, similar to the behavior in the as-processed state (Figs. 18b-d). As discussed in a previous paper on the as-processed composites [149], the initial increase in toughness over roughly one millimeter of crack extension results from the extrinsic toughening mechanisms of crack deflection (Fig. 19a and b) and crack bridging (Fig. 19c and d), both of which are promoted by interparticle/intercluster crack growth and are clearly seen in the hydrated composites. Depending on the filler shape and deflection angle, crack deflection may lead to formation of uncracked bridges when a crack locally arrests and either 1) a new crack initiates and propagates ahead of the arrest point or 2) the crack fronts on each side of the arrest point propagate and reconnect ahead. In either case, a bridge of uncracked material may be formed behind the crack tip. As intact particles, or groups of particles, span across the crack flanks, those bridges sustain part of the applied load that would otherwise be experienced at the crack tip, effectively toughening the material by lowering the near-tip stress intensity, K_{tip}, relative to the applied stress intensity, K_{app}:

$$K_{tip} = K_{app} - K_{br} \quad \textbf{(12),}$$

where K_{br} is the bridging stress intensity, which is a function of crack extension, Δa. Crack bridges are developed as the crack propagates, causing the increases in toughness seen in Fig 18. The observation of a steady state, or plateau, toughness

following the initial increase indicates that the bridging zone becomes fully developed and the bridges are forming and breaking at roughly equivalent rates in the crack wake.

From Fig. 18f, it is evident that the microhybrid composite has superior peak toughness compared to the nanofill composite in the as-processed, hydrated, and post-cured conditions. The absence of any observable decrease in the *R*-curve peak toughness of the microhybrid composite after 60 days of water hydration suggests a lack of water induced degradation, which is in agreement with no apparent change in the crack path after hydration, i.e. interparticle failure through the matrix was the dominant mechanism. Although it may seem counterintuitive that only the strength, and not the peak toughness, is decreased by hydration, it is important to note that the strength of brittle materials exhibiting *R*-curves is only partially determined by the peak toughness. Indeed, the steepness of the rising portion of the *R*-curve is also important in determining strength [122, 123]. Furthermore, there may be multiple competing effects of hydration in influencing the intrinsic resistance to crack advance, e.g., by matrix plasticization, and the extrinsic toughness mechanisms such as crack deflection and bridging. Such competition may be offsetting and not apparent when only comparing the peak toughness, but may in fact affect the rise of the *R*-curve and the strength.

On the contrary, the nanofill composite showed a significant decrease in the *R*-curve peak toughness after hydration, as observed in Fig. 18d and f. As described previously

in Sec. 5.4.1.2, most mechanisms of hydrolytic degradation reported in the literature are related to either filler, matrix or interfacial degradation, and for the present composites filler degradation has largely been ruled out. Since both interfacial debonding and a toughness decrease were only observed in the hydrated nanofill composite, it may be concluded that interfacial debonding is the most likely cause of the toughness loss with hydration for the nanofill composite. If resin degradation were the cause, such an effect would be expected in both composites.

The present results on the nanofill composite generally agree with the theoretical finite modeling results of Chan et al. who suggested that improvement in silanization can improve the fracture toughness of dental nanocomposites [77]. However, there is likely a practical limit where silanization is above a threshold level and this effect would saturate, which may have been achieved in the present microhybrid composite which showed no evidence of interfacial separation in either the as-processed or hydrated cases.

5.4.3 Effect of post-curing

Following the same trend as observed in hydrated and as-processed conditions, the microhybrid composite had a higher average post-cured peak toughness than the nanofill (Fig. 18e-f), which is likely associated with the inherent microstructural differences between the two composites [149]. There is no significant improvement in peak toughness of the nanofill composite after the post-curing treatment, compared to the as-processed condition, and although a statistical comparison between as-processed and post-cured microhybrid composite is not feasible due to limited data, average peak toughness values are essentially identical (Fig. 18f). However, there is a noticeable change in the *R*-curve shape from the as-processed to post-cured states (Figs. 18c-e). Indeed, the peak toughness is reached more quickly, within the first < 0.5 mm of crack extension. This indicates either an increase in the steepness of the *R*-curve, an increase in the initiation point of the *R*-curve, or both. Either of these factors could contribute to higher strength and apparent single value, K_{Ic}, toughness. Improvement in those mechanical properties has been reported and attributed to increases in the molecular mobility of the polymer chains which enhances the degree of polymerization [13, 74, 100], increased mobility of free radicals [74, 100] and/or relaxation of internal stresses [101] during the heat treatment.

In bridging ceramics like Al_2O_3 and Si_3N_4, which are essentially composites of crystalline ceramic grains surrounded by a weak glass matrix (e.g., ~ 10% volume in Si_3N_4) that fracture mostly intergranularly, optimal grain adhesion plays an important

role in imparting high strength and fracture toughness [122, 123]. A weak intergranular crack path is essential for imparting crack deflection, crack bridging, high toughness and strength; however, when that path is too weak the *R*-curve becomes less steep and the strength is lower [122, 123]. A similar case appears to occur in resin based composites. When the crack path is through the resin matrix, as occurs in the as-processed and post-cured states for both composites, the light-cured matrix is likely weaker than optimal and post-curing improves the matrix properties resulting in a steepening of the *R*-curve that is associated with higher strength. The relationship between the steepness of the *R*-curve, $\frac{dK_R}{da}$, and high strength may be seen by assuming an initial penny shaped flaw radius of a_i. In that case, the applied stress, σ_{app}, equals the fracture strength when the following two conditions are satisfied:

$$K_{app} = 2\sigma_{app}\sqrt{\frac{\Delta a + a_i}{\pi}} = K_R \text{ and } \frac{dK_{app}}{da} = \frac{dK_R}{da} \quad \textbf{(13),}$$

where K_R is the fracture resistance from the *R*-curve. Flexural strength predictions based on Eq. 13 have proven to be quite accurate for two Si_3N_4 ceramics provided the early part of the *R*-curve is accurately measured back to $\Delta a = 0$ [122]. This can be achieved by direct measurements using specialized experimental techniques [147], or can be deduced by independently measuring the initiation toughness, K_0, and interpolating the data [119, 122, 123]. Unfortunately, for the former case custom testing apparatus is required, and for the latter case there are experimental challenges

associated with stress relaxation of the resin matrix during K_0 measurements. While this was not possible in the present study, nonetheless, insight has been gained into the mechanisms responsible for toughness and strength in these composites.

5.5 Conclusions

Based on a study on flexural strength and *R*-curve toughness of two commercial dental restorative composites, one microhybrid and one nanofill, after subjecting them to either 60 days of water hydration or a post-cure heat treatment (120 °C for 90 min), the following conclusions can be made.

1. Hydration significantly lowers the strength of both composites, by ~ 32% in the microhybrid composite and ~ 50% in the nanofill composite. Based on crack path and fracture surface observations, this effect is attributed to resin matrix degradation in both composites, with the additional decrease in the nanofill composite attributed to interfacial degradation as evidenced by matrix-particle debonding.

2. Two extrinsic toughening mechanisms, crack deflection and crack bridging, both were identified in the composites under all conditions. The latter mechanism was responsible for the rising *R*-curve behavior, increasing the toughness of the composite by forming intact bridge regions behind the crack tip, thus sustaining some of the applied load and reducing the stresses experienced at the crack tip.

3. The peak toughness of the nanofill composite was lowered ~ 18% by water hydration, while no such effect was observed for the microhybrid composite. This reduction is attributed to degradation of the particle-matrix interface, which caused particle-matrix debonding during the fracture process.

4. Although the peak toughness was not affected by post-curing in either composite, the shape of the *R*-curve was noticeably different, reaching the peak toughness after much shorter amounts of crack extension. Such behavior can explain the increase in strength and single value apparent toughness with post-curing observed in other studies, and is likely attributed to an improvement in the resin matrix properties.

ACKNOWLEDGEMENTS

The authors would like to thank 3M™ ESPE™ for providing the necessary restorative materials for the present work, as well as Michelle Yang and Josh Hogg for helping prepare and machine the specimens used in this study.

6 MANUSCRIPT III: MECHANISTIC ASPECTS OF FATIGUE CRACK GROWTH BEHAVIOR IN RESIN BASED DENTAL RESTORATIVE COMPOSITES

M. B. Shah[a], J. L. Ferracane[b] and J. J. Kruzic[a5]

[a] School of Mechanical, Industrial, and Manufacturing Engineering, Oregon State University,
Corvallis, OR, USA

[b] Division of Biomaterials & Biomechanics, School of Dentistry, Oregon Health & Science University, Portland, OR, USA

Submitted to

Dental Materials

November 2008

[5] Corresponding author. Tel: +1-541-737-7027; fax: +1-541-737-2600.

E-mail address: jamie.kruzic@oregonstate.edu (J. J. Kruzic)

6.1 Abstract

Objective: To evaluate the fatigue crack growth behavior and related micromechanisms of two commercial resin based dental restorative composites.

Methods: After 60 days of water hydration, the fatigue crack growth resistance of two different resin composites, one microhybrid (Filtek™ Z250) and one nanofill (Filtek™ Supreme Plus), was measured in wet conditions using compact-tension, C(T), specimens at a load ratio of 0.1 and frequency of 2 Hz. Cyclic fatigue behavior was quantified in terms of the fatigue crack growth rate, *da/dN*, as a function of the stress intensity range, ΔK.

Results: A sigmoidal *da/dN*-ΔK curve with three different fatigue crack growth regions was identified for both composites. In general, fatigue crack growth ranged from ~10^{-9} to 10^{-5} m/cycle over ΔK of 0.54 to 0.63 MPa√m for the Z250 composite and ΔK of 0.41 to 0.67 MPa√m for the Supreme Plus composite. The Supreme Plus composite showed a lower fatigue threshold, ΔK_{th}, by ~ 0.13 MPa√m compared to the Z250 composite, while also showing a plateau in the fatigue crack growth curve that is likely related to environmental attack. SEM observations of the fatigue crack paths and fracture surfaces revealed an interparticle crack path and extrinsic toughening mechanisms of crack deflection and crack bridging. No fatigue degradation of reinforcing particles or clusters was found, but cluster-matrix debonding was evident in the Supreme Plus composite, also indicative of environmental attack due to water.

Significance: This study increases the understanding of both the fatigue behavior and the micromechanisms of fatigue in resin based dental composites.

KEYWORDS

Resin composite; Fatigue; Crack growth; Crack bridging; Hydration; Mechanisms

6.2 Introduction

Teeth experience cyclic loading routinely during their lifetime due to forces from mastication, grinding, and shivering. Although a single mechanical overload leading to a catastrophic failure is a possibility, repetitive loading due to mastication can lead to sub-critical crack propagation in tooth tissue and/or restorations, negatively affecting the long term functionality and structural stability of the affected teeth [159, 160]. Because such cyclic stresses are repeated more than $3x10^5$ times per year for the average person [90], dental restorative materials must be able to resist fatigue failure from cyclic loading conditions and there is a need to understand such behavior when comparing existing, or designing new, restorative materials. In that regard, resin based dental composites have experienced increased usage in direct dental restorative applications, and there is evidence that their long term clinical performance is not as good as amalgam in high load bearing posterior restorations [17, 27].

In addition to causing bulk fracture, fatigue behavior has also been related to the wear properties of resin based composites. Microcrack propagation in a subsurface layer due to repeated occlusal loading may be a precursor of clinical wear [94] and higher wear resistance has been found for restoratives with higher fatigue crack growth resistance [83]. Reduced clinical wear can enhance the lifetime of composite restorations as well as help them retain their favorable aesthetic appearance.

Two different approaches are commonly used to evaluate the cyclic fatigue behavior of a material, namely the "stress-life" and the damage tolerant methods. Cyclic fatigue is most commonly evaluated using the "stress-life" (*S/N*) method whereby the fatigue life, N_f, is determined as the number of cycles to cause material failure at a given cyclic stress amplitude. Using this method, fatigue strength may be determined for a given lifetime. Although this method is simple to apply, there are a few limitations. For example, *S/N* data is highly scattered due to the unpredictable nature of crack initiation, which may be affected by flaws and/or inhomogeneities at the surface or in the microstructure. This makes accurate lifetime predictions using the *S/N* method difficult, as actual fatigue lives may vary by several orders of magnitude. Another drawback of the *S/N* approach is that it is difficult to separately determine i) which variables affect crack initiation and growth and ii) the mechanisms governing each of those portions of the fatigue life.

The damage tolerant approach is different in that it assumes cracks or crack-like flaws exist in a material, and it focuses on understanding the crack growth portion of the lifetime. This method uses fracture mechanics to characterize the crack growth rates, which in turn can allow accurate predictions of fatigue life and the study of fatigue crack growth mechanisms. Fatigue crack growth rates, *da/dN*, are generally characterized in terms of the stress intensity range, ΔK.[6] These parameters are often

---

[6] The stress-intensity factor, *K*, is a global parameter which fully characterizes the local stress and deformation fields in the immediate vicinity of a crack tip in a linear-elastic solid, and thus can be used

related to each other at intermediate growth rates by the Paris law for fatigue crack growth [161]:

$$\frac{da}{dN} = C(\Delta K)^m \quad \textbf{(14),}$$

where $\Delta K = K_{max} - K_{min}$ and C and m are material and environment specific constants. K_{max} and K_{min} are defined as the maximum and minimum stress intensity experienced by the crack during each loading cycle. For teeth, where cracks generally exist in the enamel [162], and resin based dental restorative composites, where fracture is known to initiate at surface or internal flaws [53], this approach should be highly relevant.

It appears that only a few studies have quantified the fatigue crack growth resistance of resin based dental composites [82, 83, 95-97]. In general, it has been found that resin based dental composites have lower fatigue crack growth resistance when compared to the natural human dentin they replace [97]. Additionally, the fatigue crack growth resistance of resin composites is affected by water hydration [83, 95]; indeed one study reported continuous decline in the fatigue crack propagation resistance over 1-3 months of water storage [95] while another found changes in the Paris law exponent [83]. Similarly, a degradation in fatigue strength after a month of

---

to correlate with the extent of crack advance. It is defined for a crack of length a as $K = Y\sigma_{app}(\pi a)^{1/2}$, where σ_{app} is the applied stress and Y is a geometry factor of the order of unity [98].

water storage has also been observed by Braem et al. [163] for four different resin based composites using a modified *S/N* approach, known as the "staircase" approach. However, Lohabauer et al. [81] observed no change in the flexural fatigue limit of a resin based composite after long-term water storage (90 days) suggesting there are likely variations in the susceptibility of different resin based composites to water induced degradation of fatigue resistance.

Although a few studies have evaluated the fatigue crack growth behavior of resin based restorative composites, there is still very little data available and the understanding of the associated micromechanisms are limited. Accordingly, the purpose of the current study is to evaluate the fatigue crack growth resistance of two different commercial composites and, where possible, provide insight into the mechanisms responsible for the observed behavior.

6.3 Materials and methods

6.3.1 Materials

Two different universal dental resin composites were evaluated in the present study. The first material investigated was a microhybrid composite, commercially known as Filtek™ Z250 (3M/ESPE™), which contains 60 vol% zirconia/silica fillers with particle size ranging from 0.01 to 3.5 μm (average 0.6 μm). The second was a nanofill composite reinforced entirely with nano particles and their agglomerates and

commercially known as Filtek™ Supreme Plus (3M/ESPE™), which contains 20 nm discrete silica particles and 0.6 to 1.4 μm zirconia/silica clusters made up of 5-20 nm primary particles (59.5 vol%). According to the manufacturer, both composites have very similar matrix composition with Bis-GMA, UDMA, Bis-EMA and a small amount of TEGDMA [33].

6.3.2 Specimen preparation

For fatigue crack growth experiments, ($N = 8$) standard fracture mechanics based compact-tension, C(T), specimens were prepared for each composite. A complete description of sample preparation is in Ref. [149], but to summarize, rectangular coupons were prepared in an aluminum split mold and light cured for 40 seconds each on the top and bottom surfaces (Triad II, Dentsply International, York Division, PA). After curing, holes and a starter notch were machined into the samples using conventional machining methods. Final samples had a nominal width, $W \approx 14$ mm, and thickness, $B = 2 \pm 0.5$ mm, with a starter notch length, $a_0 = 3.5 \pm 0.2$ mm, as shown in Fig. 1. Specimen surfaces on both sides were ground with silicon carbide paper to 600 grit and polished using alumina slurries to 0.05 μm followed by a final polishing step using Buehler™ MasterPolish. All samples were stored at room temperature in deionized water for 60 days before testing. This treatment was determined to give >98% hydration through the entire thickness of the samples based on calculations using Fick's second law of non-steady state diffusion [164].

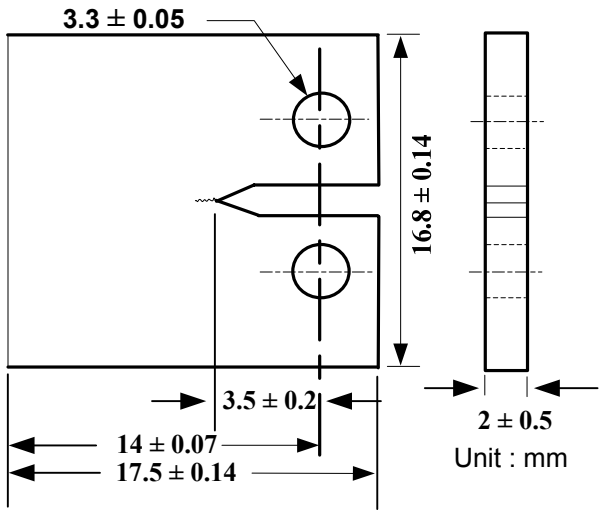

Fig. 21. Schematic of a compact tension, C(T), specimen with geometrical dimensions.

6.3.3 Fatigue crack growth testing

A custom built razor micronotching machine was used to produce a sharp pre-crack in all specimens by repeatedly sliding a razor blade over the end of the machined notch under an applied load while irrigating with a 1 μm diamond slurry. The diamond slurry ground a razor sharp micronotch into the sample and this process was continued until the applied load caused a sharp pre-crack to initiate from the micronotch. Following pre-cracking, fatigue cycling was performed using a computer controlled servo-hydraulic mechanical testing machine (Instron© 8501, Canton, MA) at a frequency, υ, of 2 Hz (sine wave) and a constant load ratio ($R=P_{min}/P_{max}$, ratio of minimum to maximum load) of 0.1. Fatigue crack growth rates, da/dN, were determined as a function of applied stress intensity range, ΔK, in general accordance with ASTM standard E-647 [165]. As both composites showed rising fracture

resistance over the first ~1 mm of crack extension [149, 164], crack growth rate measurements were taken only after the fatigue crack had grown more than 1 mm from the end of the notch.

Throughout the fatigue testing, each sample was kept wet and hydrated by taping a wet sponge around it and keeping the sponge hydrated throughout the test. Growth rates approaching the fatigue threshold, ΔK_{th}, which is often operationally defined as minimum crack growth rate below 10-10 m/cycle where cracking is essentially dormant, was achieved by decreasing ΔK (load-shedding) using a normalized K-gradient ($1/\Delta K$ [$d\Delta K/da$]) of -0.08 mm-1. Alternatively, the high velocity portion of the crack growth curve, $da/dN > 10^{-8}$ m/cycle, was measured using increasing ΔK conditions (K-gradient = +0.08 mm-1). Load-point displacements were monitored in-situ using a capacitance displacement gauge (HPT150, Capacitec, Inc., Ayer, MA) which was connected to the clevis grips. Crack lengths were then deduced from the elastic unloading compliance calibrations for the standard C(T) specimen geometry [135] and proved reasonably accurate when compared with post-test optical crack length measurements. When required, any crack length errors were corrected during data analysis by assuming that error accumulated linearly with crack extension. Crack growth rates, da/dN, and ΔK values were calculated by averaging over crack extensions of ~100-200 μm.

6.3.4 Mechanism characterization

After concluding crack growth experiments on hydrated resin composites, microscopic observations of fatigue samples were performed to understand the crack path interaction with the salient microstructural features. Uncoated polished specimen surfaces (crack profiles) and fracture surfaces were examined using both an optical microscope and a field emission gun scanning electron microscope (FEI Quanta) in low vacuum mode at a pressure of 110 Pa.

6.4 Results

Fatigue crack growth data for both composites is shown in Fig. 22 where crack growth rates, *da/dN*, are plotted as a function of the applied stress intensity range, ΔK, on a log-log plot. Several samples fractured inadvertently prior to successful data collection; accordingly, data are shown from a total of five specimens (three Supreme Plus and two Z250). In each case, sufficient data was collected so that the upper and lower portions of the *da/dN* curves, measured using increasing and decreasing ΔK conditions, respectively, met up with each other. Additionally, *da/dN* data for a different microhybrid composite (Vit-1-escence, 0.7 μm average particle size, Bis-GMA-based resin) and hydrated human dentin in the Paris regime, are also shown for comparison purposes (room temperature, υ = 5 Hz and R = 0.1) [68, 97].

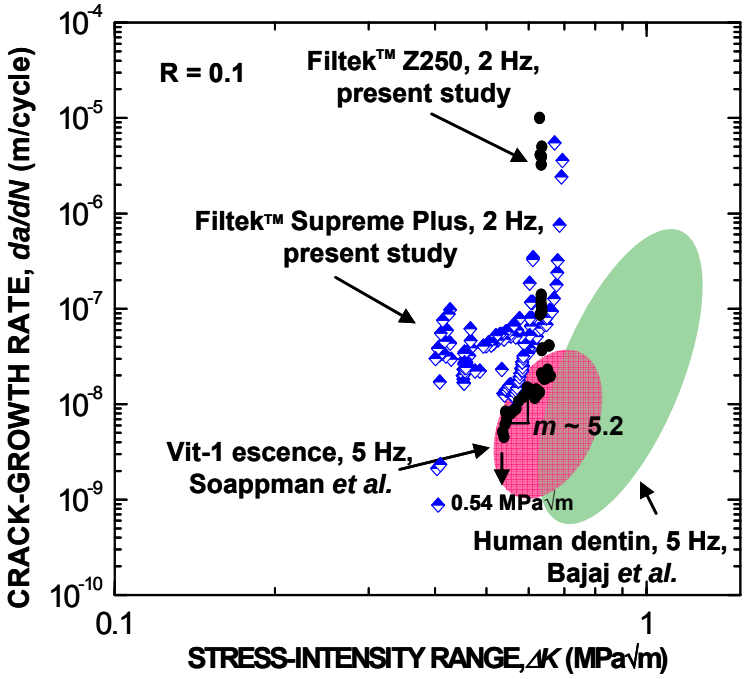

Fig. 22. Fatigue crack growth rates, *da/dN*, as a function of stress-intensity range, ΔK, for the two commercial dental restorative composites tested: Z250 (solid circular symbols) and Supreme Plus (half filled diamond symbols) (υ = 2 Hz, R = 0.1). Both composites were hydrated in water for 60 days and tested under wet conditions. The Paris regime data from a fatigue crack growth study on a different microhybrid composite (υ = 5 Hz, R = 0.1) [97] and hydrated dentin (υ = 5 Hz, R = 0.1) [166] are displayed for comparison purposes.

For both composites, three different growth rate regions may be identified on sigmoidal fatigue crack growth curves. Region I is the near-threshold region where the crack growth rate is highly sensitive to the applied ΔK, and both composites showed a well defined fatigue threshold, ΔK_{th}, at which measurable crack growth ceased. The fatigue threshold was determined to be ~0.54 MPa√m for the Z250 composite and ~0.41 MPa√m for the Supreme Plus composite.

Next, region II for both composites is characterized by an abrupt change in the slope in Fig. 22. For the Z250 composite, region II is characterized well by the Paris law

(Eq. 14), showing a roughly linear slope in Fig. 22. By fitting the data to Eq. 14, the scaling constants *m* and *C* were determined to be 5.2 ± 1.0 and ~ 2 x 10^{-7} (m/cycle) (MPa√m)$^{-m}$ respectively, with a correlation coefficient of $R^2 = 0.67$. Conversely, region II for the Supreme Plus composite showed a very weak dependence on the stress intensity range. Thus, the Paris law was not used to fit the data in that regime. Finally, both composites exhibit a sharp transition to region III behavior, where the crack growth rate accelerated as K_{max} approached the toughness of the composite. In this region, there was considerable overlap in the behavior of the two composites. In general, the Supreme Plus composite was more susceptible to fatigue crack growth as crack propagation occurred over a larger range of stress intensities (0.26 MPa√m vs. 0.09 MPa√m) while the fatigue threshold was lower.

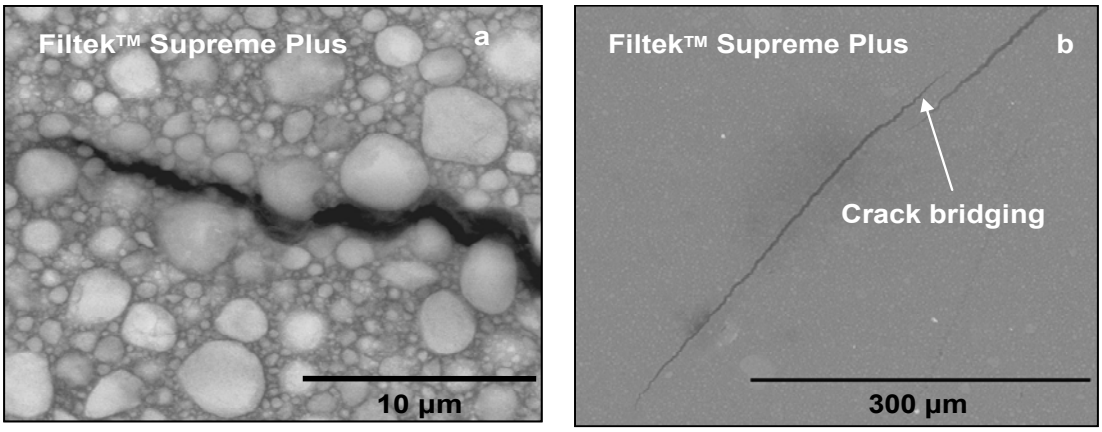

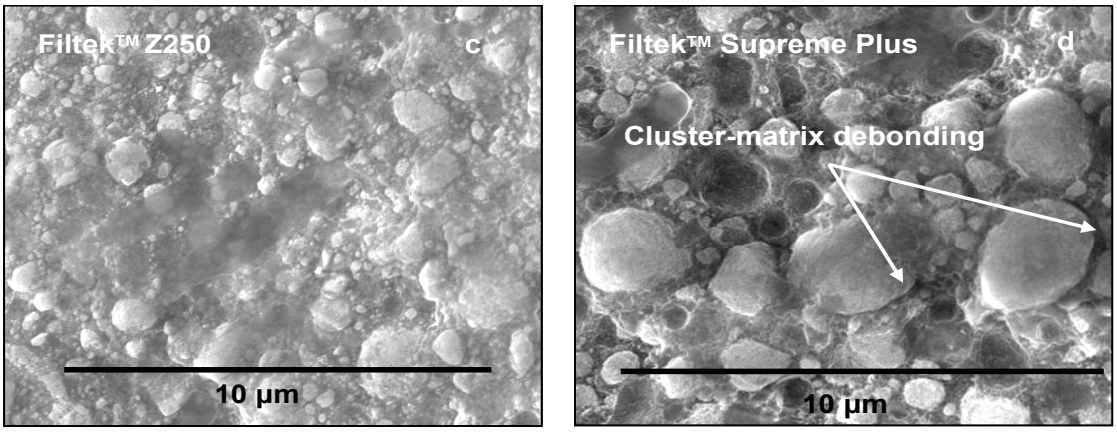

Fig. 23. (a) SEM micrograph showing representative fatigue crack path in the Supreme Plus composite. Z250 also showed similar interparticle crack propagation. (b) An uncracked bridge in the crack wake for the Supreme Plus composite. Similar features were seen in the Z250 composite. (c) Microscopic fracture surfaces showing mostly interparticle crack growth through the resin matrix in Z250 but (d) protruding filler particles with cluster-matrix debonding suggests more interfacial crack growth in Supreme Plus composite. General direction of crack growth is from right to left.

SEM observations of fatigue crack paths in both composites showed interparticle crack growth (Fig. 23a). Additionally, both crack deflection and crack bridging (Fig. 23b) were observed as extrinsic toughening mechanisms that help increase the resistance to crack propagation. Little filler-matrix debonding was seen for the Z250 composite (Fig. 23c) but cluster-matrix interfacial debonding, evidenced by protruding filler particles, was observed in the Supreme Plus composite (Fig. 23d).

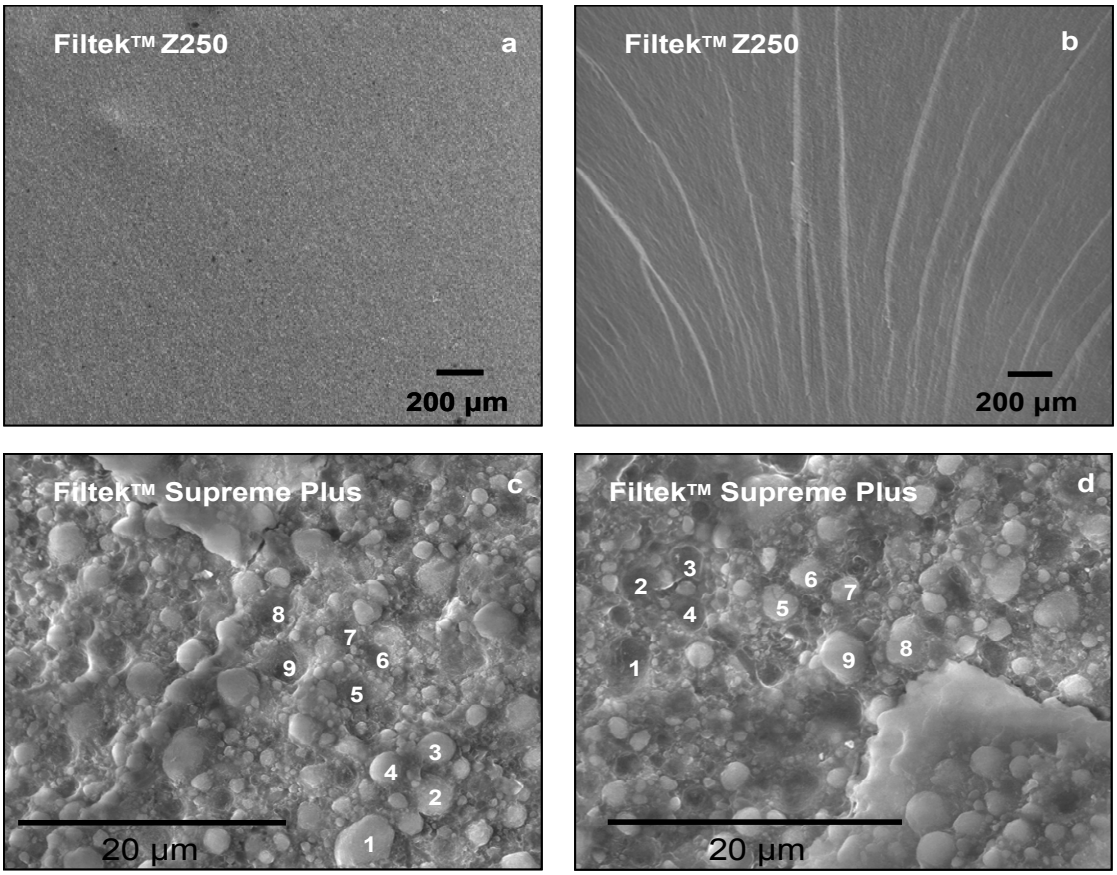

Fig. 24. Low magnification fracture surface micrograph showing how (a) the fracture surface of the Z250 composite from previous fracture tests was relatively smooth [164] while (b) fatigue samples had relatively rough surface showing crack propagation on different planes. Similar behavior was observed for the Supreme Plus composite as well. (c) and (d) show mirror images of the same location on the opposite fatigue fracture surfaces of a Supreme Plus composite sample. Interparticle crack growth is confirmed at every location where a particle on one surface corresponds to hole on the other and vice versa. Points labeled 1-9 are examples of matching locations. The Z250 composite also showed a similar lack of particle failure. General direction of crack growth is from bottom to top.

Post-test low magnification SEM micrographs of Fig. 24 shows a fracture surface for a fracture experiment sample from a previous study (Fig. 24a) [164] compared with a fatigue fracture surface from the present study (Fig. 24b). Very smooth fracture surfaces were observed for the *R*-curve fracture test samples whereas relatively rough

surfaces with extrusions and intrusions (peaks and valleys) were observed for the cyclically loaded samples, suggesting crack propagation on multiple planes.

Finally, a lack of particle or agglomerate fracture was confirmed by imaging the fatigue fracture surfaces. An example evaluation of the exact same location on opposite fracture surfaces is shown in Figs. 24c & 24d. Sites 1-9 give examples of how each particle or cluster on one surface corresponds to a hole on the other and vice versa. Similar behavior was seen for both composites and no evidence of particle or cluster splitting due to cyclic loading was observed on any of the fracture surface images taken.

6.5 Discussion

6.5.1 Fatigue crack propagation rates

In this study, a test frequency of 2 Hz was selected because it matches the upper range of the typical human chewing frequency [167] and thus allows experiments to be conducted as quickly as possible and also be considered clinically relevant. Due to the viscoelastic properties of the resin matrix, higher test frequencies may affect fatigue results. For example, it has been suggested that high test frequencies could lead to internal heating during fatigue testing [96].

Both composites showed a sigmoidal fatigue crack growth curve with three apparent crack growth regimes and a well defined threshold where measurable crack growth essentially ceased. This is in contrast to fatigue crack growth studies on some other resin based dental composites, which generally found only a single regime of crack growth [82, 83, 95-97]. In some cases, this difference may be attributed to the fact that data was collected over a limited range of growth rates, but that may not explain it completely. Rather, it is likely that there are fundamental differences between the fatigue crack growth behavior of different composites, and/or there may be a role of different test conditions.

Two separate studies have measured the 10^5 cycle flexural fatigue limit (FFL) for the same commercial composites examined in the present work. The results were very similar for the composites, with one study reporting a FFL of 45.9 ± 7 MPa for the Z250 composite [168] and another study reporting a FFL of 49.6 ± 3.8 for the Supreme Plus composite [169]. However, it should be pointed out that water hydration times were very short in those studies, two weeks for the Z250 and 24 hours for the Supreme Plus. Recent results have shown that both the strength and fracture resistance of the Supreme Plus composite to be more susceptible to long term water induced degradation than the Z250 composite [164]. In that study, a relatively higher degradation in properties with hydration for the Supreme Plus composite was associated with interfacial debonding, which is also seen here (Fig. 23). Considering that the short hydration FFL results from other studies indicate similar fatigue behavior for the two composites while the present longer hydration results suggest a

lower fatigue threshold for the Supreme Plus composite, it is likely that the fatigue properties of Supreme Plus are also more susceptible to water degradation than the Z250 composite and that may be associated with increased interfacial debonding.

Only Z250 showed a clear Paris regime with a Paris exponent, *m*, of ~5.2 MPa√m. Soappman *et al*. recently studied fatigue crack growth response of a different microhybrid composite (Vit-1-escence, 0.7 μm average particle size, Bis-GMA based resin) and reported the m value to be ~ 5.3 [97]. This value is in very good agreement with our results despite the fact that the samples in that study were soaked for 24 hrs in the Hanks Balanced Salt Solution (HBSS) compared to 60 days water hydration in our study. This may indicate that the fatigue crack growth resistance of these two microhybrid composites has relatively low susceptibility to water degradation.

Most metals have Paris exponents in the range of 2-4, while the *m* values for brittle materials and their composites are much larger, even as high as 100 [103]. The intermediate value found for the Z250 composite suggests that potentially both ductile and brittle fatigue mechanisms operate in these composites. For comparison, the *m* value for hydrated human dentin (υ = 5 Hz, R = 0.1) has been reported to be 13–22 for samples from individual donors depending on age, with the higher values corresponding to specimens from older donors [68].

For the Supreme Plus nanofill composite, a well defined Paris regime was not found and instead there was a plateau in the da/dN-ΔK curve in the range of 10^{-8}–10^{-7} m/cycle where the fatigue crack growth rate was relatively insensitive to the applied

stress intensity range. In general, when fatigue crack growth rates are largely insensitive to the stress intensity it is because the growth rate is determined by some process other than mechanical fatigue, such as mass transfer of, or reactions with, a chemical species from the environment [170]. As was mentioned previously, the Supreme Plus composite has shown higher susceptibility to water degradation of the strength and fracture properties [149, 164]. This was associated with clear evidence of interfacial debonding that does not occur in the dry as-processed condition, nor does interfacial debonding occur in the Z250 composite in either the hydrated or dry as-processed test conditions. Thus, environmental attack from water would appear to be the most likely reason for the observed plateau in the da/dN-ΔK curve for the Supreme Plus composite.

As growth progresses to final fracture, the final K_{max} values were ~ 0.7 MPa√m for both composites in this study. This is lower compared to the peak R-curve toughness values of 1.3 and 0.8 MPa√m for the Z250 and Supreme Plus composites, respectively [164]. A key difference between the studies is the strain rate, which is much higher in the present dynamic tests. Resin based polymer composites exhibit viscoelastic behavior and thus may be expected to behave differently at different strain rates.

6.5.2 Fatigue threshold behavior

As seen in Fig. 22, the fatigue threshold, ΔK_{th}, for the Z250 composite was 0.54 MPa√m while that of the Supreme Plus composite was 0.41 MPa√m. A higher fatigue threshold is beneficial as it suggests that Z250 can sustain relatively higher cyclic stresses without causing crack extension. In general, both resin composites showed lower fatigue thresholds compared to human dentin. Nalla *et al*. [171] have reported a threshold of 1.06 MPa√m, whereas Bajaj *et al*. [68] found a lower value of ~0.7 MPa√m for young hydrated dentin.

The fatigue threshold may be influenced by a number of factors, including the inherent microstructure, extrinsic toughening mechanisms, and environment. Recent studies have found the fracture resistance of both composites to be governed by crack deflection and bridging mechanisms, with the fracture resistance of the Z250 being higher than the Supreme Plus composite in both hydrated and as-processed conditions [149, 164]. In materials toughened by crack deflection and bridging, it is often found that the fatigue threshold scales with the fracture toughness [146, 172, 173], as is found here for these two resin based dental composites. In those cases, toughening due to crack bridging can influence the fatigue threshold by reducing the crack-tip stress intensity, and thus slowing crack growth.

Other than microstructure and toughening mechanisms, environment can also significantly affect the fatigue threshold. Evidence of interfacial degradation seen as

particle and/or cluster-matrix debonding due to water hydration has been observed in the Supreme Plus composite both in the present study (Fig. 23d) and in a previous study on the fracture and strength properties [164]. An environmental influence on fatigue threshold was recently demonstrated by Takeshige *et al*. [95] where the fatigue threshold of a resin based dental composite was found to progressively decrease over 3 months of water hydration. Those authors suggested either enhanced crack tip blunting due to resin plasticization, internal stress relaxation, and/or residual compressive stresses at the crack tip as the possible mechanisms for water influencing the crack growth behavior of the composite they tested. In the present study, however, it appears interfacial degradation is the most likely mechanism influencing the fatigue properties of the Supreme Plus composite.

6.5.3 Fatigue micromechanisms

Similar toughening micromechanisms, namely crack deflection and bridging, were found in the present fatigue study as have been previously reported for the fracture of these same composites in both the hydrated and as-processed conditions [149, 164]. Both mechanisms are promoted by the interparticle crack path observed in the fatigue of these composites (Figs. 23a, 24c & 24d). Cyclic degradation of the Supreme Plus nanoparticle clusters (Fig. 24c and d) or the solid particles of the Z250 composite was not observed indicating that differences in the fatigue crack growth behavior between two resin composites may not be related to hydrolytic or cyclic degradation of the filler. Z250 showed interparticle crack growth with crack propagation mostly through

the matrix whereas Supreme Plus composite demonstrated considerable interfacial debonding along the particle and/or cluster-matrix interfaces. Interfacial debonding suggests there is some hydrolytic degradation of the silane coupling agent for the Supreme Plus composite. Although the fillers in both composites are silane treated, differences in hydrolytic degradation may be attributed to different interfacial properties due to the larger surface area to volume ratio and more irregular porous structure of the nanoparticle clusters [51] compared to the solid particles in the Z250 composite. The porous surfaces associated with the agglomerates may not as effectively accept the silane treatment or may simply be more prone to hydrolytic degradation.

6.6 Conclusions

Based on investigations of the fatigue crack growth behavior of one commercial microhybrid (Z250) and one commercial nanofill (Supreme Plus) restorative composite tested under wet conditions after 60 days of water hydration, the following conclusions can be made:

1. Fatigue crack growth was found to follow an intergranular crack path in both composites, with crack deflection and crack bridging contributing to the fatigue crack growth resistance. No evidence was found of hydrolytic or cyclic degradation of the fillers in either composite; however, in the case of the Supreme Plus nanofill composite, there was evidence of interfacial debonding between the matrix and filler.

2. Both composites exhibited a sigmoidal fatigue crack growth curve with three distinct regimes of fatigue crack growth. The intermediate growth region for the Z250 composite was characterized well by the Paris power law with a scaling exponent, $m \sim 5.2$.

3. For the Supreme Plus composite, in the intermediate regime the crack growth rate was largely insensitive to the applied stress intensity range. This suggests that an environmental effect likely controlled the growth rate such as water degradation of the matrix-filler interface, as was observed in the crack profiles and fracture surfaces.

4. The Supreme Plus composite showed lower fatigue threshold, ΔK_{th}, by ~0.13 MPa√m when compared to the Z250 composite. This is likely associated with the lower fracture resistance and/or the higher susceptibility to hydrolytic degradation for that composite.

ACKNOWLEDGEMENTS

The authors would like to express their gratitude to 3M for providing all the necessary materials for conducting the research, Rawley Green for helping with the fatigue crack growth experiments, and Josh Hogg for machining the samples. Also, the authors thank John Donovan and Kurt Langworthy for their help and support with the SEM analysis.

7 SUMMARY AND CONCLUSIONS

A mechanistic study of fracture and fatigue resistance was performed on two particulate reinforced commercial resin based dental restorative composites, one micohybrid (Filtek™ Z250) and one nanofill (Filtek™ Supreme Plus).

The present study made quantitative measurements of the fracture resistance in terms of *R*-curves and qualitative evaluations of fracture and/or toughening micromechanisms by crack path and fracture surface observations of double notched and compact-tension, C(T), specimens. The flexural strength of both composites was also measured in four point bending using un-notched beam samples. In addition to the as-processed condition, both composites were tested after 60 days of water hydration and post-cure heat treatment at 120 ºC for 90 min.

Rising *R*-curve behavior was observed for both composites irrespective of the pre-test treatment, which was attributed to crack deflection and crack bridging toughening mechanisms. Interparticle crack growth promoted crack deflection and the formation of intact regions in the crack wake provided crack bridging. SEM observation of the crack path and fracture surfaces evidenced particle-matrix debonding in the hydrated nanofill composite, negatively influencing the peak toughness of the composite. Following hydration, flexural strength of both composites deteriorated, suggesting hydrolytic degradation of the resin matrix, as both composite have very similar filler composition and filler volume percentages with no evidence of filler fracture.

Additional strength degradation in the nanofill composite was attributed to filler/matrix interfacial degradation. Post-cured heat treatment changed the shape of the *R*-curve by reaching the peak toughness at a very small crack extension, which helps explain the reported increase in strength in the literature due to matrix toughening.

As resin composites are routinely subjected to relatively weak but repetitive masticatory forces, the fatigue resistance of both composites was evaluated after 60 days of water hydration using the damage tolerant approach. The cyclic loading response was quantified in terms of fatigue crack growth rate, *da/dN*, as a function of the stress intensity range, ΔK. Both composites showed a sigmoidal *da/dN*- ΔK curve with three different fatigue crack growth regions. In case of the microhybrid composite, the mid-growth region was characterized using the Paris power law, with exponent, *m*, of ~ 5.2. In general, fatigue crack growth ranged from ~ 10^{-9} to 10^{-5} m/cycle over ΔK of 0.54 to 0.63 MPa√m for the microhybrid composite and ΔK of 0.41 to 0.67 MPa√m for the nanofill dental composite. Crack deflection and crack bridging were observed extrinsic toughening mechanisms in fatigue with evidence of cluster-matrix debonding for the nanofill composite. The latter mechanism of interfacial debonding due to environmental attack is likely responsible for lower fatigue threshold and observed plateau in the fatigue crack growth curve of the nanofill composite.

8 FUTURE WORK

The research outlined in the previous three manuscripts clearly showed the importance of crack deflection and bridging toughening mechanisms in governing the toughness of the resin composites. As crack deflection is highly influenced by the geometrical configuration of the second phase particles, additions of high aspect ratio rod or plate shape particles could enhance the overall toughness of the composites. It is known that the twist component induced by rod shape particles is more effective in deflecting the crack [105] and thus improving the crack resistance compared to the spherical configuration. Furthermore, increased filler volumes with optimum packing densities can also be explored for its affect on increasing the strength and toughness of the resin composites.

In addition to the steady state toughness, quantitative measurements of the crack initiation and growth toughness for both composites could also be useful in modeling and designing a material with optimal toughness and strength. Such quantification further allows understanding of the strength-toughness relationship, and it has been shown for bridging ceramics that steeper and faster rising R-curves give relative insensitivity to the flaw size and higher fracture strength [119, 122, 123].

The nanofill composite showed a lower fatigue threshold and plateau behavior in the fatigue crack growth study. As hydration and wet environment are likely influencing

this behavior, it would be useful to study the fatigue crack growth behavior in the as processed condition as well, to discern the effect of environment.

9 REFERENCES

[1] Kishen A. Mechanisms and risk factors for fracture prediction in endodontically treated teeth. Endodontic Topics, 2006; **13(1)**:57-83.

[2] Bowen RL, Rodriguez MS. Tensile strength and modulus of elasticity of tooth structure and several restorative materials. Journal of the American Dental Association, 1962; **64**:378-387.

[3] Powers JM, Sakaguchi RL. Craig's restorative dental materials. 2006. Twelfth edition, Mosby.

[4] Manhart J, Chen H, Hamm G, Hickel R. Review of the clinical survival of direct and indirect restorations in posterior teeth of the permanent dentition. Operative Dentistry, 2004; **29(5)**:481-508.

[5] Roulet JF. The problems associated with substituting composite resins for amalgam - A status report on posterior composites. Journal of Dentistry, 1988; **16(3)**:101-113.

[6] Manhart J, Kunzelmann KH, Chen HY, Hickel R. Mechanical properties of new composite restorative materials. Journal of Biomedical Materials Research, 2000; **53(4)**:353-361.

[7] Kahler WA, Kotousov A, Borkowski K. On fracture of restored teeth. Key Engineering Materials, 2005; **293-294**:245-251.

[8] Bonilla ED, Mardirossian G, Caputo AA. Fracture toughness of posterior resin composites. Dental Materials, 2001; **32(3)**:206-210.

[9] Davis DM, Waters NE. An investigation into the fracture-behavior of a particulate-filled Bis-GMA resin. Journal of Dental Research, 1987; **66(6)**:1128-1133.

[10] Brunthaler A, König F, Lucas T, Sperr W, Schedle A. Longevity of direct resin composite restorations in posterior teeth: a review. Clinical Oral Investigations, 2003; **7(2)**:63-70.

[11] Watanabe H, Khera SC, Vargas MA, Qian F. Fracture toughness comparison of six resin composites. Dental Materials, 2008; **24(3)**:418-425.

[12] Sakaguchi RL, Wiltbank BD, Murchison CF. Cure induced stresses and damage in particulate reinforced polymer matrix composites: a review of the scientific literature. Dental Materials, 2005; **21(1)**:43-46.

[13] Yamaga T, Sato Y, Akagawa Y, Taira M, Wakasa K, Yamaka M. Effects of post-curing by light and heat on hardness and fracture toughness of four commercial visible-light-cured dental composite resins for crown and bridge veneers. Journal of Materials Science Letters, 1994; **13(20)**:1494-1496.

[14] Soderholm KJ, Roberts MJ. Influence of water exposure on the tensile strength of composites. Journal of Dental Research, 1990; **69(12)**:1812-1816.

[15] Sideridou I, Achilias DS, Spyroudi C, Karabela M. Water sorption characteristics of light-cured dental resins and composites based on Bis-EMA/PCDMA. Biomaterials, 2004; **25(2)**:367-376.

[16] Poon ECM, Smales RJ, Yip KH-K. Clinical evaluation of packable and conventional hybrid posterior resin-based composites: Results at 3.5 years. Journal of the American Dental Association, 2005; **136(11)**:1533-1540.
[17] Bernardo M, Luis H, Martin M, Leroux B, Rue T, Leitão J, DeRouen T. Survival and reasons for failure of amalgam versus composite posterior restorations placed in a randomized clinical trial. Journal of American Dental Association, 2007; **138(6)**:775-783.
[18] Papadogiannis Y, Lakes R, Palaghias G, Helvatjoglu-Antoniades M, Papadogiannis D. Fatigue of packable dental composites. Dental Materials, 2007; **23(2)**:235-242.
[19] Tantbirojn D, Versluis A, Cheng YS, Douglas WH. Fracture toughness and microhardness of a composite: do they correlate? Journal of Dentistry, 2003; **31(2)**:89-95.
[20] Zhou ZR, Zheng J. Tribology of dental materials: a review. Journal of Applied Physics D: Applied Physics, 2008; **41(11)**:1-22 (113001).
[21] He LH, Swain MV. Understanding the mechanical behavior of human enamel from its structural and compositional characteristics. Journal of the Mechanical Behavior of Biomedical Materials, 2008; **1(1)**:18-29.
[22] Imbeni V, Kruzic JJ, Marshall GW, Marshall SJ, Ritchie RO. The dentin-enamel junction and the fracture of human teeth. Nature Materials, 2005; **4(3)**:229-232.
[23] Scheid RC. Woelfel's dental anatomy: Its relevance to dentistry. 2007. Seventh edition, Lippincott Williams & Wilkins.
[24] Peutzfeldt A. Indirect resin and ceramic systems. Operative Dentistry, 2001; **26(6)**:153-176.
[25] Jung YG, Peterson IM, Kim DK, Lawn BR. Lifetime-limiting strength degradation from contact fatigue in dental ceramics. Journal of Dental Research, 2000; **79(2)**:722-731.
[26] Lawn B, Bhowmick S, Bush M, Qasim T, Rekow ED, Zhang Y. Failure modes in ceramic-based layer structures: A basis for materials design of dental crowns. Journal of the American Ceramic Society, 2007; **90(6)**:2007.
[27] Collins CJ, Bryant RW, Hodge K-LV. A clinical evaluation of posterior composite resin restorations: 8-year findings. Journal of Dentistry, 1998; **26(4)**:311-317.
[28] Kovarik RE, Haubenreich JE, Gore D. Glass ionomer cements: A review of composition, chemistry, and biocompatibility as a dental and medical implant material. Journal of Long-Term Effects of Medical Implants, 2005; **15(6)**:655-671.
[29] Hickel RA, Folwaczny M. Various forms of glass ionomers and compomers. Operative Dentistry, 2001; **26(6)**:177-190.
[30] Azevedo C, Forestier J-P, Tavernier B. Effect of time on the flexural strength of glass ionomer and composite orthodontic adhesives. The Angle Orthodontist, 2004; **75(1)**:114-118.
[31] Sideridou I, Tserki V, Papanastasiou G. Study of water sorption, solubility and modulus of elasticity of light-cured dimethacrylate-based dental resins. Biomaterials, 2003; **24(4)**:655-665.

[32] Kahler B, Kotousov A, Borkowski K. Effect of material properties on stresses at the restoration-dentin interface of composite restorations during polymerization. Dental Materials, 2006; **22(2)**:942-947.
[33] Mitra SB, Wu D, Holmes BN. An application of nanotechnology in advanced dental materials. Journal of the American Dental Association, 2003; **134(10)**:1382-1390.
[34] Sideridou ID, Karabela MM, Bikiaris DN. Aging studies of light cured dimethacrylate-based dental resins and a resin composite in water or ethanol/water. Dental Materials, 2007; **23(9)**:1142-1149.
[35] Drummond JL. Degradation, fatigue, and failure of resin dental composite materials. Journal of Dental Research, 2008; **87(8)**:710-719.
[36] Santos C, Clarke RL, Braden M, Guitian F, Davy KWM. Water absorption characteristics of dental composites incorporating hydroxyapatite filler. Biomaterials, 2002; **23(8)**:1897-1904.
[37] Li Y, Swartz ML, Phillips RW, Moore BK, Roberts TA. Effect of filler content and size on properties of composites. Journal of Dental Research 1985; **64(12)**:1396-1401.
[38] Meric G, Dahl JE, Ruyter IE. Physicochemical evaluation of silica-glass fiber reinforced polymers for prosthodontic applications. European Journal of Oral Sciences, 2005; **113(3)**:258-264.
[39] van Dijken JWV, Sunnegardh-Gronberg K. Fiber-reinforced packable resin composites in class II cavities. Journal of Dentistry, 2006; **34(10)**:763-769.
[40] Freilich MA, Meiers JC, Duncan JP. Fiber-reinforced composites in clinical dentistry. 2000. First edition, Quintessence Publishing.
[41] Xu HHK. Long-term water-aging of whisker-reinforced polymer-matrix composites. Journal of Dental Research, 2003; **82(1)**:48-52.
[42] Asmussen E, Peutzfeldt A. Influence of UEDMA, BisGMA and TEGDMA on selected mechanical properties of experimental resin composites. Dental Materials, 1998; **14(1)**:51-56.
[43] Musanje L, Davell BW. Aspects of water sorption from the air, water and artificial saliva in resin composite restorative materials. Dental Materials, 2003; **19(5)**:414-422.
[44] Ferracane JL. Hygroscopic and hydrolytic effects in dental polymer networks. Dental Materials, 2006; **22(3)**:211-222.
[45] Ferracane JL, Hopkin JK, Condon JR. Properties of heat-treated composites after aging in water. Dental Materials, 1995; **11(5)**:354-358.
[46] Antonucci JM, Dickens SH, Fowler BO, Xu HHK, McDonough WG. Chemistry of silanes: interfaces in dental polymers and composites. Journal of Research of the National Institute of Standards and Technology, 2005; **110(5)**:541-558.
[47] Eick J, Kotha S, Chappelow C, Kilway K, Giese G, Glaros A, Pinzino C. Properties of silorane-based dental resins and composites containing a stress-reducing monomer. Dental Materials, 2007; **23(8)**:1011-1017.
[48] Rueggeberg FA. From vulcanite to vinyl, a history of resins in restorative dentistry. Journal of Prosthetic Dentistry, 2002; **87(4)**:364-379.

[49] Ferracane JL, Ferracane LL, Musanje L. Effect of light activation method on flexural properties of dental composites. American Journal of Dentistry, 2003; **16(5)**:318-322.
[50] International Standards Organization ISO 4049. Dentistry-polymer-based filling, restorative and luting materials. 2000.
[51] Curtis AR, Shortall AC, Marquis PM, Palin WM. Water uptake and strength characteristics of a nanofilled resin-based composite. Journal of Dentistry, 2008; **36(3)**:186-193.
[52] Chung SM, Yap AUJ, Chandra SP, Lim CT. Flexural strength of dental composite restoratives: Comparison of biaxial and three-point bending test. Journal of Biomedical Materials Research, 2004; **71B(2)**:278-283.
[53] Rodrigues Jr. SA, Ferracane JL, Della Bona A. Flexural strength and Weibull analysis of a microhybrid and a nanofill composite evaluated by 3- and 4-point bending tests. Dental Materials, 2008; **24(3)**:426-431.
[54] Rodrigues Jr. SA, Zanchi CH, de Carvalho RV, Demarco FF. Flexural strength and modulus of elasticity of different types of resin-based composites. Brazilian Oral Research, 2007; **21(1)**:16-21.
[55] Debnath S, Ranade R, Wunder SL, McCool J, Boberick K, Baran G. Interface effects on mechanical properties of particle-reinforced composites. Dental Materials, 2004; **20(7)**:677-686.
[56] Soderholm KJM, Mukherjee R, Longmate J. Filler leachability of composites stored in distilled water or artificial saliva. Journal of Dental Research, 1996; **75(9)**:1692-1699.
[57] Musanje L, Ferracane JL. Effects of resin formulation and nanofiller surface treatment on the properties of experimental hybrid resin composite. Biomaterials, 2004; **25(18)**:4065-4071.
[58] Tyas MJ. Correlation between fracture properties and clinical-performance of composite resins in class-IV cavities. Australian Dental Journal, 1990; **35(1)**:46-49.
[59] Scherrer SS, Botsis J, Studer M. Fracture toughness of aged dental composites in combined mode I and mode II loading. Journal of Biomedical Materials Research, 2000; **53(4)**:362-370.
[60] Lloyd CH, Ianetta RV. The fracture toughness of dental composites, Part I: The development of strength and fracture toughness. Journal of Oral Rehabilitation, 1982; **9(2)**:55-66.
[61] Fujishima A, Ferracane JL. Comparison of four modes of fracture toughness testing for dental composites. Dental Materials, 1996; **12(1)**:38-43.
[62] Ferracane JL, Antonio RC, Matsumoto H. Variables affecting the fracture toughness of dental composites. Journal of Dental Research, 1987; **66(6)**:1140-1145.
[63] Zhao D, Botsis J, Drummond JL. Fracture studies of selected dental restorative composites. Dental Materials, 1997; **13(3)**:198-207.
[64] Rodrigues Jr. SA, Scherrer S, Ferracane JL. Microstructural characterization and fracture behavior of a microhybrid and a nanofill composite. Dental Materials, 2008; **24(9)**:1281-1288.

[65] Ferracane JL, Berge HX. Fracture toughness of experimental dental composites aged in ethanol. Journal of Dental Research, 1995; **74(7)**:1418-1423.
[66] Zhang D, Nazari A, Soappman M, Bajaj D, Arola D. Methods for examining the fatigue and fracture behavior of hard tissues. Experimental Mechanics, 2007; **47(3)**:325-336.
[67] Xu HHK, Smith DT, Jahanmir S, Romberg E, Kelly JR, Thompson VP, Rekow ED. Indentation damage and mechanical properties of human enamel and dentin. Journal of Dental Research, 1998; **77(3)**:472-480.
[68] Bajaj D, Sundaram N, Nazari A, Arola D. Age, dehydration and fatigue crack growth in dentin. Biomaterials, 2006; **27(11)**:2507-2517.
[69] Indrani DJ, Cook WD, Televantos F, Tyas MJ, Harcourt JK. Fracture toughness of water-aged resin composite restorative materials. Dental Materials, 1995; **11(3)**:201-207.
[70] Pilliar RM, Smith DC, Maric B. Fracture toughness of dental composites determined using the short-rod fracture toughness test. Journal of Dental Research, 1986; **65(11)**:1308-1314.
[71] Söderholm KJ. Degradation of glass filler in experimental composites. Journal of Dental Research, 1981; **60(11)**:1867-1875.
[72] Ferracane JL, Marker VA. Solvent degradation and reduced fracture toughness in aged composites. Journal of Dental Research, 1992; **71(1)**:13-19.
[73] Ferracane JL, Berge HX, Condon JR. In vitro aging of dental composites in water-effect of degree of conversion, filler volume, and filler/matrix coupling. Journal of Biomedical Materials Research, 1998; **42(3)**:465-472.
[74] Ferracane JL, Condon JR. Post-cure heat treatments for composites: properties and fractography. Dental Materials, 1992; **8(5-6)**:290-295.
[75] Kim KH, Ong JL, Okuno O. The effect of filler loading and morphology on the mechanical properties of contemporary composites. Journal of Prosthetic Dentistry, 2002; **87(6)**:642-649.
[76] Xu HHK, Schumacher GE, Eichmiller FC, Peterson RC, Antonucci JM, Mueller HJ. Continuous-fiber preform reinforcement of dental resin composite restorations. Dental Materials, 2003; **19(6)**:523-530.
[77] Chan KS, Lee YD, Nicolella DP, Furman BR, Wellinghoff S, Rawls R. Improving fracture toughness of dental nanocomposites by interface engineering and micromechanics. Engineering Fracture Mechanics, 2007; **74(12)**:1857-1871.
[78] Cannillo V, Bondioli F, Lusvarghi L, Montorsi M, Avella M, Errico ME, Malinconico M. Modeling of ceramic particles filled polymer-matrix nanocomposites. Composites Science and Technology, 2006; **66(7-8)**:1030-1037.
[79] Mesquita RV, Axmann D, Geis-Gerstorfer A. Dynamic visco-elastic properties of dental composite resins. Dental Materials, 2006; **22(3)**:258-267.
[80] Momoi Y, McCabe JF. Hygroscopic expansion of resin based composites during 6 months of water storage. British Dental Journal, 1994; **176(3)**:91-96.

[81] Lohbauer U, Frankenberger R, Kramer N, Petschelt A. Time-dependent strength and fatigue resistance of dental direct restorative materials. Journal of Materials Science-Materials in Medicine, 2003; **14(12)**:1047-1053.
[82] Kawakami Y, Takeshige F, Hayashi M, Ebisu S. Fatigue of tooth-colored restoratives in aqueous environment. Dental Materials, 2007; **26(1)**:1-6.
[83] Truong VT, Cock DJ, Padmanathan N. Fatigue crack propagation in posterior dental composites and prediction of clinical wear. Journal of Applied Biomaterials, 1990; **1(1)**:21-30.
[84] Baran G, Boberick K, McCool J. Fatigue of restorative materials. Critical Reviews in Oral Biology & Medicine, 2001; **12(4)**:350-360.
[85] Htang A, Ohsawa M, Matsumoto H. Fatigue resistance of composite restorations: effect of filler content. Dental Materials, 1995; **11(1)**:7-13.
[86] Staninec M, Kim P, Marshall GW, Ritchie RO, Marshall SJ. Fatigue of dentin-composite interfaces with four-point bend. Dental Materials, 2008; **24(6)**:799-803.
[87] McCabe JF, Wang Y, Braem M. Surface contact fatigue and flexural fatigue of dental restorative materials. Journal of Biomedical Materials Research, 2000; **50(3)**:375-380.
[88] Nagarajan VS, Hockey BJ, Jahanmir S, Thompson VP. Contact wear mechanisms of a dental composite with high filler content. Journal of Materials Science, 2000; **35(2)**:487-496.
[89] Bae J-M, Kim K-N, Hattori M, Hasegawa K, Yoshinari M, Kawada E, Oda Y. Fatigue strengths of particulate filler composites reinforced with fibers. Dental Materials, 2004; **23(2)**:166-174.
[90] Garoushi S, Lassila LVJ, Tezvergil A, Vallittu PK. Static and fatigue compression test for particulate filler composite resin with fiber-reinforced composite substructure. Dental Materials, 2007; **23(1)**:17-23.
[91] Spanoudakis J, Young RJ. Crack propagation in a glass particle-filled epoxy resin. Part 2. Effect of particle-matrix adhesion. Journal of Materials Science, 1984; **19(2)**:487-496.
[92] McCool J, Boberick K, Baran G. Lifetime predictions for resin-based composites using cyclic and dynamic fatigue. Journal of Biomedical Materials Research, 2001; **58(3)**:247-253.
[93] Montes-G GM, Draughn RA. Slow crack propagation in composite restorative materials. Journal of Biomedical Materials Research, 1987; **21(5)**:629-642.
[94] Truong VT, Tyas MJ. Prediction of in vivo wear in posterior composite resins: a fracture mechanics approach. Dental Materials, 1988; **4(6)**:318-327.
[95] Takeshige F, Kawakami Y, Hayashi M, Ebisu S. Fatigue behavior of resin composites in aqueous environments. Dental Materials, 2007; **23(7)**:893-899.
[96] Loughran GM, Versluis A, Douglas WH. Evaluation of sub-critical fatigue crack propagation in a restorative composite. Dental Materials, 2005; **21(3)**:252-261.
[97] Soappman M, Nazari A, Porter J, Arola D. A comparison of fatigue crack growth in resin composite, dentin and the interface. Dental Materials, 2007; **23(5)**:608-614.

[98] Anderson TL. Fracture Mechanics: Fundamentals and Applications. 2005. Third edition, CRC, Taylor and Francis Group, Florida.
[99] Bagis YH, Rueggeberg FA. The effect of post-cure heating on residual, unreacted monomer in a commercial resin composite. Dental Materials, 2000; **16(4)**:244-247.
[100] Cook WD, Johannson M. The influence of postcuring on the fracture properties of photo-cured dimethacrylate based dental composite resin. Journal of Biomedical Materials Research, 1987; **21(8)**:979-989.
[101] de Gee AJ, Pallav P, Werner A, Davidson CL. Annealing as a mechanism of increasing wear resistance of composites. Dental Materials, 1990; **6(4)**:266-270.
[102] Ritchie RO. Mechanisms of fatigue crack-propagation in metals, ceramics and composites - role of crack tip shielding. Materials Science and Engineering A-Structural Materials Properties Microstructure and Processing, 1988; **103(1)**:15-28.
[103] Ritchie RO. Mechanisms of fatigue-crack propagation in ductile and brittle solids. International Journal of Fracture, 1999; **100(1)**:55-83.
[104] Kaur S, Shetty DK, Cutler RA. R Curves and crack-stability map: application to Ce-TZP/AL_2O_3. Journal of the American Ceramic Society, 2007; **90(11)**:3554-3558.
[105] Lawn B. Fracture of Brittle Solids. 1993. second ed. edition, Cambridge University Press, Cambridge, UK.
[106] Evans AG. Perspective on the development of high-toughness ceramics. Journal of the American Ceramic Society, 1990; **73(2)**:187-206.
[107] Nalla RK, Kruzic JJ, Kinney JH, Ritchie RO. Mechanistic aspects of fracture and R-curve behavior in human cortical bone. Biomaterials, 2005; **26(2)**:217-231.
[108] Ritchie RO, Kinney JH, Kruzic JJ, Nalla RK. A fracture mechanics and mechanistic approach to the failure of cortical bone. Fatigue & Fracture of Engineering Materials & Structures, 2005; **28(4)**:345-371.
[109] Kruzic JJ, Schneibel JH, Ritchie RO. Fracture and fatigue resistance of Mo-Si-B alloys for ultrahigh-temperature structural applications. Scripta Materialia, 2004; **50(4)**:459-464.
[110] Sheu C, Dauskardt RH, De Jonghe L. Toughness and fatigue of encapsulation-processed silicon carbide-polymer matrix particulate composites. Journal of Materials Science, 1993; **28(8)**:2196-2206.
[111] Boddapati SR, Rodel J, Jayaram V. Crack growth resistance (R-curve) behavior and thermo-physical properties of Al2O3 particle-reinforced AlN/Al matrix composites. Composites Part A-Applied Science and Manufacturing, 2007; **38(3)**:1038-1050.
[112] Nalla RK, Kruzic JJ, Kinney JH, Ritchie RO. Effect of aging on the toughness of human cortical bone: Evaluation by R-curves. Bone, 2004; **35(6)**:1240-1246.
[113] Nalla RK, Kinney JH, Tomsia AP, Ritchie RO. Role of alcohol in the fracture resistance of teeth. Journal of Dental Research, 2006; **85(11)**:1022-1026.

[114] Kruzic JJ, Nalla RK, Kinney JH, Ritchie RO. Crack blunting, crack bridging and resistance-curve fracture mechanics in dentin: effect of hydration. Biomaterials, 2003; **24(28)**:5209-5221.
[115] Munz D. What can we learn from R-curve measurements? Journal of the American Ceramic Society, 2007; **90(1)**:1-15.
[116] Nalla RK, Kruzic JJ, Ritchie RO. On the origin of the toughness of mineralized tissue: microcracking or crack bridging? Bone, 2004; **34(5)**:790-798.
[117] Sigl LS. Microcrack toughening in brittle materials containing weak and strong interfaces. Acta Materialia, 1996; **44(9)**:3599-3609.
[118] Tomaž K, Aleš D, Čedomir O, Peter J. The strength and hydrothermal stability of Y-TZP ceramics for dental applications. International Journal of Applied Ceramic Technology, 2007; **4(2)**:164-174.
[119] Kruzic JJ, Cannon RM, Ritchie RO. Crack-size effects on cyclic and monotonic crack growth in polycrystalline alumina: Quantification of the role of grain bridging. Journal of the American Ceramic Society, 2004; **87(1)**:93-103.
[120] Foulk III JW, Cannon RM, Johnson GC, Klein PA, Ritchie RO. A micromechanical basis for partitioning the evolution of grain bridging in brittle materials. Journal of the Mechanics and Physics of Solids, 2007; **55(4)**:719-743.
[121] Becher PF, Sun EY, Plucknett KP, Alexander KB, Hsueh CH, Lin HT, Waters SB, et al. Microstructural design of silicon nitride with improved fracture toughness: I, effects of grain shape and size. Journal of the American Ceramic Society, 1998; **81(11)**:2821-2830.
[122] Kruzic JJ, Satet RL, Hoffmann MJ, Cannon RM, Ritchie RO. The utility of R-curves for understanding fracture toughness-strength relations in bridging ceramics. Journal of the American Ceramic Society, 2008; **91(6)**:1986-1994.
[123] Kruzic JJ, Cannon RM, Ritchie RO. Effects of moisture on grain boundary strength, fracture and fatigue properties of alumina. Journal of the American Ceramic Society, 2005; **88(8)**:2236-2245.
[124] Hu XZ, Mai YW. Crack-bridging analysis for alumina ceramics under monotonic and cyclic loading. Journal of the American Ceramic Society, 1992; **75 (4)**:848-853.
[125] Leung CKY, Chi J. Crack-bridging force in random ductile fiber brittle matrix composites. Journal of Engineering Mechanics-ASCE, 1995; **121(12)**:1315-1324.
[126] Moon RJ, Hoffman M, Hilden J, Bowman KJ, Trumble KP, Rodel J. R-curve behavior in alumina-zirconia composites with repeating graded layers. Engineering Fracture Mechanics, 2002; **69(14 -16)**:1647-1665.
[127] Nalla RK, Stolken JS, Kinney JH, Ritchie RO. Fracture in human cortical bone: local fracture criteria and toughening mechanisms. Journal of Biomechanics, 2005; **38(7)**:1517-1525.
[128] Lohbauer U, Frankenberger R., Kramer N., Petschelt A. Strength and fatigue performance versus filler fraction of different types of direct dental restoratives. Journal of Biomedical Materials Research, 2006; **76B(1)**:114-120.

[129] Wilson NH, Dunne SM, Gainsford ID. Current materials and techniques for direct restorations in posterior teeth. Part 2: Resin composite systems. International Dental Journal, 1997; **47(4)**:185-193.
[130] Hickel RA, Manhart J, Garcia-Godoy F. Clinical results and new developments of direct posterior restorations. American Journal of Dentistry, 2000; **13(Special Issue SI)**:41D-54D.
[131] Combe EC, Burke FJT. Contemporary resin-based composite materials for direct placement restorations: packables, flowables and others. Dental Update, 2000; **27(7)**:326-332, 334-326.
[132] Palin WM, Fleming GJP, Burke FJT, Marquis PM, Randall RC. The influence of short and medium-term water immersion on the hydrolytic stability of novel low-shrink dental composites. Dental Materials, 2005; **21(9)**:852-863.
[133] van Dijken JWV. Direct resin composite inlays/onlays: An 11 year follow-up. Journal of Dentistry, 2000; **28(5)**:299-306.
[134] Fischer H, Rentzsch W, Marx R. R-Curve behavior of dental ceramic materials. Journal of Dental Research, 2002; **81(8)**:547-551.
[135] Newman JC. Stress-intensity factors and crack-opening displacements for round compact specimens. International Journal of Fracture, 1981; **17(6)**:567-578.
[136] Murakami Y. Stress intensity factors handbook. 1987. First edition, Pergamon Press, Elmsford, NY.
[137] Chung SM, Yap AUJ, Koh WK, Tsai KT, Lim CT. Measurement of Poisson's ratio of dental composite restorative materials. Biomaterials, 2004; **25(13)**:2455-2460.
[138] Papadogiannis DY, Lakes RS, Papadogiannis Y, Palaghias G, Helvatjoglu-Antoniades M. The effect of temperature on the viscoelastic properties of nano-hybrid composites. Dental Materials, 2008; **24(2)**:257-266.
[139] Njiwa ABK, Fett T, Lupascu DC, Rodel J. Crack-tip toughness of a soft lead zirconate titanate. Journal of the American Ceramic Society, 2003; **86(11)**:1973-1975.
[140] Kim KH, Park JH, Imai Y, Kishi T. Microfracture mechanisms of dental resin composites containing spherically-shaped filler particles. Journal of Dental Research, 1994; **73(2)**:499-504.
[141] Calais JG, Soderholm K-JM. Influence of filler type and water exposure on flexural strength of experimental composite resins. Journal of Dental Research, 1988; **67(5)**:836-840.
[142] Kinloch AJ, Maxwell D, Young RJ. Micromechanisms of crack propagation in hybrid-particulate composites. Journal of Materials Science Letters, 1985; **4(10)**:1276-1279.
[143] Nalla RK, Kinney JH, Ritchie RO. On the fracture of human dentin: Is it stress- or strain-controlled? Journal of Biomedical Materials Research, 2003; **67A(2)**:484-495.
[144] Kahler B, Swain MV, Moule A. Fracture-toughening mechanisms responsible for differences in work to fracture of hydrated and dehydrated dentine. Journal of Biomechanics, 2003; **36(2)**:229-237.

[145] Swain MV. R-curve behavior in a polycrystalline alumina material. Journal of Materials Science Letters, 1986; **5(12)**:1313-1315.
[146] Yuan R, Kruzic JJ, Zhang XF, De JongheL C, Ritchie RO. Ambient to high-temperature fracture toughness and cyclic fatigue behavior in Al-containing silicon carbide ceramics. Acta Materialia, 2003; **51(20)**:6477-6491.
[147] Jelitto H, Felten F, Swain MV, Balke H, Schneider GA. Measurement of the total energy release rate for cracks in PZT under combined mechanical and electrical loading. Journal of Applied Mechanics-Transactions of the ASME, 2007; **74(6)**:1197-1211.
[148] Kovarik RE, Fairhurst CW. Effect of Griffith precracks on measurement of composite fracture toughness. Dental Materials, 1993; **9(4)**:222-228.
[149] Shah MB, Ferracane JL, Kruzic JJ. R-curve behavior and micromechanisms of fracture in resin based dental restorative composites. Journal of the Mechanical Behavior of Biomedical Materials, 2008; **in review**.
[150] Evans AG, Heuer AH. Transformation toughening in ceramics - martensitic transformations in crack-tip stress-fields. Journal of American Ceramic Society, 1980; **63(5-6)**:241-248.
[151] Munz D, Fett T. Ceramics: Mechanical Properties, Failure Behaviour, Materials Selection. 2001. Second edition, Springer-Verlag Berlin Heidelberg, NY.
[152] Schütt A, Bürki G, Schwaller P, Michler J, Cattani-Lorente M, Vallitu P, Bouillaguet S. Mechanical properties of fibre-reinforced dental composites subjected to hydrothermal and mechanical ageing. European Cells and Materials, 2004; **7(2)**:55-56.
[153] Lagouvardos PE, Pissis P, Kyritsis A, Daoukaki D. Water sorption and water-induced molecular mobility in dental composite resins. Journal of Materials Science-Materials in Medicine, 2003; **14(9)**:753-759.
[154] Soderholm KJ, Zigan M, Ragan M, Fischlschweiger W, Bergman M. Hydrolytic degradation of dental composites. Journal of Dental Research, 1984; **63(10)**:1248-1254.
[155] Martos J, Osinaga P, Oliveira E, Castro L. Hydrolytic degradation of composite resins: effects on the microhardness. Materials Research, 2003; **6(4)**:599-604.
[156] Trujillo M, Newman SM, Stansbury JW. Use of near-IR to monitor the influence of external heating on dental composite photopolymerization. Dental Materials, 2004; **20(8)**:766-777.
[157] Mayworm CD, da Rocha-Leão MHM, Bastian FL. Artificial saliva sorption of two hybrid nanoparticle resin-based restorative dental composites. 2nd Mercosur Congress on Chemical Engineering, 4th Mercosur Congress on Process Systems Engineering, 2005. p. 1-9.
[158] Ortengren U, Wellendorf H, Karlsson S, Ruyter I. Water sorption and solubility of dental composites and identification of monomers released in an aqueous environment. Journal of Oral Rehabilitation, 2001; **28(12)**:1106-1115.
[159] Drummond JL. Cyclic fatigue of composite restorative materials. Journal of Oral Rehabilitation, 1989; **16(5)**:509-520.

[160] Kruzic JJ, Nalla RK, Kinney JH, Ritchie RO. Mechanistic aspects of in vitro fatigue-crack growth in dentin. Biomaterials, 2005; **26(10)**:1195-1204.
[161] Paris PC, Erdogan F. A critical analysis of crack propagation laws. Journal of Basic Engineering, 1963; **85(4)**:528-534.
[162] Brown WS, Jacobs HR, Thompson RE. Thermal fatigue in teeth. Journal of Dental Research, 1972; **51(2)**:461-467.
[163] Braem M, Lambrechts P, Gladys S, Vanherle G. In vitro fatigue behavior of restorative composites and glass ionomers. Dental Materials, 1995; **11(2)**:137-141.
[164] Shah MB, Ferracane JL, Kruzic JJ. R-curve behavior and toughening mechanisms of resin based dental composites: Effects of hydration and post-cure heat treatment. Dental Materials, 2008:Accepted for publication.
[165] ASTM E647. Standard test method for measurement of fatigue crack growth rates. 2000.
[166] Bajaj D, Sundaram N, Nazari A, Arola D. Age, dehydration and fatigue crack growth in dentin. Biomaterials 2006; **27(11)**:2507-2517.
[167] Braem M, Lambrechts P, Vanherle G. Clinical relevance of laboratory fatigue studies. Journal of Dentistry, 1994; **22(2)**:97-102.
[168] Lohbauer U, von der Horst T, Frankenberger R, Kramer N, Petschelt A. Flexural fatigue behavior of resin composite dental restoratives. Dental Materials, 2003; **19(5)**:435-440.
[169] Turssi CP, Ferracane JL, Ferracane LL. Wear and fatigue behavior of nano-structured dental resin composites. Journal of Biomedical Materials Research Part B: Applied Biomaterials, 2006; **78B(1)**:196-203.
[170] Suresh S. Fatigue of Materials. 1998. Second edition, Cambridge University Press, UK.
[171] Nalla RK, Imbeni V, Kinney JH, Staninec M, Marshall SJ, Ritchie RO. In vitro fatigue behavior of human dentin with implications for life prediction. Journal of Biomedical Materials Research A, 2003; **66A(1)**:10-20.
[172] Gilbert CJ, Ritchie RO. Mechanisms of cyclic fatigue-crack propagation in a fine-grained alumina ceramic: the role of crack closure. Fatigue & fracture of engineering materials & structures, 1997; **20(10)**:1453-1466.
[173] Campbell JP, Venkateswara Rao KT, Ritchie RO. The effect of microstructure on fracture toughness and fatigue-crack growth behavior in g-based titanium aluminide intermetallics. Metallurgical and Materials Transactions A, 1999; **30A(3)**:563-577.